Characteristics of Dividing and Combining Flows

Weimin Zhu

A thesis

in

The Department

of

Civil Engineering

Presented in Partial Fulfillment of the Requirements
for the Degree of Doctor of Philosophy at
Concordia University
Montreal, Quebec, Canada

June 1995

ISBN 0-612-05069-6

Canada

ABSTRACT

Characteristics of Dividing and Combining Flows

Weimin Zhu, Ph.D.

Concordia University, 1995

In the present thesis, some aspects of dividing and combining flows are studied. The first part of the study considers the discharge characteristics of flow past a two-dimensional lateral slot located in a rectangular conduit. Existing theoretical solutions to this problem are based on free streamline theory. The test results provide data to verify the predictions of the theoretical model related to the dependence of the slot discharge coefficient on discharge ratios and the ratio of the kinetic energy to the total energy of the flow approaching the slot. The test results validate the model predictions.

A theoretical expression for the outflow through a rectangular lateral weir located in a circular open channel is derived. The theoretical weir discharge coefficient is expressed as a function of the parameters relating the geometry of the weir and the channel, and a velocity parameter that is a function of the dimensionless flow depth, the weir sill height and the approach Froude number. Experimental results are presented to verify the proposed theoretical model.

The characteristics of dividing flows in closed rectangular conduits are studied in the next section. The contraction coefficient and the loss coefficients of branching flows are determined using results of an existing model dealing with a two-dimensional lateral outlet fitted with an external barrier. For dividing closed conduit flows, two different

procedures are used to obtain the variation of an energy loss coefficient and the contraction coefficient with the discharge ratio. Detailed velocity and pressure distribution profiles are presented to describe the flow processes.

In the final part of the thesis, the characteristics of combining flows past 90° junctions of a rectangular closed conduit are presented. Detailed pressure and velocity distribution data are obtained to understand the flow processes. Both the mean and fluctuating components of the velocity field are determined in the two flow sections immediately downstream of the junction. Simple empirical models are developed to determine the transfer of momentum and the contraction coefficient. Experimental data are used to verify the predicted results of the proposed models.

ACKNOWLEDGMENT

I wish to thank Dr. A. S. Ramamurthy for suggesting the research topic. The help provided by Dr. L. B. Carballada during the initial period of the study is thankfully acknowledged. Thanks are also due to Mr. N. Lang and the staff members of the machine shop of the faculty of Engineering and Computer Science.

TABLE OF CONTENTS

		PAGE
LIST OF NOTATIONS		x
LIST OF FIGURES		xv
LIST OF TABLES		xvii
Chapter 1	Introduction	1
1.1	General remarks	1
1.2	Literature review	2
1.2.1	Dividing flows	2
1.2.2	Combining Flows	8
1.2.3	Lateral weir flows	9
1.3	Scope of the present investigation	10
Chapter 2	Two Dimensional Slot in a Closed Rectangular Conduit	13
2.1	General remarks	13
2.2	Governing relations	13
2.3	Experimental set-up and procedures	15
2.4	Results	17
2.4.1	Profiles of axial and lateral velocities at various conduit locations (L/B=0.11)	17
2.4.2	Profiles of axial and lateral velocities at various conduit locations (L/B=1.0)	19

2.4.3 Verification of the free-streamline model of slot flow with experimental result {2-D conduit (channel) model} 20

2.4.4 Pressure distribution near the slot 21

2.4.5 Other remarks 21

2.5 Conclusions 22

Chapter 3 Rectangular Lateral Weirs in Circular Open Channels 23

3.1 General remarks 23

3.2 Governing relations 23

3.2.1 Two-dimensional conduit outlet model 24

3.2.2 Rectangular lateral weir in a circular channel 25

3.3 Experimental set-up and procedures 29

3.4 Analysis of results 30

3.4.1 Verification of the proposed mean discharge coefficient relationship 30

3.4.2 Comparison of the present model with a previous model (Uyumaz, 1985) 31

3.4.3 Variation of $\bar{C}_d$ with η_o^2 32

3.4.4 Variation of $\bar{C}_d$ with s/D, Y_1/D, $V_1^2/2gD$ and L/D 33

3.4.5 A typical example 33

3.5 Conclusions 35

Chapter 4	Dividing Rectangular Closed Conduit Flows	36
4.1	General remarks	36
4.2	Governing relations	37
4.2.1	Contraction coefficient for dividing flows in a branching rectangular conduit	37
4.2.2	Energy loss coefficient K_{12}	39
4.2.3	Energy loss coefficient K_{13}	40
4.3	Experimental set-up and procedures	41
4.4	Results	43
4.4.1	Energy loss coefficient K_{12}	43
4.4.2	Energy loss coefficient K_{13}	44
4.4.3	Flow pattern and contraction coefficient C_c	44
4.5	Conclusions	46
Chapter 5	Combining Flows at 90° Junctions of Rectangular Closed Conduits	48
5.1	General remarks	48
5.2	Governing relations	49
5.3	Experimental set-up and procedures	51
5.4	Results	53
5.4.1	Energy loss coefficients	53
5.4.2	Flow pattern	54
5.4.3	Turbulent characteristics	57

5.4.4 Power coefficient K_p 58

5.4.5 Expansion loss and contraction coefficient C_c 59

5.4.6 Momentum transfer and average entry angle δ 60

5.5 Conclusions 60

Chapter 6 Conclusions and Scope for Further Study 62

6.1 Validation of the theoretical solution for two-dimensional lateral conduit outlet 62

6.2 Rectangular lateral weir in a circular open channel 62

6.3 Dividing flows in rectangular closed conduits 63

6.4 Combining flows in rectangular closed conduits 63

6.5 Practical applications and benefits 64

6.6 Scope for further studies 64

Appendix 1 References 65

Appendix 2 Figures 71

Appendix 3 Tabulation of data 98

Appendix 4 Experimental uncertainties 158

Appendix 5 Specimen computations 160

LIST OF NOTATIONS

The following symbols are used in the thesis. Common notations are listed to begin with. This is followed by topic specific notations.

1) Common notations:

A_1 = cross-sectional area of flow at depth Y_1 in open channel or at upstream main in closed conduit;

$A_2 = A_1$ cross-sectional area of main conduit;

A_3 = area of slot outlet or branch conduit;

B = channel or main conduit width;

C = length of barrier (Fig.1.1);

C_d = discharge coefficient for free outlet of conduits and local discharge coefficient for lateral weirs;

C_c = contraction coefficient in main conduit downstream of junction for combining flow and in branch conduit for dividing flow (for dividing flow $C_c = C_d$);

$F()$ = a function in Eq.1.3;

g = acceleration due to gravity;

$G()$ = a function in Eq.1.3;

$H()$ = a function in Eq.1.4;

L = length of weir or width of slot or branch conduit;

Q_1 = discharge in upstream channel (main conduit);

Q_2 = discharge in downstream channel (main conduit);

Q_3 = lateral discharge;

R_e = Reynolds number;

V_1 = mean velocity in upstream section;

V_2 = mean velocity in downstream section;

V_3 = velocity in branch (for slot $V_3 = V_j$);

V_j = velocity of jet;

x, X = horizontal axial co-ordinate;

y, Y = vertical co-ordinate;

z, Z = horizontal lateral co-ordinate;

γ = specific weight of water;

η = velocity parameter.

2) For Lateral Slot Flow:

c_1, c_2, c_3 = coefficient for polynomial fit

u = mean axial velocity at measuring point

u_{max} = maximum mean point axial velocity in the test section

$\hat{u} = u/u_{max}$

v = mean lateral velocity at measuring points

v_{max} = maximum for the mean lateral velocity in the test section

$\hat{v} = v/v_{max}$

W = depth of the closed conduit

$\hat{x} = x/L$

$\hat{y} = y/B$

$\hat{z} = z/W$

3) For the Lateral Weir Flows:

A_w = projected area of the weir on the vertical plane through the channel axis;

B_1 = channel width at depth Y_1;

B_h = channel width at depth h;

$\bar{C}_d$ = mean discharge coefficient for lateral weirs;

c_0, c_1, c_2, c_3 = coefficient for polynomial fit;

D = diameter of circular pipes;

F_1 = Froude number of the approach flow;

dh = thickness of infinitesimal layer;

h = depth of layer (Fig.3.2);

h_0 = head over sill (=Y_1-s);

Q_M = measured discharge of weir;

Q_t = theoretical discharge of weir;

s = sill height of weir;

$\bar{V}_j$ = mean velocity of weir outflow;

Y_1 = depth of flow in the approach section;

η_0 = jet velocity parameter at $h = h_0$ (Eq.3.9).

4) For Rectangular Closed Dividing Conduit Flows:

K_{12} = energy loss coefficient between sections 1 and 2 (Fig.4.1);

K_{13} = energy loss coefficient between sections 1 and 3 (Fig.4.1);

p_c = pressure at "c" (Fig.4.1);

p_j = pressure at "j" (Fig.4.1);

$Q_r = (Q_3/Q_1)$ discharge ratio;

$\Delta p = p_1 - p_c \ (\approx p_1 - p_j)$.

5) For Combining Flows:

E_L = energy loss in the expansion section;

K_{12} = energy loss coefficient between sections 1 and 2 (Fig.5.1);

K_{32} = energy loss coefficient between sections 3 and 2 (Fig.5.1);

K_p = power loss coefficient for combining flow (Eq.5.6);

ΔM = momentum difference between M_1 and M_2;

N = number of subsections at the entry section "*eb*" of Fig.5.1;

P_d = pressure force on the downstream side wall of the branch;

P_u = pressure force on the upstream side wall of the branch;

$Q_r = (Q_3/Q_2)$ discharge ratio;

u' = turbulent intensity in the X direction;

U_{max} = maximum for the mean axial velocity at the section;

$-u'v'$ = turbulent shear stress term;

V_c = average flow velocity at the vena contracta;

v' = turbulent intensity in Y direction;

δ = average entry angle for branch flow (Fig.5.1).

LIST OF FIGURES

FIGURE		PAGE
1.1	Two-dimensional flow configurations	71
1.2	Lateral weir model	71
2.1	Two-dimensional slot test set-up	72
2.2	Detail of the slot Q-R	72
2.3	Conduit geometry	72
2.4a	Velocity profile and streamline pattern (L/B = 0.11, Q_3/Q_1 = 0.04)	73
2.4b	Velocity profile and streamline pattern (L/B = 0.11, Q_3/Q_1 = 0.10)	73
2.4c	Velocity profile and streamline pattern (L/B = 1.0, Q_3/Q_1 = 0.65)	74
2.4d	Velocity profile and streamline pattern (L/B = 0.11, Q_3/Q_1 = 0.33)	74
2.5	Variation of C_d versus η_{12}	75
2.6	Variation of C_d with Q_r	76
2.7	Typical pressure head distribution	77
3.1	Two-dimensional conduit outlet model	78
3.2	A rectangular lateral weir in a circular channel	78
3.3	Experimental set-up	78
3.4	Measured weir discharge Q_M vs theoretical discharge Q_t	79
3.5	Comparison of present model with Uyumaz's model (1985)	80
3.6	Variation of $\bar{C}_d$ *and* $\bar{C}_{dM}$ with η_o^2	81
4.1	Dividing rectangular conduit flow	82
4.2	Dividing rectangular conduit flow test set-up	82

4.3	Energy loss coefficient K_{12} for dividing closed conduit flow	83
4.4	Energy loss coefficient K_{13} for dividing closed conduit flow	84
4.5a	Flow field and pressure profiles for dividing conduit flow L/B = 1.0, $Q_3/Q_1 = 0.46$	85
4.5b	Flow field and pressure profiles for dividing conduit flow L/B = 0.77, $Q_3/Q_1 = 0.42$	86
4.5c	Flow field and pressure profiles for dividing conduit flow L/B = 0.77, $Q_3/Q_1 = 0.57$	87
4.5d	Flow field and pressure profiles for dividing conduit flow L/B = 0.22, $Q_3/Q_1 = 0.30$	88
4.6	Dividing streamline pattern	89
5.1	Combining rectangular conduit flow junction	90
5.2	Combining rectangular conduit flow test set-up	90
5.3a	Combining conduit flow K_{12} vs Q_3/Q_2	91
5.3b	Combining conduit flow K_{32} vs Q_3/Q_2	92
5.4	Flow pattern and pressure profiles in combining conduit flows L/B = 1.0	93
5.5	Flow pattern and pressure profiles in combining conduit flows L/B = 0.77	94
5.6	Flow pattern and pressure profiles in combining conduit flows L/B = 0.22	95
5.7	Turbulent intensity and shear in the main conduit of rectangular combining flows, L/B = 1.0, $Q_3/Q_2 = 0.49$	96
5.8	Turbulent intensity and shear in the main conduit of rectangular combining flows, L/B = 0.22, $Q_3/Q_2 = 0.50$	97

LIST OF TABLES

TABLE		PAGE
2.1	Experimental data of two-dimensional slot flow $L/B = 1.0$	98
2.2	Experimental data of two-dimensional slot flow $L/B = 0.78$	100
2.3	Experimental data of two-dimensional slot flow $L/B = 0.11$	102
3.1	Range of geometric variables: Lateral weirs in circular channels	104
3.2	Experimental data of rectangular side weirs in a circular channel D = 30 cm, L = 30 cm, s = 3.81 cm	105
3.3	Experimental data of rectangular side weirs in a circular channel D = 30 cm, L = 22.5 cm, s = 3.81 cm	106
3.4	Experimental data of rectangular side weirs in a circular channel D = 30 cm, L = 15 cm, s = 3.81 cm	107
3.5	Experimental data of rectangular side weirs in a circular channel D = 30 cm, L = 30 cm, s = 8.46 cm	108
3.6	Experimental data of rectangular side weirs in a circular channel D = 30 cm, L = 22.5 cm, s = 8.46 cm	109
3.7	Experimental data of rectangular side weirs in a circular channel D = 30 cm, L = 15 cm, s = 8.46 cm	110
3.8	Experimental data of rectangular side weirs in a circular channel D = 30 cm, L = 30 cm, s = 13.75 cm	111
3.9	Experimental data of rectangular side weirs in a circular channel D = 30 cm, L = 22.5 cm, s = 13.75 cm	112

3.10 Experimental data of rectangular side weirs in a circular channel
D = 30 cm, L = 15 cm, s = 13.75 cm 113

4.1 Experimental data of dividing closed conduit flows L/B = 1.0 114

4.2 Experimental data of dividing closed conduit flows L/B = 0.77 123

4.3 Experimental data of dividing closed conduit flows L/B = 0.22 132

4.4 The contraction coefficient C_c 138

5.1 Experimental data of combining closed conduit flows L/B = 1.0 139

5.2 Experimental data of combining closed conduit flows L/B = 0.77 145

5.3 Experimental data of combining closed conduit flows L/B = 0.22 151

5.4 Contraction coefficient for combining flows 157

5.5 Average entry angle "δ" for momentum transfer 157

CHAPTER 1

INTRODUCTION

1.1 General remarks

Dividing and combining flows are encountered in the design of open channels and closed conduit engineering systems, such as water and wastewater treatment plants, water distribution networks, irrigation systems, heating, ventilating, and air conditioning systems, automobile engine systems and even electrical machine cooling systems. There are many variables which influence the system performance. For example, the shape of the conduits and orifices can alter the flow characteristics. The area ratio and discharge ratio of the branches, the conditions at the inlet and outlet, and the nature of the conveying system (open channel or closed conduit) can alter the characteristics of dividing and combining flows. To understand the characteristics of a lateral flow system, it is essential to study the behavior of flow past outlets of the simplest form to begin with. Lateral flows commonly encountered in practice can occur in several ways. Fig.1.1 shows some typical lateral flow configurations. There are a great number of studies dealing with lateral flows related to combining and dividing flow problems. Crow and Wharton (1968), Ward-Smith (1980) and Miller (1990) have provided very good reviews of previous studies on these topics. In this chapter, some of the pervious studies related to combining and dividing flow problems are reviewed and discussed. Based on this discussion, the scope of the current study is presented.

1.2 Literature review

1.2.1 Dividing flows

Theoretically, the hydrodynamic model or momentum equation has been used to solve the problem of dividing flows and combining flows. Michell (1890) was the first to use the free-streamline theory to solve problems related to dividing flows (Fig.1.1a). For the problem of flow past a slot in two-dimensional conduits, he gave the solution between the jet angle θ and the parameters involving the flow velocities at the upstream and downstream sections of the slot. For the specific case in which the downstream velocity $V_2 = 0$, von Mises (1917) found the dependence of the contraction coefficient C_c and the jet angle θ (Fig.1.1a) on the relative size of the opening L/B. McNown and Hsu (1951) extended the earlier studies on lateral flows and determined the dependence of the discharge coefficient C_d and jet angle θ on the velocity ratio V_2/V_1. Here, V_1 denotes the upstream velocity in the main. It may be noted that in this case, $C_d = C_c$ (contraction coefficient). In Fig.1.1a (McNown and Hsu 1951),

$$\theta = \cos^{-1}\frac{V_1 + V_2}{2V_j} \qquad (1.1)$$

$$(V_1 - V_2)B = C_d L V_j \qquad (1.2)$$

$$L/B = F(\frac{V_1}{V_j}) - F(\frac{V_2}{V_j}) - \frac{V_1 - V_2}{V_j}G(\theta) \qquad (1.3)$$

in which,

$$F(\frac{V}{V_j}) = \frac{2}{\pi}(1 + \frac{V^2}{V_j^2})\tanh^{-1}\frac{V}{V_j}$$

and

$$G(\theta) = \frac{2}{\pi}\cos\theta \ln(\cot\frac{\theta}{2}) - \sin\theta$$

For the dividing flow past a slot fitted with an external barrier (Fig.1.1b), McNown and Hsu (1951) found the effect of the barrier on the various parameters. To this end, they used the above equations and replaced Eq. 1.1 by the following relation (Eq.1.4).

$$C/B = H(\frac{V_2}{V_j}) - H(\frac{V_1}{V_j}) + \frac{V_1 - V_2}{V_j}G(\frac{\pi}{2} - \theta) \qquad (1.4)$$

in which,

$$H(\frac{V}{V_j}) = \frac{2}{\pi}(1 - \frac{V^2}{V_j^2})\tan^{-1}\frac{V}{V_j}$$

Ramamurthy and Carballada (1979) used free streamline theory and numerical methods to solve the problem of flow past lateral outlets fitted with barriers that were set at arbitrary angles. Tsakonas (1957) studied the flow through lateral outlets located in open channels whose walls were not parallel. He concluded that the presence of very non-uniform velocity profiles in the section upstream of the lateral outlet lead to test data which do not agree with results of the free streamline theory. Gurevitch (1966) has reported that experimental data fail to confirm the predictions of the free streamline model when the jet

air flows into ambient air. He pointed out that for experimental verification, the fluid in the conduit should be denser than the fluid outside.

Earlier efforts to experimentally verify the predictions of existing two-dimensional theoretical hydrodynamic models for flow past a two-dimensional slot in a rectangular conduit were not successful (Ramamurthy et al. 1994). Verification of the theory was limited to flow past circular orifices in circular pipes (Barton 1946, McNown 1954, and Rawn 1960). Although the theoretical results were found to hold good for flow of real fluids in circular conduits, it is hardly a proper verification of the two-dimensional theoretical model, since dividing and combining flows in circular pipes are three-dimensional.

Several different methods were proposed to solve the dividing flow problem. By balancing the flow momentum at sections of the main which are upstream and downstream of the junction, Bajura (1971) proposed a parameter termed as "pressure regain coefficient" γ_{d} which accounts for the uncertainty in the axial momentum transferred from the main conduit to the branch in dividing flows. Hager (1984) proposed a simple hydraulic model to evaluate the energy losses assuming a linear pressure drop along the dividing streamline (Fig.1.1c). Based on Hager's study (1984), Tran (1988) and Perinpanathan (1992) assumed the pressure variation along the dividing streamline to be respectively parabolic and nth-order polynomial. These assumptions were validated using test data. Williamson and Rhone (1973) also proposed the expressions for the energy loss coefficients by using

Bernoulli's equation. However, Ward-Smith (1980) stated that their expressions are poorly represented .

In the past, a large number of experimental studies have provided various energy loss coefficient data for dividing flow past a branching closed circular conduit (Fig.1.1c). The first comprehensive experimental investigation in this context was carried out at the Hydraulic Institute of the Munich Technical University from 1928 to 1931 (Vogel 1929, Thoma 1929, Petermann 1929, and Kinne 1931). Later, at the Iowa Institute of Hydraulic Research, McNown (1954) reported a series of experimental results related to dividing flows. At Lausanne, Gardel (1957) carried out another set of experiments. The parameter range was similar to that of the Munich tests.

Vogel (1929) reported a series of experiments on pipes with right angled branches. In these experiments, the pipe diameters ranged from 15 to 43 mm and the Reynolds number Re varied from 5×10^3 to 1×10^5. He concluded that for a given branch configuration, the loss coefficients were functions of the discharge ratio, but was independent of the Reynolds number. Thoma (1929) extended the tests to cases of branches set at angles of 45° and 60° to the main. Petermann (1929) and Kinne (1931) repeated the studies of Vogel and Thoma with a redesigned apparatus and a more accurate measuring equipment.

The Iowa tests (McNown 1954) were performed in a 2 in. (51 mm) diameter main made of brass pipes and 2 in. (51 mm), 1 in. (25 mm), and 1/2 in. (13 mm) branch pipes with 90°

sharp edged junctions. The comparison of the results of the Iowa and Munich tests show that the energy loss coefficients from the main to branch are close only for a branch having a diameter equal to that of the main. When the branch diameter was less than the diameter of the main, the Munich tests gave considerably larger loss coefficients than those reported in the Iowa tests.

Gardel (1957) conducted a series of experiments at the University of Lausanne. The main pipe was 150 mm and branches varied from 150 mm to 60 mm. The maximum Reynolds number was about 4×10^5. When the energy loss coefficient K_{13} from the main to branch is compared with Munich data, the data agreed only for the specific case in which the branch and main had the same diameter. The values of the energy loss from the main to branch for the other Munich tests were significantly greater than those reported by Gardel.

Escobar (McNown, 1954) performed experiments in which the region of lateral flow from the main circular conduit was visualized by observing streams of fine air bubbles or dye injected into the flow upstream of the slot. Using the velocity distribution described by the von Karman equation (logarithmic distribution of velocity), he tried to account for the deviations of previous experimental data and the theoretical predictions for small discharge ratios. Fu et al. (1991) used a numerical model to analyze the three-dimensional flow past a rectangular branch conduit fitted to a rectangular conduit and verified the predictions using laser Doppler velocimetry (LDV) test data. In a very limited range of discharge ratios, for flow past a branching square conduit, Miller (1971) has obtained the

experimental energy loss coefficients. He asserts that the data of branching circular conduits are directly applicable to branching non-circular conduits. Popp and Sallet (1983) used LDV to obtain the velocity field data for dividing flow past a rectangular tee junction for which the ratio $L/B = 1$ (Fig.1.1c). Unfortunately, in their tests, fully developed turbulent velocity profiles were not attained in the approach section.

Based on experimental data, several empirical formulas have been proposed to relate the loss coefficient K_{12} and K_{13} with the discharge ratio Q_r. Here, K_{13} denotes the energy loss coefficient from the main to the branch, and K_{12} is the energy loss coefficient related to the flow in the main. Based on his test data, Gardel (1957) obtained the following empirical equations for dividing flows.

$$K_{12} = 0.03(1-Q_r)^2 + 0.35Q_r^2 - 0.2Q_r(1-Q_r) \qquad (1.5)$$

$$K_{13} = 0.95(1-Q_r)^2 + 0.4Q_r(1-Q_r)\left(\frac{1+A_3/A_1}{A_3/A_1}\right)\tan\frac{\phi}{2} + Q_r^2\left\{\left(1.3\tan\frac{\phi}{2} - 0.3 + \frac{0.4-0.1(A_3/A_1)}{(A_3/A_1)^2}\right)\left(1-0.9\left(\frac{r}{A_3/A_1}\right)^{0.5}\right)\right\} \qquad (1.6)$$

Here, A_1 and A_3 are cross sectional areas of the main and the branch, and ϕ is the angle between the branch and the main. Lastly, r is the ratio of radius of the branch corner fillet to the diameter of the main.

Ito and Imai (1973) used all the experimental results available to them and fitted the empirical relations for the loss coefficients of 90° sharp-edged branches with $A_3 / A_1 = 1$.

$$K_{12} = 1.55(0.22 - Q_r)^2 - 0.03 \qquad 0 \le Q_r \le 0.22 \qquad (1.7)$$

$$K_{12} = 0.65(Q_r - 0.22)^2 - 0.03 \qquad 0.22 \le Q_r \le 1 \qquad (1.7a)$$

$$K_{13} = 0.99 - 0.82Q_r + 1.02Q_r^2 \qquad 0 \le Q_r \le 1 \qquad (1.8)$$

1.2.2 Combining Flows

Modi, et al. (1981) presented an analytical solution for two-dimensional combining flows (Fig.1d) using conformal transformation techniques. Best and Reid (1984) found that the theoretical predictions (Modi, et al. 1981) overestimate the width of the separation zone. Blaisdell and Manson (1967) derived a theoretical relation for the loss in the combining flows, which was criticized to be based on unsound reasoning (Ward-Smith 1980). Bajura (1971) proposed a "pressure regain coefficient" γ_c which accounts for the uncertainty in the axial momentum transferred from the branch to the main conduit in combining flows.

Vogel (1929), McNown (1954), Gardel (1957), Miller (1971), Ito and Imai (1973) and recently Serre et al. (1994) performed experimental studies on combining flows in closed conduits. Except for Miller who used a square conduit, all the others obtained test data for circular pipes.

On the basis of the experimental data, Gardel (1957) provided the following empirical equations.

$$K_{32} = -0.92(1-Q_r)^2 + (2-A_3/A_2)(1-Q_r)Q_r$$
$$-Q_r^2\{(1.2-r^{0.5})(\frac{\cos(\pi-\phi)}{A_3/A_2}-1)+0.8[1-(A_2/A_3)^2]-(A_2/A_3-1)\cos(\pi-\phi)\} \quad (1.9)$$

$$K_{12} = 0.03(1-Q_r)^2 + (2-A_3/A_2)(1-Q_r)Q_r$$
$$-Q_r^2\{1+(1.62-r^{0.5})[\frac{\cos(\pi-\phi)}{A_3/A_2}-1]-0.38(1-A_3/A_2)\} \quad (1.10)$$

For 90^0 sharp-edged junction with $A_3 / A_2 = 1$, Ito and Imai (1973) suggested the relations

$$K_{32} = 1.09 - 0.53(1-Q_r) - 1.48(1-Q_r)^2 \quad (1.11)$$

$$K_{12} = 0.045 + 1.38Q_r - 0.90Q_r^2 \quad (1.12)$$

Since most of the existing test results are restricted to pressure loss data only, information related to the flow processes associated with combining closed conduit flows is scarce (Ward-Smith, 1980). Only Serre et al. (1994) provide some insight into the flow features of combining flows in the range $A_3/A_2 \leq 0.2$ on the basis of visual observations of the branch flow entering the main.

1.2.3 Lateral weir flows

Since lateral weir flows have very practical applications in irrigation and draining systems as well as in the design of equipment for water and wastewater treatment plants, they have been studied extensively in rectangular (Nimmo 1928; De Marchi 1934; Collinge

1957; Rajaratnam, 1967; Subramanya and Awasthy, 1972; and Hager, 1987a), trapezoidal (El-Khashab and Smith 1976), circular (Allen 1957, Uyumaz and Muslu, 1985) and "*U*" shaped (Volkart 1983) open channels. Hager (1987b) provided a critical analysis of the study on lateral weirs in circular channels by Uyumaz and Muslu (1985) and presented an interesting empirical solution to the lateral weir flow problem. Ramamurthy and Carballada (1980) applied the free streamline model of McNown (1951) to solve the rectangular lateral weir flow problem. The model related the characteristics of flow through rectangular lateral weirs located in the side of rectangular channels. In this model, the weir outflow was considered as the sum of the efflux through a large number of infinitesimal horizontal layers. The infinitesimal layers (Fig.1.2) were viewed as two-dimensional lateral flow elements (Fig.1.1a) which possessed a lateral outlet. The mean discharge coefficient of the weir was determined with the velocity parameter and the ratio *L/B*. Later, similar procedures were used to solve the lateral weir flow problem in trapezoidal channels (Ramamurthy et al. 1986).

1.3 Scope of the present investigation

Because of the complex nature of analyzing the lateral flow problem, it is almost impossible at present to provide general solutions with the available information. Free streamline theory offers analytical solutions to some selected cases of flow distribution in closed two-dimensional conduits. For dividing and combining closed conduit flows (Fig.1.1c and d), no theoretical solution is available at the present time. The present

study is initiated to use the result of two-dimensional free streamline theory to obtain solutions to problems dealing with some selected engineering applications of dividing and combining flows. Specifically, the following aspects of dividing and combining flows are studied and reported in the present thesis:

1. **Rectangular lateral slot in a rectangular conduit:** The characteristics of flow past a rectangular slot located in the wall of a rectangular conduit (Fig.1.1a) are studied experimentally and the results are used to verify an existing free streamline slot flow model. Detailed velocity and pressure measurements will be obtained to understand the flow processes that are involved.

2. **Rectangular weir in a circular open channel:** A theoretical expression for the discharge coefficient of a rectangular lateral weir located in the side of a circular open channel (Fig.1.2) will be obtained using the above lateral slot flow model as the basis. Test data obtained will be used to verify the dependence of the weir discharge coefficient on the velocity parameter η ($=V_1/V_j$), the geometric parameter L/B, and the sill parameter s/Y_1. Here, s is the weir sill height and Y_1 is the depth of flow in the approach channel.

3. **Dividing flow in rectangular conduit:** The contraction coefficient for the branch flow and the energy loss coefficient K_{13} will be determined as functions of L/B and Q_3/Q_1 for dividing flows in rectangular conduits (Fig.1.1c). The results will be verified using test data.

4. **Combining flow in rectangular closed conduit junction:** For rectangular closed conduit junctions (Fig.1.1d), the energy loss and power loss coefficient will be determined as a function of Q_3/Q_2 and L/B. The experimentally determined values of the parameters such as the mean entry angle δ of the branch flow as it enters the main and the contraction coefficient C_c of the combining flow will be compared with the predictions of empirical models. Test data related to the flow characteristics of a rectangular conduit junction will be compared with the flow characteristics of circular conduit junctions to assess the similarity and dissimilarity of the flow processes in the two systems.

In summary, in the following chapters, the characteristics of flow past the following configurations which are studied will be reported:

1). Dividing flow past a lateral outlet (Chapter 2),

2). Dividing flow past a rectangular weir in a circular channel (Chapter 3),

3). Dividing flow past a rectangular closed conduit branch (Chapter 4), and

4). Combining flow at a rectangular conduit junction (Chapter 5).

CHAPTER 2

TWO DIMENSIONAL SLOT IN A CLOSED RECTANGULAR CONDUIT

2.1 General remarks

The flow past a two-dimensional lateral slot of width L (Fig.2.2) located in the wall of a closed rectangular conduit of width B finds applications in the design of equipment used for distributing flow in water and wastewater treatment plants and drainage systems (Benefield et al. 1984, Gill 1987). In this thesis, the characteristics of a two-dimensional lateral slot located in the wall of a rectangular closed conduit is studied. Specifically, the theoretical dependence of the discharge coefficient C_d for the slot on the velocity parameter $\eta_1^2 = V_1^2/(2gE_1)$ and the slot geometric parameter L/B is verified using test data. Here, g and E_1 denote respectively the gravitational acceleration and the total energy of the flow upstream of the slot reckoned with respect to the horizontal jet exit plane (QR Fig.2.1). Experimental data related to typical velocity distributions in the conduit at sections upstream and downstream of the slot are also presented to explain the processes associated with the slot flow.

2.2 Governing relations

Figs.2.2 and 2.3 show the lateral flow through a two dimensional rectangular slot located at the side of a rectangular conduit. For this flow configuration, the characteristics of flow

have been theoretically determined on the basis of a free streamline flow model (McNown and Hsu, 1951). Using the results of this model, the dependence of the slot discharge coefficient C_d on the parameters $\eta_l^2 = V_l^2/(2gE_l)$ and L/B can be obtained (Ramamurthy and Carballada, 1980). Here, C_d relates the slot discharge Q_3, the slot area A and the velocity $V_j = \sqrt{2gE_l}$ of the jet emerging from the slot. Thus,

$$Q_3 = C_d A \sqrt{2gE_l} \tag{2.1}$$

Further,

$$C_d = f_l(\eta_l^2, L/B) \tag{2.2a}$$

here, f_1 denotes a function. For the range $\eta_{min} < \eta_1 \leq 1$ and $0 < L/B \leq 1$, the following relations are valid (Ramamurthy and Carballada, 1980):

$$C_d = 0.61 + c_1\eta^2 + c_2\eta^4 + c_3\eta^6 \tag{2.2b}$$

in which,

$$c_1 = -0.54 + 0.25(L/B)$$
$$c_2 = 0.058 + 0.234(L/B)$$
$$c_3 = -0.13 - 0.49(L/B)$$

Here, η_{min} = minimum value of η_1 attainable for a given L/B. An alternate way of presenting the results is to express C_d in terms of the discharge ratio Q_r denoting the ratio

of the lateral outflow Q_3 to the total approach flow Q_1 (Fig.2.3). Thus, for a different function f_2,

$$C_d = f_2(Q_r, L/B) \tag{2.3}$$

here, $Q_r = \frac{Q_3}{Q_1} = C_d \eta^{-1} L/B$.

2.3 Experimental set-up and procedures

Fig.2.1 shows the equipment used for the tests on lateral slots. The closed rectangular Plexiglas conduit was 41.3 mm x 91.5 mm in cross section. It was nearly 4 m long upstream of the slot to provide fully developed flow in the approach section. A constant head supply tank ensured steady flow. The downstream slot edge was sharp and was beveled to a very small angle (Fig.2.2) to let the jet emerge freely from the slot. The slot was oriented horizontally and the outflow through the slot was confined to the conduit depth W by the extended side plates (Fig.2.3). These ensured that the two-dimensional infinitesimal layers forming the jet flow would lie in vertical planes and remain parallel to each other as they emerge from the slot. For the fixed value of B = 91.5 mm, the geometry of the slot system used yielded L/B = 0.11, 0.78, and 1.0. A large number of 1 mm wall pressure taps spaced closely near the entry and exit sections of the slot enabled detailed mapping of the pressure field in the vicinity of the slot. The water manometer connected to the taps could be read to the nearest millimeter. Q_3 and Q_2 (Fig.2.1) were measured with the help of standard V notches. The maximum error in the discharge measurement was estimated to be 3%.

The measured pressure head profile in the approach section upstream of the slot which was unaffected by the presence of the slot was extrapolated to the center of the slot (FG in Fig.2.7) to determine p_l/γ. This pressure head was used to find the upstream total energy $E_l = p_l/\gamma + V_l^2/2g$. Typical pressure head profiles are presented in a subsequent section. A venturi meter in the pipe system provided a check on the total flow Q_t passing through the system.

A Dantec two-dimensional LDV unit equipped with a two-dimensional fiber-optic probe was used to obtain the velocity surveys. The laser power was 300 mw. Its measuring volume was 0.078 mm wide and 0.66 mm long. The light scattered in the measuring volume was collected by photo multipliers and processed to get the flow velocity. The maximum error in the velocity measurement was estimated to be 1%. The fiber-optic probe was positioned with the help of an automated traverse which could move in the x, y and z directions (Fig.2.3) and provide a resolution of 0.0025 mm.

While using the LDV measurement, 1000 samples were used to calculate a single mean velocity. The maximum Reynolds number in the all the tests was 1.744×10^5. In Fig. 2.5, the few dark circles shown denote the data related to tests in which the velocity profiles were also obtained. Fig.2.5 will be described in a subsequent section.

The maximum axial velocity u_{max} in the approach section was used to normalize axial velocities and the maximum lateral velocity v_{max} in the region PS of Fig.2.1 was used to

normalized the lateral velocities. In Fig.2.4, the x, y, and z locations were normalized by L, B, and W respectively. Thus, $\hat{x} = x/L$; $\hat{y} = y/B$; $\hat{z} = z/W$; $\hat{u} = u/u_{max}$; *and* $\hat{v} = v/v_{max}$. The velocity profiles shown in Fig.2.4 were obtained at the centerline of the channel ($\hat{z} = 0.5$) except for the profiles obtained at the upstream edge of the slot in Fig.2.4c ($\hat{x} = 0.0$). Here, velocities were measured at $\hat{z} = 0.35,\ 0.5$ *and* 0.65.

2.4 Results

The test data obtained in the two-dimensional slot model are used to verify the predictions according to the proposed model (Eq. 2.2). The measured pressure heads and other results of the tests are summarized in tables 2.1, 2.2 and 2.3. The temperature of water was 20°C. Typical axial and lateral velocity distributions at different sections along the conduit length were obtained to describe the flow characteristics. To this end, in Fig.2.4, the velocity survey data are plotted for the slot length ratios which were the largest (*L/B=1.0*) and the smallest (*L/B=0.11*). For each slot, two typical discharge ratios Q_3/Q_1 were selected to obtain the velocity profiles.

2.4.1 Profiles of axial and lateral velocities at various conduit locations (L/B=0.11)

When the discharge ratio Q_r is small (Q_r=*0.04*) and the slot width ratio L/B is also small, the profiles of the axial velocity *u=u(y)* at i) the approach section *(x/L<0)*, ii) the downstream section *(x/L>1)* and iii) in the vicinity of the slot *(0.0<x/L<1.0)* are very

similar (Fig.2.4a). However, since the flow has to turn to emerge as a jet through the slot, the vertical velocity component $v=v(y)$ increases in the vicinity of the slot ($x/L \approx 0$ to $x/L \approx 1$) and vanishes at a section downstream of the slot (x/L=5.77). Q_r was too small to permit one to trace the changes in the streamline patterns that were originally parallel when no slot was present. Hence, the streamline pattern in the presence of the slot is not shown in Fig.2.4a.

When Q_r was increased to 0.10, for the same slot width ratio of $L/B=0.11$, the flow close to the conduit wall in which the slot was located experiences considerable acceleration in the axial direction, in the region just upstream of the slot. Also, the flow at a section x/L=0.96 which is just upstream of the end of the slot ($x/L=1.0$) indicates that the axial velocity component u registers a local flow reversal. At this location, the vertical velocity component v is quite large (Fig.2.4b). The velocity distributions $u=u(y)$ in the conduit were used to obtain the streamline pattern (Fig.2.4b) for the $L/B=0.11$ and $Q_r=0.10$. The dashed line of the sketch shows the dividing streamline for the slot flow pattern. The dividing streamline reaches the conduit wall at right angles (not shown). One branch of this dividing streamline forms the boundary of the emerging jet flow Q_3 and the other branch forms part of the flow Q_2 in the downstream section of the main.

2.4.2 Profiles of axial and lateral velocities at various conduit locations (L/B=1.0)

Figs.2.4c and 2.4d show the velocity profiles and streamline patterns for the largest slot width *(L/B=1.0)* and two discharge ratios. In Fig.2.4c, both Q_r and L/B are large (Q_r=*0.65*, *L/B=1.0*), and hence one can notice the reversal of flow occurring at the conduit wall opposite to the slot at $x/L \approx 0.71$. The reversal of flow can also be seen on the conduit wall containing the slot at a location just downstream of the slot ($x/L \approx 1.02$). The streamline patterns for the slot flow are shown in Fig.2.4c. Fig.2.4c includes the velocity profile $\hat{u}(y)$ taken at a location across the span of the conduit (x/L=0.0, z/W=0.35, 0.5, and 0.65). These velocity distributions indicate that the flow was essentially two-dimensional.

Popp and Sallet (1983), who conducted the study of flow past a two-dimensional outlet to which a two-dimensional branch conduit was attached, state that for L/B=1.0, flow separation on the conduit wall, which was opposite to the branch conduit, occurred only at a much higher Q_r value (Q_r=*0.81*). In the present tests dealing with flow past a two-dimensional lateral slot, for *L/B=1*, flow separation was noticed on the conduit wall opposite to the slot at Q_r=*0.65*.

Fig.2.4d shows the velocity distribution and streamline pattern for Q_r=*0.33*, *L/B=1.0*. Here, Q_r is very small and hence the flow does not separate at the wall opposite to the slot.

2.4.3 Verification of the free-streamline model of slot flow with experimental result {2-D conduit (channel) model}:

Figs.2.5 and 2.6 show the variation of the slot discharge coefficient C_d with the velocity parameter η_1^2 and the discharge ratio Q_r for three slot length ratios L/B. The theoretical variations of C_d with η_1^2 at fixed values of L/B, given by Eq.2.2, are denoted by the solid lines in the Fig.2.5, for L/B=0.11, 0.78 and 1.0. The insert of Fig.2.5c gives the group of all the three different solutions in a single sketch. As indicated, the minimum values of η_1^2 which can be achieved increase with an increase in the value of L/B. This is similar to the existence of a minimum approach Froude number that can be achieved in a rectangular open channel fitted with a rectangular branch channel at right angles to the main channel (Ramamurthy 1988).

Fig.2.6 provides an alternate method for the verification of the theory with the present experimental data. The solid line of Fig.2.6 denotes the relationship given by Eq.(2.3). For all the L/B values tested, the present experimental data provided a good verification of the free-streamline model. It must be noted that Eqs. 2.2 and 2.3 are directly derived from the existing free-streamline theory.

2.4.4 Pressure distribution near the slot:

Fig.2.7 shows a typical pressure distribution for $Q_r=0.10$ and $x/L=0.11$. As stated earlier, the large accelerations experienced by the flow in the axial direction near the entrance to the slot cause a large pressure gradient in the section AB of the insert of Fig.2.7. The point C in the insert of Fig.2.7 is close to the stagnation point and the flow quickly tends to revert back to fully developed conduit flow and a velocity profile for which the v component is nearly zero (location D at x/L=5.77 in Fig.2.7 insert).

2.4.5 Other remarks:

As stated earlier, to verify the theoretical two-dimensional free-streamline slot flow model, the available test data are restricted to the flow through circular orifices in circular pipes (McNown 1954). Alternative solutions to the problem of slot flow proposed by Gill (1987) need experimental values of the slot discharge coefficient C_d to find the slot discharge. Toch (1953) solved the general free-streamline model of manifold efflux. He was able to verify his results only with the experimental data of a three-dimensional flow through circular orifices located in the wall of circular pipes. He noted: "... although this agreement is heartening, it must be viewed as fortuitous. The attempt at experimentally verifying the model (2-D) ... was completely unsuccessful."

In the tests, the Reynolds number of the flow was quite large and hence the flow characteristics did not depend on it. The Reynolds number is not explicitly included in the formulation of Eqs. 2.2 and 2.3. It may be noted that the slopes denoting the pressure gradient in the upstream conduit section (FG in Fig.2.7) depends on the Reynolds number of the flow, for flows which are not fully turbulent. A specimen computation related to lateral slot flow is given in Appendix 5 (pp. 160).

2.5 Conclusions

The solution to the problem of the two-dimensional efflux through a rectangular slot located in a two-dimensional wide rectangular closed conduit was solved earlier on the basis of the free-streamline theory. However, in the past, its verification was obtained only through experimental data pertaining to flow through circular orifices located in the wall of circular pipes. Eqs.2.2 and 2.3 are derived directly from the results of free-streamline theory solution to two-dimensional slot flows. The present experimental data provide a direct verification of the theoretical solutions of the two-dimensional slot flow. The agreement between the theoretical predictions and test data is quite good for the dependence of C_d on the slot flow parameters $\eta_1 = V_1/\sqrt{2gE_1}$ and $Q_r = Q_3 / Q_1$ (Eqs.2.2 and 2.3). The results find applications in treatment plant hydraulics for environmental engineers dealing with dividing flows.

CHAPTER 3
RECTANGULAR LATERAL WEIRS IN CIRCULAR OPEN CHANNELS

3.1 General remarks

The hydrodynamic characteristics of flow through lateral slots(outlets) of two-dimensional channels (Fig.3.1) have been determined theoretically by Michell (1890), McNown and Hsu (1951) and Gurevitch (1966). A model related to the characteristics of flow through rectangular weirs located in the side of rectangular channels has been reported by Ramamurthy and Carballada (1980). In that model, the weir outflow was considered as the sum of the efflux through a large number of infinitesimal horizontal layers of flow. These layers were viewed as two-dimensional channel flow elements having lateral outlets.

Lateral weirs are used in irrigation and drainage systems to divert part of the flow in open channels. They are also commonly used to bypass excess storm water flow in wastewater treatment plants (Benefield et al. 1984). In this chapter, a theoretical expression for the discharge through a rectangular lateral weir located in a circular open channel (Fig. 3.2) is developed and this expression is verified on the basis of experimental data.

3.2 Governing Relations

The development of the governing relations describing the characteristics of flow through a rectangular weir located in the side of a circular open channel is very similar to an earlier

development of the relations for the flow through a rectangular lateral weir located in a rectangular open channel (Ramamurthy and Carballada, 1980).

3.2.1 Two-dimensional conduit outlet model

For a rectangular lateral outlet of length L set in a two-dimensional conduit of width B (Fig.3.1), following McNown and Hsu (1951), the discharge coefficient C_d can be defined as,

$$C_d = \frac{jet\ discharge\ per\ unit\ depth\ of\ conduit}{LV_j} \tag{3.1}$$

where, C_d is a function of the geometric parameter L/B (Fig.3.1) and the velocity parameter η (Ramamurthy and Carballada, 1980) which can be defined as:

$$\eta = \frac{V_l}{V_j} \tag{3.2}$$

In the above expressions, V_l is the axial flow velocity in the approach section and V_j is the velocity of the jet emerging from the outlet. In other words, the results of McNown and Hsu (1951) link the theoretical discharge coefficient C_d with η and L/B. *i.e.*

$$C_d = C_d(\eta, L/B) \tag{3.3}$$

The above relationship between C_d, η and L/B which is implicit can be approximated by an explicit cubic expression in η^2 for the range $0 < L/B \leq 1.0$ and $0 < \eta \leq 1.0$ (Ramamurthy and Carballada, 1980). The ranges of the variables L/B and η covered in the present experimental study are $0 < L/B \leq 1.5$ and $0 < \eta \leq 1.0$. Hence, the following explicit relation between C_d, L/B and η was obtained for these ranges of L/B and η.

$$C_d = c_0 + c_1\eta^2 + c_2\eta^4 + c_3\eta^6 \qquad (3.4)$$

in which,

$$c_0 = 0.618 - 0.020(L/B) + 0.009(L/B)^2$$

$$c_1 = -0.528 + 0.595(L/B) + 0.028(L/B)^2 - 0.248(L/B)^3$$

$$c_2 = -0.029 - 1.001(L/B) + 0.700(L/B)^2 + 0.241(L/B)^3$$

$$c_3 = -0.058 + 0.420(L/B) - 0.712(L/B)^2$$

Equation (3.4) is an explicit cubic in η^2 and is adopted easily for the development of the following model for a rectangular lateral weir in a circular open channel.

3.2.2 Rectangular lateral weir in a circular open channel

The existing theoretical two-dimensional lateral conduit outlet model is adopted to develop an expression for the discharge through a rectangular lateral weir of length L

located on one side of a circular open channel of diameter D (Fig. 3.2). The following assumptions are made to develop the weir discharge relation.

(i) The bed of the channel and the free surface of water are horizontal.

(ii) The axial velocity component of the jet emerging from the lateral weir is V_l = velocity of the approach flow. The lateral velocity component of the jet emerging from the outlet of the infinitesimal flow element of thickness dh (Fig. 3.2) is equal to $\sqrt{2gh}$. Here, h is the depth of the layer below the free surface.

(iii) The velocity coefficient $\alpha = 1.0$ at the approach section.

The total outflow through the rectangular lateral weir is obtained by adding the flow through the large number of infinitesimal two-dimensional parallel rectangular flow elements (Fig. 3.2) that give rise to the emerging jet. These flow elements are assumed to represent two-dimensional conduits of infinitesimal thickness which have lateral outlets. For any such flow element, the axial velocity component V_l and the lateral velocity component $\sqrt{2gh}$ can be added vectorially (Subramanya and Awasthy, 1970) to obtain the jet velocity V_j (Fig. 3.1):

$$V_j = \sqrt{2gh + V_l^2} \tag{3.5}$$

For the weir outflow through the flow elements outlet area Ldh, the local weir outlet discharge coefficient C_d is a function of L/B_h (Fig. 3.2) and the velocity parameter $\eta = V_l/V_j$ (Eq. 3.4, with $B=B_h$). Here, B_h denotes the varying widths of the flow elements at different depths (h) below the free surface (Fig. 3.2). For the flow elements

constituting the lateral weir flow, the parameter h has a range of 0 to h_o ($=Y_l$-s). As such, both the width of the flow element, B_h, and the outflow jet velocity, V_j vary with the depth h of the flow element below the free surface. Consequently, the local discharge coefficient C_d for the flow element will vary for each flow element. The width of the outflow from the flow element contracts, since it emerges as a jet and has an effective flow area of $C_d L dh$.

Three new parameters are defined as follows,

$$a = \frac{Y_l}{D} \qquad b = \frac{L}{D} \qquad c = \frac{V_l^2}{2gD} \tag{3.6}$$

Using Eq.(3.2), Eq.(3.5), Eq.(3.6) and the geometric relations of the circular channel, L/B_h can be expressed as:

$$\frac{L}{B_h} = \frac{b}{\sqrt{1-4[a-0.5-c(\eta^{-2}-1)]^2}} \tag{3.7}$$

The expression for the theoretical outflow, Q_t, through the rectangular lateral weir is:

$$Q_t = \int_0^{h_o} C_d V_j L dh \tag{3.8}$$

Expressing V_j in terms of η and V_l (Eqs. 3.2 and 3.5), Q_t can be expressed as:

$$Q_t = \frac{V_l^3 L}{g} \int_{\eta_o}^{1} \frac{C_d}{\eta^4} d\eta \tag{3.9}$$

Here,

$$\eta_o = \frac{\frac{V_1}{\sqrt{2gD}}}{\sqrt{\frac{V_1^2}{2gD} + (\frac{Y_1}{D} - \frac{s}{D})}} \qquad (3.10)$$

denotes the lower limiting value of η for the infinitesimal layer located just above the weir sill of height s. The parameter η_o depends on the dimensionless sill height s/D, the parameter $V_1/\sqrt{2gD}$ and the dimensionless flow depth Y_1/D at the approach section.

For the theoretical weir outflow Q_t, the following alternate relation may be stated in terms of a mean weir discharge coefficient $\bar{C}_d$ and a mean jet velocity $\bar{V}_j$. Thus,

$$Q_t = \bar{C}_d A_w \bar{V}_j \qquad (3.11)$$

where, for the weir jet outflow the mean velocity $\bar{V}_j = \int_0^{h_o} \frac{V_j}{h_o} dh = \frac{V_1^3}{3gh_o}(\frac{1}{\eta_o^3} - 1)$ and the flow area $A_w = h_o L$. Here, A_w is the projected area of the weir on the vertical plane through the channel axis. Since the local discharge coefficient C_d is a function of η and L/B_h (Eq.3.4), from Eqs.(3.9) and (3.11), one can express the mean weir discharge coefficient $\bar{C}_d$ as,

$$\bar{C}_d = \frac{Q_t}{A_w \bar{V}_j} = \frac{\int_{\eta_o}^{1} \frac{C_d}{\eta^4} d\eta}{(\frac{1}{\eta_o^3} - 1)} = f(\eta_o, \frac{L}{D}, \frac{Y_1}{D}, \frac{V_1^2}{2gD}) \qquad (3.12)$$

It may be noted that η_o contains the parameter *s/D* in its definition (Eq. 3.10). The experimental data which are presented in a following section will indicate that $\bar{C}_d$ is dependent mainly on the parameter η_o and *L/D* and that the influence of the Y_1/D and $V_1^2/(2gD)$ are not dominant. The parameter η_o is related to the approach Froude number $F_1 = V_1/\sqrt{gA_1/B_1}$. Thus:

$$\eta_o^2 = \left[\frac{\frac{V_1}{\sqrt{2gD}}}{\sqrt{\frac{V_1^2}{2gD} + (\frac{Y_1}{D} - \frac{s}{D})}} \right]^2 = \frac{F_1^2}{F_1^2 + 32(\frac{Y_1}{D} - \frac{s}{D})(\frac{\sqrt{\frac{Y_1}{D} - (\frac{Y_1}{D})^2}}{\theta_1 - \sin\theta_1})} \qquad (3.13)$$

where, $\theta_1 = \pi - 2\arctan(\frac{\frac{1}{2} - \frac{Y_1}{D}}{\sqrt{\frac{Y_1}{D} - (\frac{Y_1}{D})^2}})$, g = the acceleration due to gravity. Also, A_1 and B_1 denote respectively the flow area and top width at the flow depth Y_1 in the approach section.

3.3 Experimental Set-Up And Procedures

Tests were conducted in a smooth PVC pipe of nominal diameter 30 cm which was laid horizontally (Fig.3.3). Machined 12 mm thick plexiglas plates bent to have their inner radius matching with the pipe's inner radius were located in the side of the pipe to form the sharp-edged lateral weir models (Table 3.1). A system of baffles and screens reduced large-scale turbulence at the inlet section. The flow depth was always measured at the channel center using point gages (Fig.3.3) that could be read to the nearest 0.1 mm. In all the weir test series, the nappes were fully ventilated. A spline fit was used to determine

the measured water surface profile over the weir span L (Fig. 3.3). Based on this, the average depth of flow Y_1 was determined. Standard V-notches were used to measure the through discharge and the weir outflow. The maximum error in the discharge measurement is estimated to be 3%.

3.4 Analysis Of Results

The test data for nine different L/D and s/D combinations are listed in tables 3.2 to 3.10. The temperature of water during the experiment was 20°C.

3.4.1 Verification of the proposed mean discharge coefficient relationship

For a given circular channel of diameter D and lateral weir of sill height s and length L, and a set of approach flow conditions such as Y_1 and Q_1 (Fig.3.2), one can obtain the jet velocity V_j of each flow element (Eq.3.5). The mean jet velocity for the total outflow is $\bar{V}_j = \frac{V_1^3}{3gh_o}(\frac{1}{\eta_o^3} - 1)$ which is expressed in terms of η_o. η_o itself can be determined from the known quantities (Eq.3.10). The experimental data related to the directly measured discharge Q_M for a range of parameters L/D and s/D (Table 3.1) are compared with the predicted discharge Q_t (Fig.3.4) which is based solely on theoretical considerations (Eq.3.11). The solid line in the sketch denotes a perfect correlation. For the case when L/D = 0.5 and s/D = 0.13 (Fig. 3.4*c*), the predicted discharge Q_t is 14% less than the measured discharge Q_M . In the other cases (Figs. 3.4a, b and *d* to *i*), the agreement between Q_t and Q_M is reasonable.

3.4.2 Comparison of the present model with a previous model (Uyumaz 1985)

Uyumaz (1985) has given a semi-empirical relation to predict the lateral weir discharge Q_t based on a spatially varied flow model and has proposed a discharge coefficient m on the basis of empirical relations. His model is a highly improved version of the model originally presented by De Marchi (1934). The range of L/D covered in his test series was $0.6 < L/D < 3.4$ and the range of L/D covered in the present tests is from 0.5 to 1.0. As such, the comparison of test data based on Uyumaz's tests and the present tests are possible only in a narrow L/D range. $L/D = 1.0$ is chosen as a typical example for the comparison of Q_M with Q_t based on Uyumaz's model (1985) and the present model (Eq.3.11). Although in the subcritical range ($F_1 < 1.0$), the values of Q_M agree with Q_t for both the models (Fig. 3.5), in the supercritical range, agreement between Q_M and Q_t is better for the present model (Eq.3.11) than for the model of Uyumaz (1985). Uyumaz (1985) developed his semi-empirical model by considering the flow depth present at the start of the weir as the reference depth Y_1. However, in his analysis, he states that for his test data, "calculating the mean of several intermediate heads proved more satisfactory" to obtain Y_1. It should be added that in the field example provided by Uyumaz (1987), he reverts back to the use of the single reference depth Y_1 at the upstream end of the weir.

3.4.3 Variation of $\bar{C}_d$ with η_o^2

The value of the weir discharge coefficient based on the discharge measured directly, $\bar{C}_{dM}$, can be determined using the following relation

$$Q_M = \bar{C}_{dM} A_w \bar{V}_f \qquad (3.14)$$

Fig. 3.6 and the insert of Fig. 3.6 show the variation of the mean discharge coefficient $\bar{C}_d$ with the parameters η_o^2. In these sketches, the solid lines denote the theoretical relationship between $\bar{C}_d$ and η_o^2 (Eq.3.12). As stated earlier, the experimental values of the mean discharge coefficient that are derived from test data (Eq.3.14) for the case in which L/D = 0.5 and s/D = 0.13 appear to have a slightly larger deviation from the predicted values. Except for this case, the present experimental values of the mean discharge coefficient $\bar{C}_{dM}$ (Eq.3.14, based on the measured discharges) follow the general trend of the predicted $\bar{C}_d$ - η_o^2 relation given by Eq.3.12 (Fig.3.6). The stated deviation of the experimental values of the mean discharge coefficient $\bar{C}_{dM}$ (Eq. 3.14) from the predicted values of $\bar{C}_d$ (Eq.3.12) could be due to two facts. For instance, the model developed is based on the two-dimensional ideal flow theory in which the velocity distribution in the approach channel is uniform. Further, in the experiments, the outflow through the weir was not strictly two-dimensional when the depth of flow over the weir was large. The reasonable agreement obtained between Q_M and Q_t can be traced to the fact that experimental discharge Q_M denotes the integrated value of the discharge passing through several horizontal layers located over the lateral weir sill.

3.4.4 Variation of $\bar{C}_d$ with *s/D*, Y_1/D, $V_1^2/(2gD)$ and *L/D*

The parameter η_o includes *s/D*, Y_1/D and $V_1^2/(2gD)$ in its definition (Eq. 3.10). Figs. 3.6*a*, *b* and *c* denote the variation of $\bar{C}_d$ with η_o and indicate that *s/D*, Y_1/D and $V_1^2/(2gD)$ are not dominant parameters as stated earlier when one expresses $\bar{C}_d$ as a function of η_o and *L/D*. The present hydrodynamic weir model is based on the theory of lateral flow through outlets of two-dimensional channels, which predicts a slight increase in the discharge coefficient with an increase in the outlet opening *L/D* (Insert, Fig. 3.6*c*). The present weir test results also indicate a slight increase in the weir discharge coefficient with an increase in *L/D*.

3.4.5 A typical example

For a given set of flow conditions in the circular channel and the weir geometry, one can get the prediction of the lateral weir discharge Q_l:

Given: $D = 30\ cm$, $L = 30\ cm$, $s = 3.81\ cm$, $Y_1 = 12.1\ cm$, $Q_l = 18{,}900\ cm^3/sec$ and $g = 981\ cm/sec^2$

Find: the side weir discharge Q_l.

$$\theta_l = \pi - 2\arctan\left(\frac{\frac{1}{2} - \frac{Y_l}{D}}{\sqrt{\frac{Y_l}{D} - \left(\frac{Y_l}{D}\right)^2}}\right) = 2.75 \text{ radians}$$

$$A_l = \frac{1}{8}(\theta_l - \sin\theta_l)D^2 = 267 cm^2$$

$$B_1 = 2\sqrt{Y_1 D - Y_1^2} = 29.4cm$$

$$V_1 = \frac{Q_1}{A_1} = 70.8cm/s$$

$$h_o = Y_1 - s = 8.29cm$$

From Eq.(3.10),

$$\eta_o = \frac{\frac{V_1}{\sqrt{2gD}}}{\sqrt{\frac{V_1^2}{2gD} + (\frac{Y_1}{D} - \frac{s}{D})}} = 0.485$$

From Fig.3.6 for η_o^2 = 0.235 and L/B = *1.0*, one can get $\bar{C}_d$ = 0.49 (dotted lines of Fig.3.6c) or the same value may be obtained from numerically integrating Eq. (3.12). For this, use Eqs. (3.4) and (3.7) respectively to substitute C_d and L/B . For the weir $L/B=L/B_h$.

$$\bar{V}_j = \frac{V_1^3}{3gh_o}(\frac{1}{\eta_o^3} - 1) = 113cm/s$$

$$A_w = h_o L = 249\ cm^2$$

From Eq.(3.11),

$$Q_1 = \bar{C}_d A_w \bar{V}_j = 13,800cm^3/s$$

3.5 Conclusions

A theoretical expression (Eq. 3.12) is developed to relate the mean weir discharge coefficient $\bar{C}_d$ with the parameter η_o and L/D for rectangular lateral weirs located in the side of circular channels. Unlike earlier studies, $\bar{C}_d$ (Eq.3.12) derived on the basis of theoretical considerations is independent of experimental data. When $\bar{C}_d$ is expressed as a function of η_o and L/D, the effect of the other parameters such as s/D and Y_1/D are not significant in the range of variables covered by these tests. $\bar{C}_d$ increases when the parameter L/D is increased. The experimental data presented for L/D=0.5, 0.75 and 1.0 provides a verification of the proposed expression for the lateral weir discharge for both subcritical and supercritical approach flow conditions (Fig.3.4).

CHAPTER 4

DIVIDING RECTANGULAR CLOSED CONDUIT FLOWS

4.1 General remarks

Division of flow past 90° branches of closed conduits (Fig.4.1) is encountered in internal flow systems of water and wastewater purification plants and conduit network systems associated with heating, ventilation and air conditioning. Chapter four deals with the characteristics of dividing flows in closed rectangular conduits. Test results covering a range of discharge ratios Q_3/Q_1 and three width ratios L/B are obtained to verify the proposed model. Here, Q_3 and Q_1 respectively denote the discharge in the branch of width L and the main of width B (Fig.4.1). In particular, the contraction coefficient C_c for the branch flow, the energy loss coefficients K_{12} related only to the main and the energy loss coefficient K_{13} related to the main and the branch are determined using test data. An empirical method is used to predict C_c and in turn yield K_{13}. For this, the result of an existing lateral outlet model (McNown and Hsu 1951) for two dimensional flow past a lateral slot fitted with a single 90° barrier of infinite length (Insert Fig.4.1) is used as the basis. The value of C_c determined by this method is compared with the value of C_c obtained graphically from the flow pattern sketched on the basis of measured velocity distributions. Detailed velocity and pressure data are obtained to describe the flow processes in dividing closed rectangular conduit flows.

4.2 Governing relations

4.2.1 Contraction coefficient for dividing flows in a branching rectangular conduit

The development of the governing relations describing the characteristics of dividing flow in rectangular closed conduits is very similar to the development of the relations for flow through a rectangular lateral weir located in a circular channel (Ramamurthy et al. 1995).

The insert of Fig.4.1 shows a rectangular lateral outlet of length L fitted with a single barrier of infinite length set in a two-dimensional conduit of width B. Following McNown and Hsu (1951), C_c can be defined as,

$$C_c = \frac{\textit{jet discharge per unit depth of conduit}}{LV_j} \qquad (4.1)$$

Here, C_c is a function of the geometric parameter L/B (Fig.4.1) and the velocity parameter η (Ramamurthy et al. 1995) which can be defined as in Eq.(4.2). Denoting the specific weight of water as γ and the gravitational acceleration as g,

$$\eta = \frac{V_1}{V_j} = \sqrt{\frac{\frac{V_1^2}{2g}}{\frac{V_1^2}{2g} + \frac{p_1}{\gamma}}} \qquad (4.2)$$

Here, V_1 and p_1 are the axial flow velocity and pressure at the approach section and $V_j = \sqrt{V_1^2/2g + p_1/\gamma}$ is the velocity of the jet emerging from the lateral outlet (Insert Fig.4.1). Theoretically, the speed of the fluid particles along the free streamline "*bc*" is constant. It may be noted that test data shows that the velocity is nearly uniform at the

contracted section "*cg*". The procedure to find p_1 experimentally is described in the section on experimental procedures.

The existing results of McNown and Hsu (1951) for a slot-barrier configuration (Insert Fig.4.1) can be used to link the theoretical contraction coefficient C_c with η and L/B. *i.e.*

$$C_c = C_c(\eta, L/B) \tag{4.3}$$

The above relationship among C_c, η and L/B is implicit and can be approximated by an explicit cubic expression in η for the range $0 < L/B \leq 1.0$ and $0 < \eta \leq 1.0$. For instance, the following explicit relation between C_c, L/B and η can be obtained for two dimensional flow past a lateral slot fitted with a 90° barrier (Insert Fig.4.1).

$$C_c = c_0 + c_1\eta + c_2\eta^2 + c_3\eta^3 \tag{4.4}$$

in which,

$$c_0 = 0.618 + 0.144(L/B) + 0.225(L/B)^2;$$
$$c_1 = -0.096 - 0.286(L/B) - 0.977(L/B)^2;$$
$$c_2 = -0.700 + 0.822(L/B) + 1.41(L/B)^2;$$
$$c_3 = 0.200 - 0.685(L/B) - 0.644(L/B)^2.$$

Eq.(4.4) is assumed to be valid to calculate C_c for dividing flow in a branching rectangular conduit (Fig.4.1) when p_1 is replaced by $\Delta p=(p_1-p_c)$ in Eq.(4.2), since the pressure p_c at

"c" is not in general zero. Accordingly, Eq.(4.2) denoting η for branch conduit flows is rewritten as,

$$\eta = \frac{V_1}{V_j} = \sqrt{\frac{\frac{V_1^2}{2g}}{\frac{V_1^2}{2g} + \frac{\Delta p}{\gamma}}} \qquad (4.5)$$

The pressure decreases along "cj" from "c" to the point where the velocity is zero in the branch separation bubble (Fig.4.1) and increases from there up to "j". Further, the velocity in the bubble is very small. Hence, the pressure difference is in general not expected to be large between "j" and "c" (Fig.4.1). The measured pressure p_j at "j" can be used in place of p_c at "c" to get Δp in Eq.(4.5).

4.2.2 Energy loss coefficient K_{12}

The energy loss coefficient related only to the main rectangular conduit is given by,

$$K_{12} = \frac{E_1 - E_2}{\frac{V_1^2}{2g}} \qquad (4.6)$$

$$E_2 = \frac{V_2^2}{2g} + \frac{p_2}{\gamma} \qquad (4.7)$$

Here, the energy , velocity and pressure are respectively denoted by E, V and p. The subscript 1, 2 and 3 relate to sections 1, 2 and 3 of Fig.4.1.

4.2.3 Energy loss coefficient K_{13}

The energy loss coefficient K_{13} for the main and branch conduits is defined in terms of the following expressions. Denoting the discharge ratio $Q_r = Q_3/Q_1$,

$$K_{13} = \frac{E_1 - E_3}{\frac{V_1^2}{2g}} \tag{4.8}$$

where,

$$V_1 = \frac{V_3 \frac{L}{B}}{Q_r} \tag{4.9}$$

$$E_1 = \frac{V_1^2}{2g} + \frac{p_1}{\gamma} \tag{4.10}$$

$$E_3 = \frac{V_3^2}{2g} + \frac{p_3}{\gamma} \tag{4.11}$$

The flow entering the branch contracts in the region "*bc*", expands in the region "*cd*", and reattaches at "*d*". Following flow recovery in the region "*de*", fully developed flow occurs beyond the section "*e*" which is far away from "*d*" (Fig.4.1). The flow expanding in the region "*cd*" experiences considerable energy loss. This loss depends on the value of C_c which itself is a function of L/B and η (Eq.4.5). Assuming the expression (Eq.4.12) for the sudden expansion of flow in a conduit to be approximately valid for the expansion of the flow in the branch, the loss coefficient K_{13} can be written as,

$$K_{13} = \frac{Q_r}{\frac{L}{B}} \left(\frac{1}{C_c} - 1\right)^2 \tag{4.12}$$

In sudden expansions, the separating flow does not strictly follow the profile of the sudden conduit expansion. As such, Eq.(4.12) can be used as an approximation to obtain a relation for K_{13}.

4.3 Experimental set-up and procedures

Fig.4.2 shows the equipment used for the tests to determine the characteristics of dividing flows. *12* mm thick large Plexiglas plates were used to form *90°* rectangular closed conduit branches without too many joints. The main rectangular conduit was *41.2* mm x *91.5* mm in cross section. It was about *4* m long upstream of the junction to provide fully developed flow in the approach section. For the branch conduits, three different cross sections (*20.4* mm x *41.2* mm, *70.5* mm x *41.5* mm, and *91.5* mm x *41.5* mm) were used. This resulted in the three geometric ratios of L/B = *0.22*, *0.77* and *1.0*. A constant head supply tank provided steady flow in the main conduit. Q_2 and Q_3 were measured with the help of *30°* V-notches (Fig.4.2). The point gages measuring the driving head of the V-notches had a least count of 0.1 mm. The maximum error in the discharge measurement was *3*%.

Many closely spaced *1* mm pressure taps were provided along the wall centerlines of the main and the branch. The spacing of the wall pressure taps was reduced to *3* mm near the two corners "*h*" and "*b*" of the branch (Fig.4.1). This enabled detailed mapping of the pressure field near the branch. The water manometers connected to the wall taps of the

conduit could be read to the nearest millimeter. Far away from the branching point, the pressure profiles at sections of the main and branch were linear and were unaffected by the presence of the branch. These linear pressure profiles were noted and extrapolated to the center of the junction to find the pressures p_1, p_2 and p_3 experimentally. This procedure eliminates the need to account for the boundary friction losses which are present in real flows between the conduit branch center and sections 1, 2 and 3. These experimentally determined pressures p_1, p_2 and p_3 were used to find the total energies E_1, E_2 and E_3 (Eqs.4.7, 4.10 and 4.11), which in turn yield the energy loss coefficients.

The total energy of the main flow just before it enters the branch was experimentally determined by adding the experimentally determined pressure head p_1/γ and the velocity head at the exit section "*bs*" of the main. The mean velocity at sections 1 and "*bs*" (Fig.4.1) are the same. Since the loss in the converging section "*bhcg*" is very small, $V_j^2/2g + p_c/\gamma \approx V_1^2/2g + p_1/\gamma$. Thus, knowing V_1, p_1 and p_c, one may find V_j and in turn η and C_c. In the present study, η was determined using Eq.(4.5), since the pressure along the free streamline "*bc*" is not zero as in the case of the lateral slot model (McNown and Hsu 1951). Using the plotted streamline pattern (Fig.4.5), C_c was determined graphically.

The laser Doppler velocimetry *(LDV)* unit was used to measure velocities in the test section. Detailed distribution data of the mean velocity components were obtained at various cross sections for each of the three area ratios at two typical discharge ratios

Q_3/Q_1. The velocity data was used to determine the flow pattern by plotting the streamline. The x and y locations were normalized respectively by the branch width L and the main width B.

4.4 Results

Experimental data for three different L/B ratios are summarized in tables 4.1, 4.2 and 4.3, respectively. The temperature of water was 20°C.

4.4.1 Energy Loss coefficient K_{12}

The data (Fig.4.3) show that for rectangular branching conduits, L/B is not a significant variable controlling the variation of K_{12} with Q_3/Q_1. The negative loss coefficients in the low Q_3/Q_1 range for circular conduits can be attributed to the fact that the low energy three dimensional flow in the conduit boundary layer enters the branch leaving the through flow to possess higher energy (Escobar 1954). This fact is well supported by the two-dimensional flow pattern of rectangular conduits sketched in Fig.4.5c. For instance, at low Q_3/Q_1 , the low energy flow in the boundary layer entering the branch is clearly trapped by the dividing streamline "*nh*" (Fig.4.5c). Further, at low Q_3/Q_1 values, the energy loss due to expansion of flow in the main is small.

4.4.2 Energy Loss coefficient K_{13}

The energy loss coefficient K_{13} was determined as a function of Q_3/Q_1 using Eq.(4.8) and plotted in Fig. 4.4. Fig. 4.4 also contains the relation between K_{13} and Q_3/Q_1 for circular and square pipes. The data for square pipes presented by Miller (1971) in Fig.4.4 is for L/B=1 and for a limited range of Q_3/Q_1. Although no specific arguments are given, Miller (1971) states that variations of K_{12} and K_{13} with Q_3/Q_1 for circular and rectangular pipes are nearly identical. Unfortunately, even for circular pipes, one notices a wide range of variation in the experimental values of K_{13} and K_{12} reported by different investigators (Figs.4.3 and 4.4). The empirical relations between K_{13} and $Q_3/Q_1 = Q_r$ determined on the basis of Eq.(4.12) for rectangular conduits are shown in Fig.4.4 together with the variation of K_{13} with Q_3/Q_1 obtained on the basis of Eq.(4.8). These two relations are in close agreement.

4.4.3 Flow pattern and contraction coefficient C_c

The wall pressure taps are very closely spaced (3 mm center to center) near the branch corners "*b*" and "*h*". Still, the pressure data indicated that a finer resolution was needed to locate the stagnation points. Stagnation occurred either on the main wall or branch wall depending on both L/B and Q_3/Q_1. The point where the velocity very near the wall was zero denoted the stagnation point and the reattachment point of the separation flow. However, at the stagnation point the pressure is generally larger. The stagnation points

could be located accurately only in a few cases. For instance, at Q_3/Q_1=0.3 and L/B=0.22 (Fig.4.5c) the stagnation was on the main wall and at about 6 mm from the corner "b". Fig.4.5 shows the shape of the separation bubble geometry and the variation of pressure and velocity along the main and the branch. Table 4.4 shows the value of C_c determined graphically for a few specific cases for which the detailed velocity and pressure profile were determined. The agreement between C_c values based on flow pattern and Eq.(4.4) is reasonable. The flow in the converging section "*bhgc*" was essentially two dimensional. In the expanding region beyond "*cg*", the flow was not strictly two dimensional. As such, the profile of the bubble "*cd*" was determined only approximately. The velocity distribution data (not shown in Fig.4.5) indicated that the tendency for flow to separate from the main wall "*lm*" starts when Q_3 is close to Q_2, for all L/B ratios.

Fig.4.6 shows the dividing streamline (DSL) profiles for the case L/B= 1.0, 0.77 and 0.22 at Q_3/Q_1=0.42. The value of Q_3/Q_1 = 0.42 for L/B=0.77 was chosen as a reference discharge ratio. For L/B=1.0 and 0.22, the profiles of DSL corresponding to Q_3/Q_1 close to 0.42 were chosen. Slight adjustments were made to these profiles using interpolation or extrapolation techniques to determine the DSL profiles for L/B=1.0 and 0.22 at Q_3/Q_1=0.42. For L/B=0.22, the downstream branch corner "h_3" is set at a location 6 mm upstream of the corners "h_1" and "h_2" at L/B=1.0 and 0.77, to account for the fact that the stagnation for L/B= 0.22 was 6 mm downstream of the branch corner and the stagnation for L/B=1.0 and 0.77 were close to the corner, for Q_3/Q_1 = 0.42. The resulting composite sketch (Fig.4.6) shows that near the entry to the branch for L/B=0.22, the DSL is slightly

steeper than it is for L/B=1.0. Still, the profiles for the three L/B ratios appear to be very similar and imply that the energy loss due to expansion of the flow in the main does not depend on the L/B ratio significantly.

A specimen computation related to dividing closed conduit flow is given in Appendix 5 (pp. 161).

4.5 Conclusions

The following conclusions can be drawn for branching flows in closed rectangular conduits:

1. The energy loss coefficient K_{12} for rectangular conduit branches depends on Q_3/Q_1 and is independent of L/B. For fixed Q_3/Q_1 values which imply fixed Q_2/Q_1 values, the streamline pattern determined on the basis of velocity data in the main are nearly identical and hence the expansion loss in the main is independent of L/B. At low values of discharge ratios ($Q_3/Q_1 < 0.2$), the flow patterns indicate that the low energy flow in the conduit boundary layer gets trapped and passes into the branch. The resulting higher energy in the through flow leads to negative K_{12} values.

2. The energy loss coefficient K_{13} is a function of Q_3/Q_1 and L/B. The value of K_{13} determined by direct energy measurements and the empirical method agree reasonably well.

3. The contraction coefficient determined graphically is close to the values of C_c obtained from the Eq.(4.4), which is based on an existing free streamline slot-barrier model.

CHAPTER 5

COMBINING FLOWS

AT 90° JUNCTIONS OF RECTANGULAR CLOSED CONDUITS

5.1 General remarks

Combination of flow past *90°* junctions of closed conduits (Fig.5.1) are encountered in internal flow systems of water and wastewater purification plants and conduit network systems associated with heating, ventilation and water distribution. In the present study, the energy and power loss coefficients of two-dimensional flows past *90°* junctions of rectangular closed conduits are determined experimentally for three area ratios (A_3/A_2 = *1.0*, *0.77* and *0.22*) and a range of discharge ratios ($0 < Q_3/Q_2 \leq 1.0$). Some of the experimental parameters such as the average entry angle δ (Fig.5.1) of the branch flows are compared with the results of a simple model based on the application of the momentum principle to two dimensional closed conduit flows. The detailed velocity and wall pressure distribution data in the vicinity of the junction are also obtained to explain the flow processes related to combining flows.

5.2 Governing relations

Fig.5.1 shows a 90^o junction for rectangular closed conduits. Downstream of the junction, both the main and branch flows attain a minimum area of cross section at a location "*mjk*" (Fig.5.1). As such, the energy loss in the contracting sections "*bsmj*" and "*ebjk*" is small. For the flow configuration shown in Fig.5.1, the following governing relations are valid. They are respectively the momentum, power, and continuity equations;

$$\Delta M = (p_2 + \rho V_2^2)A_2 - (p_1 + \rho V_1^2)A_1 \qquad (5.1)$$

$$E_1 Q_1 + E_3 Q_3 = E_c Q_2 \qquad (5.2)$$

$$Q_1 + Q_3 = Q_2 \qquad (5.3)$$

where,

$$E_1 = \frac{p_1}{\rho g} + \frac{V_1^2}{2g} \qquad (5.4a)$$

$$E_3 = \frac{p_3}{\rho g} + \frac{V_3^2}{2g} \qquad (5.4b)$$

$$E_c = \frac{p_c}{\rho g} + \frac{V_c^2}{2g} \qquad (5.4c)$$

In the above, ρ is the density of water, g is the acceleration due to gravity, ΔM is the difference of the momentum terms in the main between sections 1 and 2 (Fig.5.1). The areas at sections 1 and 2 are equal. The total energy, pressure, discharge and velocity of

flow are respectively E, p, Q and V. Suffixes *1*, *2*, *3* and *c* refer to sections *1*, *2*, *3* and the vena contracta (section *"m"* in Fig.5.1).

The coefficients K_{12}, K_{32} and K_p denote the loss of energy (Eq.5.5) and the loss of power (Eq.5.6) for combining flows (Fig.5.1). In Eq.5.6b, K_p expresses in terms of K_{12} and K_{32}. Suffix p refers to the power terms.

$$K_{12} = \frac{E_1 - E_2}{\frac{V_2^2}{2g}} \tag{5.5a}$$

$$K_{32} = \frac{E_3 - E_2}{\frac{V_2^2}{2g}} \tag{5.5b}$$

$$K_p = \frac{E_c - E_2}{\frac{V_2^2}{2g}} \tag{5.6a}$$

$$K_p = (1 - \frac{Q_3}{Q_2})K_{12} + \frac{Q_3}{Q_2}K_{32} \tag{5.6b}$$

The momentum transfer ΔM from the branch to the main conduit can be determined by the following three different methods which involve three independent relationships.

1. Measuring momentum terms $M_1 = p_1 A_2 + \rho V_1^2 A_2$ and $M_2 = p_2 A_2 + \rho V_2^2 A_2$ at sections 1 and 2 (Fig.5.1), accounting for the frictional boundary losses and using the relation $\Delta M = M_2 - M_1$ (Eq.5.1).

2. Applying the momentum equation to the branch control volume "*ebcd*" (Fig.5.1) in the axial direction of the main and relating ΔM with the wall pressure forces P_d on the downstream wall and P_u on the upstream wall (Fig.5.1). Thus, $\Delta M = P_d - P_u$.

3. Determining directly the momentum transfer ΔM using the measured velocity component u in the direction of the main channel and the velocity component v at right angles to u, at several subsections dx along the branch exit section "*eb*" (Fig.5.1). Thus,

$$\Delta M = \rho Q_3 V_3 \cot\delta = \sum_{i=1}^{N} (\rho v dx_i) u \qquad (5.7)$$

where, δ is the average entry angle of the branch flow at section "*eb*" (Fig.5.1).

5.3 Experimental set-up and procedures

Fig.5.2 shows the equipment used for the tests to determine the characteristics of combining flow. *12* mm thick large plexiglas plates were used to form *90°* rectangular closed conduit junctions without joints. The main rectangular conduit was *41.2* mm x *91.5* mm in cross section. It was about *4* m long upstream of the junction to provide fully developed flow in the approach section. For the branch conduits, three different cross sections (*20.4* mm x *41.2* mm, *70.5* mm x *41.5* mm, and *91.5* mm x *41.5* mm) were used. This resulted in the three geometric ratios of L/B = *0.22*, *0.77* and *1.0*. Here, L and B denote the widths of the branch and main conduits respectively. Constant head supply

tanks provided steady flow in the main and the branch. The main and branch flows as well as the combined flow were measured with the help of 30^{o} V-notches (Fig.5.2). The point gages measuring the driving head of the V-notches had a least count of 0.1 mm. The maximum error in the discharge measurement was 3%.

Many closely spaced 1 mm pressure taps were provided along the wall centerlines of the main and branch. The spacing of the wall pressure taps was reduced to 3 mm near the two corners "*e*" and "*b*" of the junction (Fig.5.1). This enabled detailed mapping of the pressure field in the vicinity of the junction. The water manometers connected to the wall taps of the conduit could be read to the nearest millimeter. Far away from the junction, the pressure profiles at sections of the main and branch were linear and were unaffected by the presence of the junction. These linear pressure profiles were noted and extrapolated to the center of the junction to find the pressures p_1, p_2 and p_3. These pressures were used to find the total energies E_1, E_2 and E_3 (Eq.5.4), which in turn yielded the energy loss coefficients (Figs. 5.3a and 5.3b).

Using the previously described LDV system, detailed distribution data of the mean and fluctuating velocity components were obtained at various cross sections, for each of the three area ratios at two typical discharge ratios Q_3/Q_2 for combining flows in rectangular closed conduits (Figs.5.4, 5.5 and 5.6). The x and y locations were normalized respectively by the branch width L and the main width B as before (Figs.5.4, 5.5 and 5.6).

5.4 Results

The pressure head data and other results of the tests are shown in Tables 5.1 to 5.3. The temperature of water was 20°C.

5.4.1 Energy loss coefficients

Fig.5.3a displays the dependence of the energy loss coefficients K_{12} (Eq.5.5a) on Q_3/Q_2 and A_3/A_2 for rectangular conduits. The experimental data of K_{12} for the three area ratios A_3/A_2 indicate that K_{12} decreases with an increase in A_3/A_2 at fixed Q_3/Q_2 for rectangular conduits. This characteristic is similar to the trend seen in Fig.5.3a for circular pipes. For $A_3/A_2=0.22$, up to $Q_3/Q_2 = 0.8$, the present test data for the rectangular conduit follows the mean trend of the relation between K_{12} and Q_3/Q_2 for circular pipes for $A_3/A_2=0.22$ (Gardel, 1957) and for $A_3/A_2= 0.21$ (Serre et al., 1994). For $A_3/A_2=0.77$ and 1.0, the dependence of K_{12} on Q_3/Q_2 for rectangular conduits does not closely follow the dependence of K_{12} on Q_3/Q_2 for circular pipes, although qualitatively the trends are the same. For rectangular conduits with $L/B=1$ ($A_3/A_2=1$), the values of K_{12} of the present test are slightly lower than the values of K_{12} obtained by Miller (1971) in the limited range $0.3 < Q_3/Q_2 < 0.75$.

For both circular conduits (Gardel 1957, and $A_3/A_2 = 0.21$, Serre et al. 1994) and rectangular conduits in the low range of Q_3/Q_2, Fig.5.3b and insert of the Fig.5.3b show

the good agreement in the relationship between the energy loss coefficient K_{32} and Q_3/Q_2 for $A_3/A_2=0.22$. For high Q_3/Q_2, the wide discrepancy between the present results related to K_{32} for rectangular conduits and the existing results for circular conduits (Serre 1994, Gardel 1957) can be traced to the large inherent differences in the flow structure of combining flows in rectangular conduits and circular conduits. The structure of combining flows in rectangular conduits is discussed in a subsequent section of the results (Figs.5.4, 5.5 and 5.6). For $A_3/A_2=0.77$ and 1.0, the variation of K_{32} with Q_3/Q_2 for both rectangular conduits (present tests) and circular pipes (Gardel 1957, Ito and Imai 1973) is quite similar.

5.4.2 Flow pattern

The confluence of the branch and the main flows leads to an increase in pressure near the upstream junction corner *"b"* in the vicinity of which the flow stagnates (Figs.5.4, 5.5 and 5.6). At the corner "*e*" of the junction, the flow separates while entering the main conduit and forms a separation bubble "*ekl*" in the section downstream of the junction (Figs.5.4, 5.5 and 5.6). The velocity distribution data indicate that the flow is two dimensional until the vena contracta (section "*mjk*" of Fig.5.1). By integrating the axial velocity component (u) data at the different cross sections along the axis of the main channel, the boundary of the main flow and the boundary of the branch flow can be precisely located up to the contracting section ("*bj*" and "*ek*" in Figs.5.4, 5.5 and 5.6). In the short expanding section beyond sections "*mj*" and "*jk*", the flow becomes progressively three dimensional.

Hence, as one proceeds downstream of "*j*" and "*k*" (Figs.5.4, 5.5 and 5.6), the boundaries for the main and branch flows shown downstream of the contraction are less accurate. The reattachment point *"l"* for the separation bubble was obtained more precisely by locating the position very near the wall at which the velocity components were zero. Since the flow was not strictly two dimensional in the expanding flow section downstream of "*j*" (Figs.5.4, 5.5 and 5.6), the integration of the axial velocity profiles provided only a rough estimate of the downstream boundary "*kl*" of the separation bubble. This boundary *"kl"* was slightly corrected to force it to pass through the reattachment point *"l"* which was determined more precisely from the velocity survey data close to the wall. As with the stagnation point, the velocity components are zero at the reattachment point. The downstream location where a fully developed flow characterized by a linear falling pressure profile is dependent on both A_3/A_2 and Q_3/Q_2.

Only for the case of $A_3 = A_2$ can one expect some similarity of the flow characteristics of combing flows in circular and rectangular conduits, since the branch flow in each case spans the entire width of the main conduit. Combining flows in closed circular pipes and closed rectangular conduits are expected to have different flow characteristics especially when $A_3 < A_2$. In the case of circular pipes, for $A_3 < A_2$, the main flow sees the branch flow entering the main flow as a narrow cross jet. Cross jet studies involving circular jets emerging from 90° junctions and meeting a cross flow in a wider main duct indicate that the branch jet expands continuously and is expected to develop strong horseshoe shaped vortices with their axis nearly parallel to the main conduit axis (Antani, 1977). In fact,

the flow is three dimensional for circular pipe junction flows, and hence the contracted section will be a highly curved line. Consequently, the contraction coefficient is ill defined. For circular closed conduits, except in the case of fully developed flows, the traditional use of a single row of pressure taps on the two main walls will be insufficient to describe the wall pressure distribution. In rectangular conduit systems, the flow from the branch is constricted on the sides and hence continues to contract along with the main flow until the vena contracta (section "*mjk*" Fig.5.1), and in this region, the flow remains two dimensional. As such, the energy loss up to section "*m*" is quite small and high turbulence is limited to the shear layers and the entire separation bubble region (Figs.5.7 and 5.8). However, it is fortuitous that some gross characteristics such as the energy loss and power loss coefficients for circular pipes and rectangular pipes are somewhat similar in some ranges of A_3/A_2 and Q_3/Q_2.

The geometry of the separation bubble *"ekl"* shown in Figs.5.4, 5.5 and 5.6 is largely influenced by both the ratios A_3/A_2 and Q_3/Q_2. The streamline patterns indicate that the vena contracta of the combined flow occurs at a distance of about B downstream of the corner "*b*". Here, B denotes the width of the main conduit. This is true even for the case where the reattachment length is very long (Fig.5.6a). The curvature of the flow in the region downstream of the junction affects the wall pressures on the two walls "*hi*" and "*ef*" very differently. Due to the curvilinear nature of the flow and the complex geometry of the separation bubble, the location of the contracted section of the combined flow can be estimated much less precisely by noting only the positions of the minimum wall

pressures. As such, streamline patterns sketched on the basis of detailed velocity distribution data provide a more accurate location of the contraction sections (Figs 5.4 to 5.6).

5.4.3 Turbulent characteristics

Figs.5.7 and 5.8 denote the turbulent characteristics for two typical cases of combining flows. For the conditions shown in Fig.5.4a ($Q_3/Q_2 = 0.49$, $L/B = 1.0$), the flow is nearly free from large velocity gradients up to the contracting region outside the separation bubble. In Fig.5.7a, the non-dimensional intensity of turbulence u'/U_{max} denoting the normalized root mean square (RMS) value of the axial component of turbulent fluctuations is relatively high in the separation bubble, in the expanding section and in the vicinity of the free shear layer which denotes the boundary of the separation bubble "*ekl*". This characteristic is true even for the normalized turbulent intensity v'/U_{max} which denotes the non-dimensional RMS value of the lateral velocity fluctuation (Fig.5.7b). The values of u'/U_{max} and v'/U_{max} in the bubble region indicate that the turbulence is nearly isotropic here. As stated earlier, Fig.5.7c shows that large values of the turbulent shear $-u'v'$ are confined to the separation bubble region, the vicinity of the free shear layer and the expanding region downstream of section *"mjk"*.

In Figs.5.8a and b, for which $Q_3/Q_2 = 0.50$ and $L/B = 0.22$, the intensities of turbulence u'/U_{max} and v'/U_{max} are not low in the short entry region. In this region, the velocity

gradients are large since the speed of the branch flow is nearly 4.5 times the speed of the main flow (Fig.5.6a). The velocity gradients vanish soon after the flow passes the short entry length along the boundary "*bj*". Hence, the values of u'/U_{max} and v'/U_{max} in large sections of the flow are not high except in the very short entry region from the branch to the conduit (Figs.5.8a and 5.8b). The distribution of $-u'v'$ shows that the velocity gradients along both the boundaries of the branch jet give rise to a good deal of turbulent shear. The large discharge ratio and the small area ratio cause the branch flow to behave like a jet which keeps expanding after the initial contraction which occurs near "m" (Fig.5.6a).

5.4.4 Power coefficient K_p

The power term E_cQ_2 of Eq. (5.2) at section "*mk*" of the flow (Fig.5.1) was obtained after finding the total energy E_c at the contracted section "*mk*". To obtain E_c, one needs the velocity and the pressure data in the sections "*mj*" and "*jk*" in which the flow occurs. There is a pressure gradient from the point "*m*" on the wall to the point "*k*" on the free streamline (FSL), due to the curvature of the streamlines. As such, a minor correction was applied to the recorded wall pressure at "*m*" to obtain the pressure at "*k*". To provide this minor correction, the radius of the streamline "*ekl*" can be obtained by considering the segment "*ek*" to be the part of a true circle. Further, it was noted that along "*km*" the pressure gradient $dp/dr=\rho V^2/r$, where r is the radius of the streamline and dr is the differential of r. The computed power term E_cQ_2 was found to be very close to the sum of

the power terms E_1Q_1 and E_2Q_2 (Eq. 5.2) for all cases indicating that the major energy and power losses occurred in the expanding region downstream of the section "*mk*".

5.4.5 Expansion loss and contraction coefficient C_c

Most of the energy loss due to mixing occurs in the expanding section downstream of the section *"m"* in Fig.5.1. Hence, the energy loss E_L can be estimated using test data, which in turn will yield the value of C_c as follows. In terms of the velocity V_c at the contracted section "*mk*", where the flow is nearly uniform,

$$E_c - E_2 = E_L = \frac{(V_c - V_2)^2}{2g} = (\frac{1}{C_c} - 1)^2 \frac{V_2^2}{2g} \qquad (5.8)$$

The values of C_c computed from Eq.(5.8) are compared in Table.5.4 with the values of C_c obtained directly from the flow patterns sketched on the basis of velocity data (Figs.5.4, 5.5 and 5.6). The use of Eq.(5.8), which is strictly applicable to the energy loss in sudden expansions is justified by the fact that the streamlines in the sudden expansion do not follow the contour of the expansion after leaving the narrower section.

5.4.6 Momentum transfer and average entry angle δ

The momentum transferred by the branch to the main was determined by the three independent methods described earlier. The estimate of ΔM obtained by the direct wall pressure force difference method is quite close to ΔM determined by summing the momentum transferred by the subsections of the branch at the entry section "*eb*" (Fig.5.4a) and ΔM found by noting the difference in the momentum terms at sections 1 and 2 (Eq.5.1). The average entry angle δ is related to ΔM. Hence, δ too can be determined by the same three independent methods. The values of δ determined by the three methods are generally in close agreement (Table 5.5). For small values of Q_3/Q_2 and all A_3/A_2 values, the average jet entry angle δ is expected to vary from a value of $\delta \approx 0$ at the corner *"d"* to a value $\delta = 90^o$ at the corner *"e"*. On the other hand, for small A_3/A_2 and large Q_3/Q_2 values, the branch flow will essentially enter the main as a jet at a large constant value of δ at all subsections of the entry section "*eb*" (Fig.5.6a).

5.5 Conclusions

1. Based on the test data related to the velocity and wall pressure distributions, it is noted that for combining flows at 90^o junctions of rectangular conduits, the main and branch flows generally maintain the two dimensional character up to the contracting section

downstream of the junction. This is in sharp contrast to the three dimensional nature of the entire combining flow field in circular pipes.

2. Downstream of the junction, the contracted section occurs at a distance approximately equal to one width of the main conduit. The contraction coefficient C_c determined from the flow patterns agree well with the values of C_c determined from an indirect empirical method related to expansion losses.

3. The energy loss coefficients K_{12} and K_{32} for rectangular conduit are functions of the discharge ratios Q_3/Q_2 and the area ratios A_3/A_2. The streamline pattern for the circular and rectangular conduits are different especially when $A_3/A_2<1$. As such, any similarity between the dependence of K_{12} and K_{32} on Q_3/Q_2 and A_3/A_2 is fortuitous.

4. The high degree of turbulent shear in the vicinity of the boundary streamline of the separation bubble and the high intensities of turbulence in the bubble itself further confirm the shape of separation bubble which is obtained from streamline patterns.

5. The average entry angle δ of the branch flow to the main conduit is determined from the velocity distribution data for the branch flow at the exit plane "*eb*" of the junction. This value is close to the value of δ determined by two other independent methods which are based on separate momentum balances in the axial direction of the main conduit for both the branch flow and the main flow.

CHAPTER 6

CONCLUSIONS AND SCOPE FOR FURTHER STUDY

On the basis of the present study, the following conclusions can be drawn:

6.1 Validation of the theoretical solution for two-dimensional lateral conduit outlet:

The experimental results related to flow past a rectangular slot located in a rectangular closed conduit provide a direct verification of the free streamline model for two-dimensional flow past a lateral conduit (slot).

6.2 Rectangular lateral weir in a circular open channel:

Based on an existing hydrodynamic solution for free efflux from a two-dimensional conduit, a theoretical model is developed to express the mean weir discharge coefficient C_d with the parameter η_o and L/D for rectangular lateral weirs located in the side of circular channels. The experimental data presented for L/D=0.5, 0.75 and 1.0 provides a verification of the proposed theoretical expression for the weir discharge coefficient for both subcritical and supercritical approach flow conditions.

6.3 Dividing flows in rectangular closed conduits:

The existing solution for the free efflux from a two-dimensional conduit outlet fitted with a barrier can be adopted to solve the dividing flow problem in rectangular closed conduits by noting the difference between the two configurations. The values of the energy loss coefficient and contraction coefficient obtained empirically by two different methods are found to be in close agreement. Detailed pressure and velocity distribution data provide explanations for the lack of dependence of energy loss coefficient K_{12} on L/B. The contraction coefficient C_c determined graphically is close to the values of C_c determined from the free streamline model

6.4 Combining flows in rectangular closed conduits:

The streamline pattern obtained on the basis of detailed velocity surveys related to combining flows in rectangular closed conduits indicate that the flow processes in circular and rectangular conduits are quite different. The pressure distribution data obtained during the present study tend to confirm this point of the view. As such, any similarity in the dependence of energy loss coefficients on discharge ratios in the circular and rectangular conduit junction flows should be regarded as fortuitous. The shear stress distribution along the boundary of the separation bubble confirms the shape of the separation bubble. The values of C_c and δ obtained on the basis of different methods are in close agreement (Tables 5.4 and 5.5).

6.5 Practical applications and benefits

The results of the present study find applications in dividing and combining flows encountered in the design of open channels and closed conduit engineering systems, such as water and wastewater treatment plants, water distribution networks, irrigation systems, heating, ventilating, and air conditioning system.

6.6 Scope for further studies

The present study may extended to the case of flow past multiport systems for combining and dividing closed rectangular conduit flows.

APPENDIX 1 - REFERENCES

Allen, J. W.(1957). "Discharge of water over side weirs in circular pipes", *Proc. of the Instn. of Civil Engrs*, (London), 6(2), 270-287.

Antani, D. L. (1977). "An experimental investigation of the vortices and the wake associated with a jet in crossflow," Ph.D. thesis, Georgia Institute of Technology.

Bajura, R. A. (1971). "A Model for Flow Distribution in Manifolds," J. Engg. for Power, ASME, 7-12

Barton, J. R. (1946). "A Study of Diverging Flow in Pipelines," M.S. Thesis, State University of Iowa.

Benefield, L. D., Judkins, J. K., and Parr, A. D. (1984). " Treatment Plant Hydraulics for Environmental Engineers", Prentice-Hall, Englewood Cliffs, New Jersey.

Best, J. L. and Reid, I. (1984). "Separation Zone at Open-channel Junctions," J. Hyd. Engg., 110(11), 1588-1594.

Blaisdell, F. W. and Manson, P. W. (1963). "Loss of energy at sharp-edged pipe junction in water conveyance systems," Tech. Bull 1283, US Dept. of Agric. Washington D.C.

Collinge, V. K. (1957). "The Discharge Capacity of side weirs", *Proc. of the Instn. of Civil Engrs*, (London), 6(12), 288-304.

Crow, D.A. and Wharton, R. (1968) "A Review of Literature on the Division and Combination of Flow in Closed Conduits," The British Hydromechanics Research Association.

De Marchi, G. (1934). "Essay on the performance of lateral weirs", L'Energia Electrica, Milano, Italy, 11(11), 849-860.

El-Khashab, A. and Smith, K. V. H. (1976). "Experimental Investigation of Flow over Side Weirs", *J. Hyd. Div., ASCE*, 102(9), 1255-1268.

Escobar, J. (1954). discussion of the paper "Mechanics of manifold flow," by McNown, J.S., *Trans. ASCE*, 110, 1119-1123.

Fu, H., Watkins, A.P., Tindal, M.J. and Yianneskis, M. (1991). "Turbulent Dividing Flow in a Branched Duct," Fourth International Conference on Laser Anemometry, Advances and Applications, ASME, 33-43.

Gardel, A. (1957). "Les pertes de charge dans les ecoulements au travers de branchments en Te," ["Pressure drops in flows through T-shaped pipe fittings,"] Bull. Tech. Suisse Rom. 83(9), 123-130, and 83(10), 143-148.

Gill, M. A. (1987). "Flow Through Side Slots," J. Envi. Engrg., ASCE, 113(5), 1047-1057

Gurevitch, M. I. (1966). "The Theory of Jets in an Ideal Fluid", 1st edn, Vol. 1, Pergamon Press, N.Y.

Hager, W. H. (1984). "An Approximate Treatment of Flow in Branches and Bends," Proc. Instn. Mech. Engrs., 198C(4), 63-69.

Hager, W. H. (1987a). "Lateral Outflow Over Side Weir", *J. Hyd. Engg, ASCE*, 113(4), 491-504.

Hager, W. H. (1987b). Discussion on "Flow over side weir in circular channels" by A.Uyumaz and Y. Mulslu. *J. Hyd. Engg, ASCE*, 113(5), 685-688.

Ito, H. and Imai, K. (1973). "Energy losses at 90 degree pipe junctions," J. Hydr. Div. ASCE, 99(9), 1353 - 1368.

Kinne, E. (1931). "Contributions to the Knowledge of Hydraulic Losses at Branch Pieces," Bulletin 4, Trans. of the Hydraulic Institute, Munich Technical University, Munich, Germany.

McNown, J. S. and Hsu, E. (1951). "Application of Conformal Mapping to Divided Flow", *Proc. Midwestern Conf. on Fluid Dynamics*, J. W. Edwards, Ann Arbor, Mich., pp. 143-155.

McNown, J. S. (1954). "Mechanics of manifold flow," *Trans. ASCE*, 110, 1103-1142.

Michell, J. M. (1890). "On the Theory of Free Stream Lines", *Philosophical Trans. of the Roy. Soc.*, (London), A 181, 389-431.

Miller, D. S. (1971). Internal flow, British Hydromechanics Research Association, Crainfield, Bedford, England.

Miller, D. S. (1990). Internal flow systems, 2nd Ed., Gulf Publishing Co., Houston, Tex.

Mises, R. v. (1917). "Calculation of Outflow and Overflow Coefficients," Zeits. des Vereines Deutscher Ingenieure, 61 (In German).

Modi, P. N., Ariel, P. D. and Dandekar, M. M. (1981). "Conformal Mapping for Channel Junction Flow," J. Hydr. Engg., ASCE, 107(12), 1713-1733.

Nimmo, W. H. R. (1928). "Side Spillways for Regulating Diversion Canals," Trans., ASCE, 92, 1561-1584.

Perinpanathan, M. S. (1992). "Dividing Flow in Closed Conduits with 90° Branch," Master Thesis, Concordia University, Montreal, Canada.

Petermann, F. (1929). "Loss in Oblique-angled Pipe Branches." Bulletin 3, Trans. Hydraulic Institute, Munich Technical University, Munich, Germany.

Popp, M. and Sallet, D. W. (1983). "Experimental Investigation of One- and Two-Phase Flow," *Intl. Conf. on the Physical Modelling of Multi-Phase Flow, BHRA Fluid Engg.*, 67-90

Rajaratnam, N. (1967). "Constant Velocity Concept for Supercritical Branch Channel Flow", *J. Central Board Irr. and Power*, 19(1), 17-21.

Ramamurthy, A. S. and Carballada, L. B. (1979). "Lateral Flow Past a Barrier", *J.Fluid Engg., ASME*, 101(4), 449-452.

Ramamurthy, A. S. and Carballada, L. B. (1980). "Lateral Weir Flow Model", *J. Irr. and Dr. Div., ASCE*, 106(1), 9-25.

Ramamurthy, A. S., Tim, U. S. and Carballada, L. B. (1986). "Lateral weirs in trapezoidal channels," J. of Irrigation and Drainage Engg., ASCE, 112(2),

Ramamurthy, A. S. and Satish, M. G. (1988). "Division of Open Channel Flow in Short Branches," J. Hy. Engg., ASCE, 114(4), 428-438.

Ramamurthy, A. S., Zhu, Weimin and Carballada, L. B. (1994). "Flow past a two-dimensional lateral slot," J. Env. Eng., ASCE, 120(6), 1632-8.

Ramamurthy, A. S., Zhu, Weimin and Vo, Diep (1995). "Rectangular Lateral Weirs in Circular Open Channels," J. Hydr. Engg. ASCE, 121(8), 608-612.

Rawn, A. M., Bowerman, F. R. and Brooks, N. H. (1960). "Diffusers for Disposal of Sewage in Sea Water," J. Sanit. Eng., ASCE, 86(2), 65-105

Serre, M. and Odgaard, A. J. (1994). "Energy loss at combing pipe junction," J. Hydr. Engg. ASCE, 120(7), 808-830.

Subramanya, K. and Awasthy, S. C. (1972). "Spatially Varied Flow over Side Weirs," *J. Hyd. Div., ASCE*, 98(1), 1-10.

Thoma, D. (1929). "The Hydraulic Loss in Pipes," World Power Conference, Tokyo, Japan, Vol.2, p.446.

Toch, A. and Moorman, R. W. (1953). "Manifold Efflux," State University of Iowa, Studies in Engineering, Bulletin 35, No.427, 63-72.

Tran, D. M. (1988). "Junction Flow in Open Channels," Ph.D. Thesis, Concordia University, Montreal, Canada.

Tsakonas, S. (1957). "Dividing Flow Through a Divergent Inlet Conduit," J. Hyd. Div. ASCE. 83(6), 1492-26.

Uyumaz, A., and Muslu, Y. (1985). "Flow over side weirs in circular channels." *J. Hyd. Engg., ASCE*, 111(1), 144-160.

Uyumaz, A., and Muslu, Y., (1987). Closure of paper "Flow over side weir in circular channels" *J. Hyd. Engg, ASCE*, 113(5), 688-690.

Vogel, G. (1929). Experiments to determine the loss at right angle pipe tees. In Hydraulic laboratory practice (ed. J. R. Freeman), pp. 470-2. Published by ASME (Translation, with additions, of Die Wasseebaulaboratorien Europas, 1926, published by Verein Deutscher Ingenieure).

Volkart, P. U. (1983). "Spatially Varied Flow Over Short Side-Weirs in Channels of Circular Shape," *XX_IAHR Congress, VI(D. b.), Moscow*, 519-526.

Ward-Smith, A. J. (1980). "Internal Fluid Flow," Oxford University Press, Oxford.

Williamson, J. V. and Rhone, T. J. (1973). "Dividing flow in branch and wyes," *J. Hyd. Engg. ASCE, 99(5)*, 747-769.

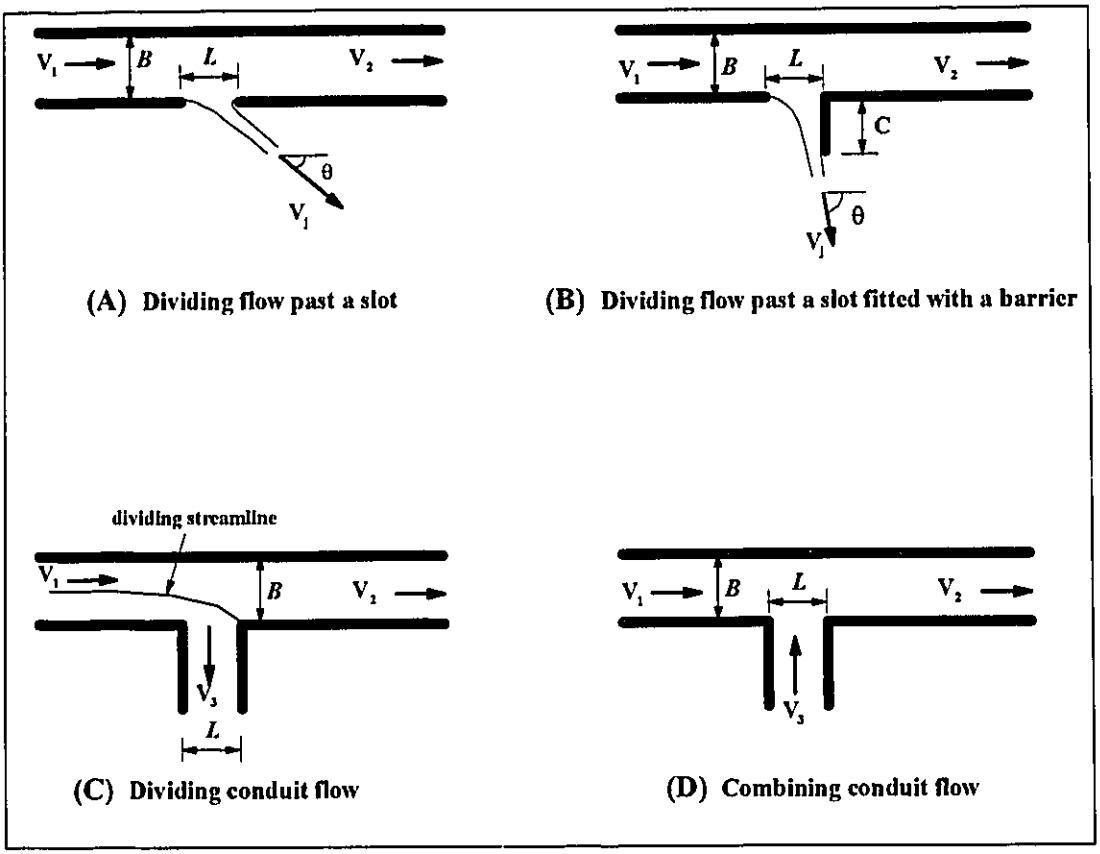

Fig. 1.1 Two-dimensional Flow Configurations

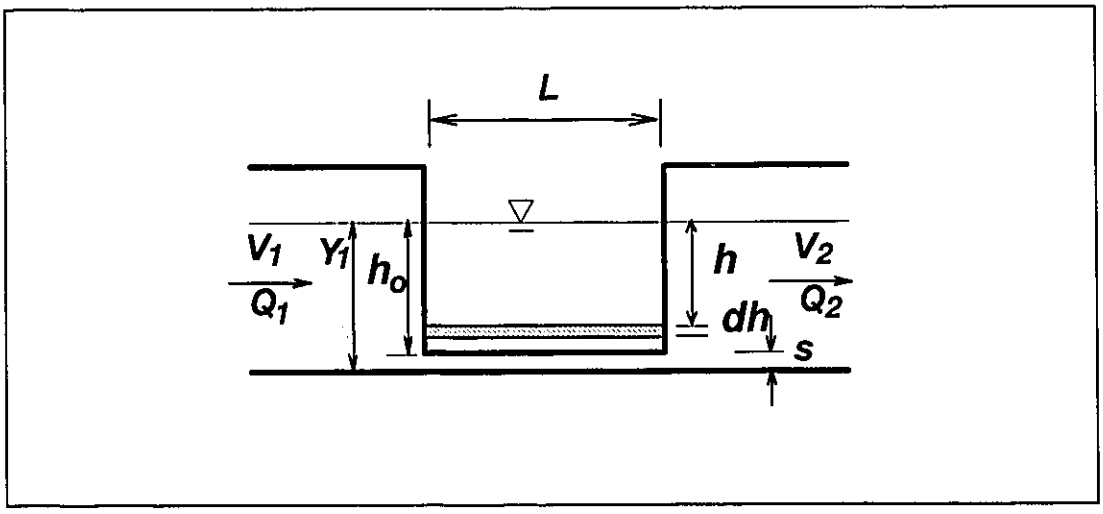

Fig.1.2 Lateral weir model

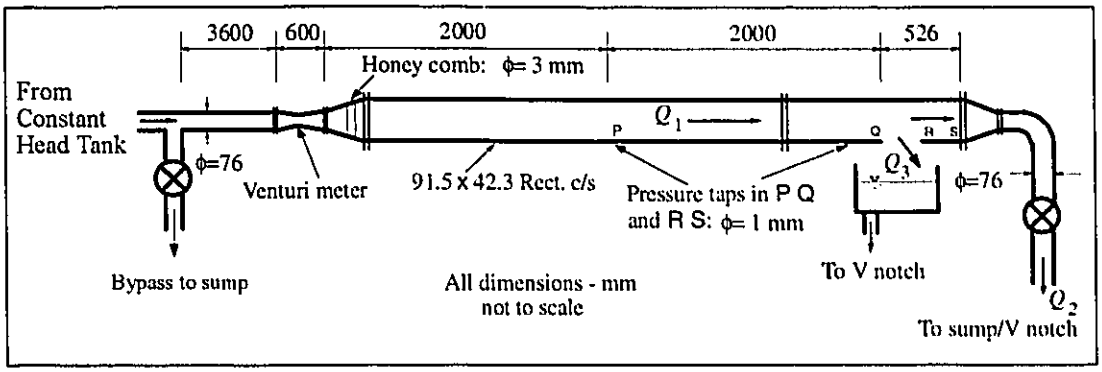

Fig. 2.1 Two-dimensional slot test set-up

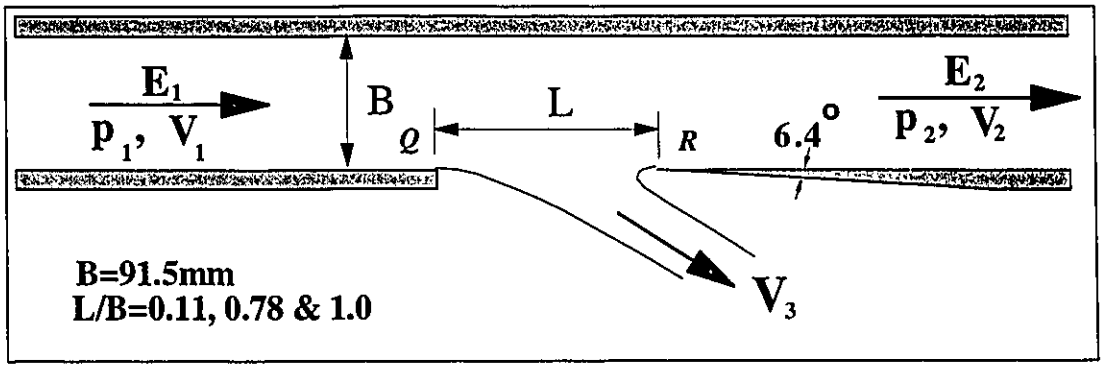

Fig. 2.2 Detail of the slot *Q-R*

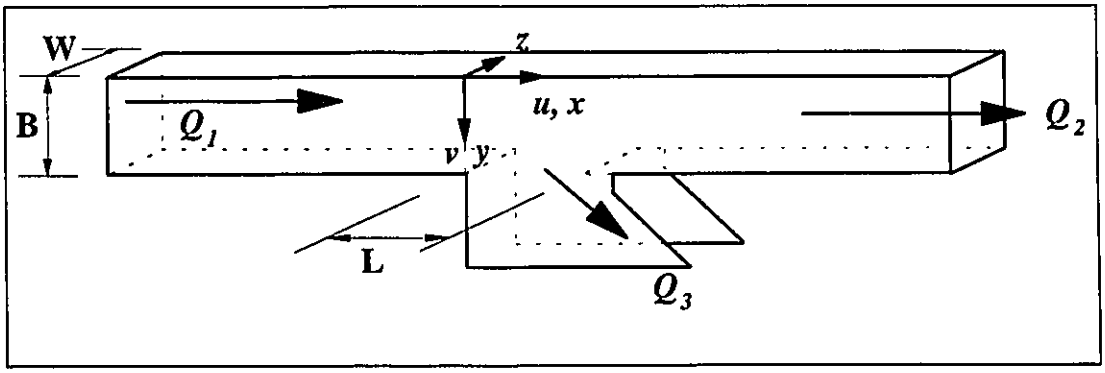

Fig. 2.3 Conduit geometry

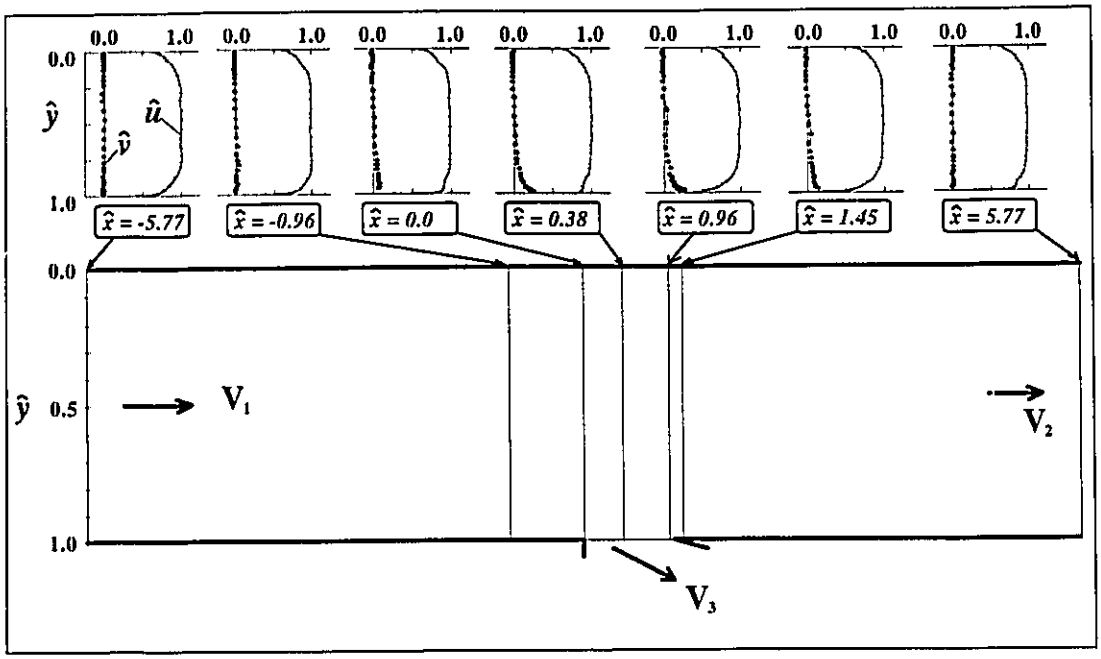

Fig. 2.4a Velocity Profile and Streamline Pattern (L/B = 0.11, Q_3/Q_1 = 0.04)
(Streamline was neglected)

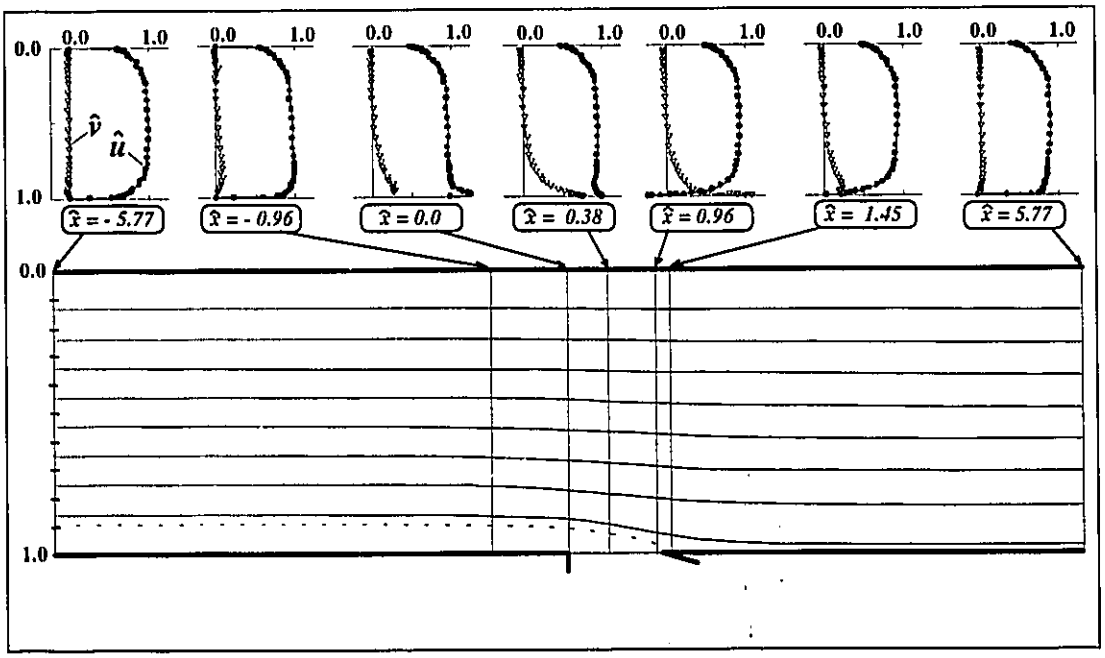

Fig. 2.4b Velocity Profile and Streamline Pattern (L/B = 0.11, Q_3/Q_1 = 0.10)

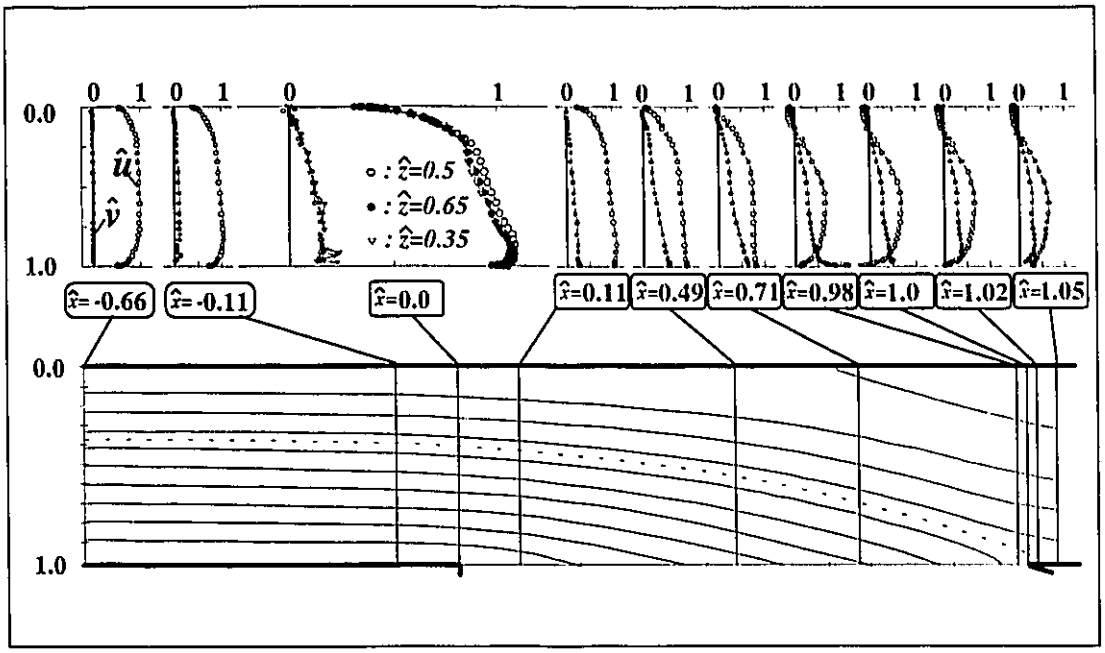

Fig. 2.4c Velocity Profile and Streamline Pattern (L/B = 1.0, Q_3/Q_1 = 0.65)

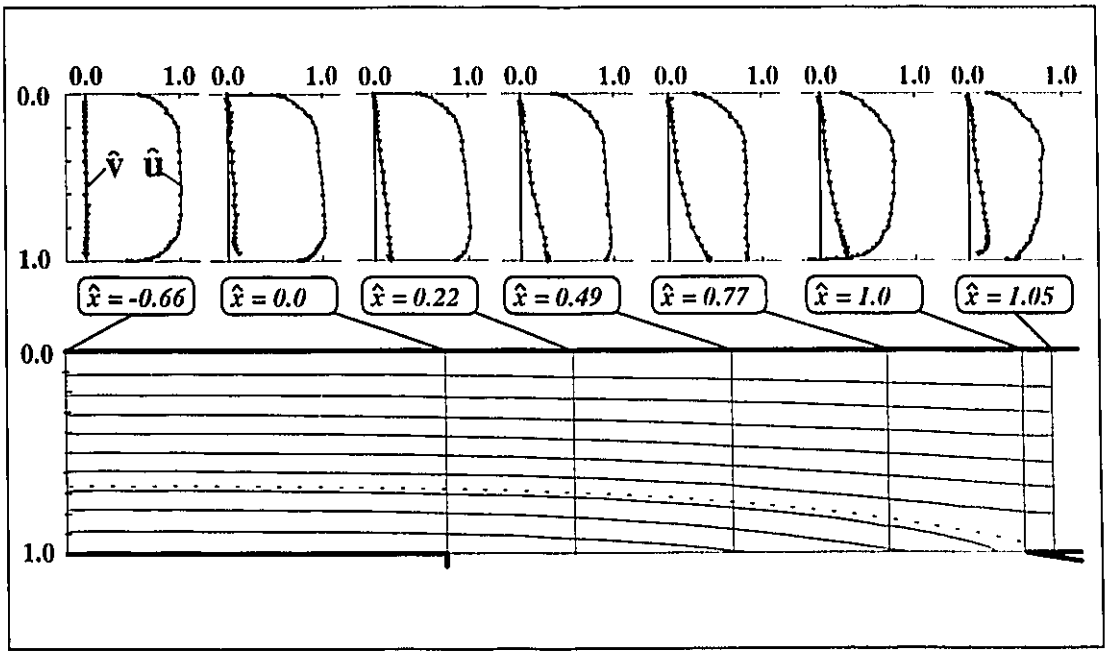

Fig. 2.4d Velocity Profile and Streamline Pattern (L/B = 1.0, Q_3/Q_1 = 0.33)

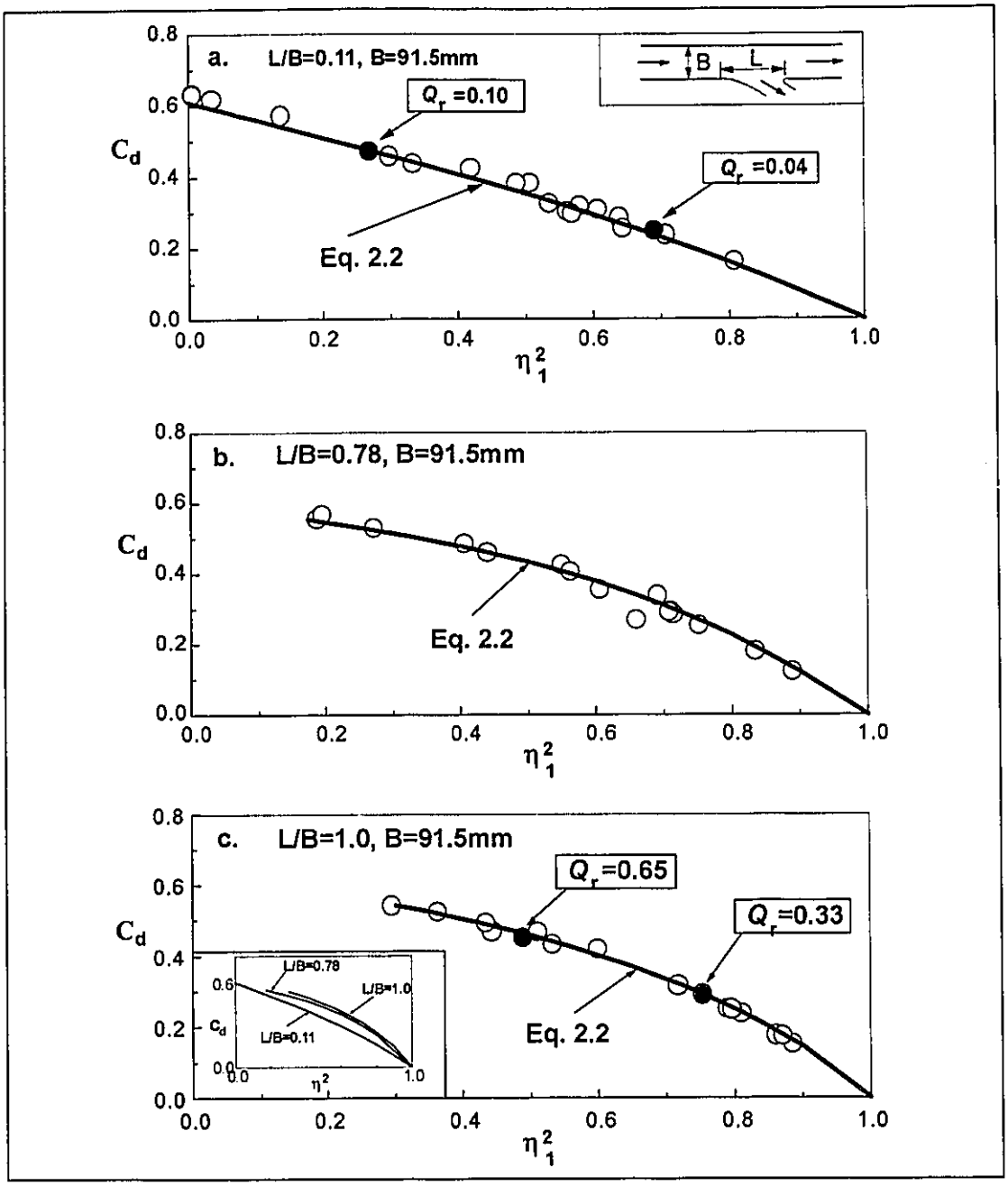

Fig. 2.5 Variation of C_d versus η_1^2

● — Tests with LDV measurements

○ — Tests without LDV measurements

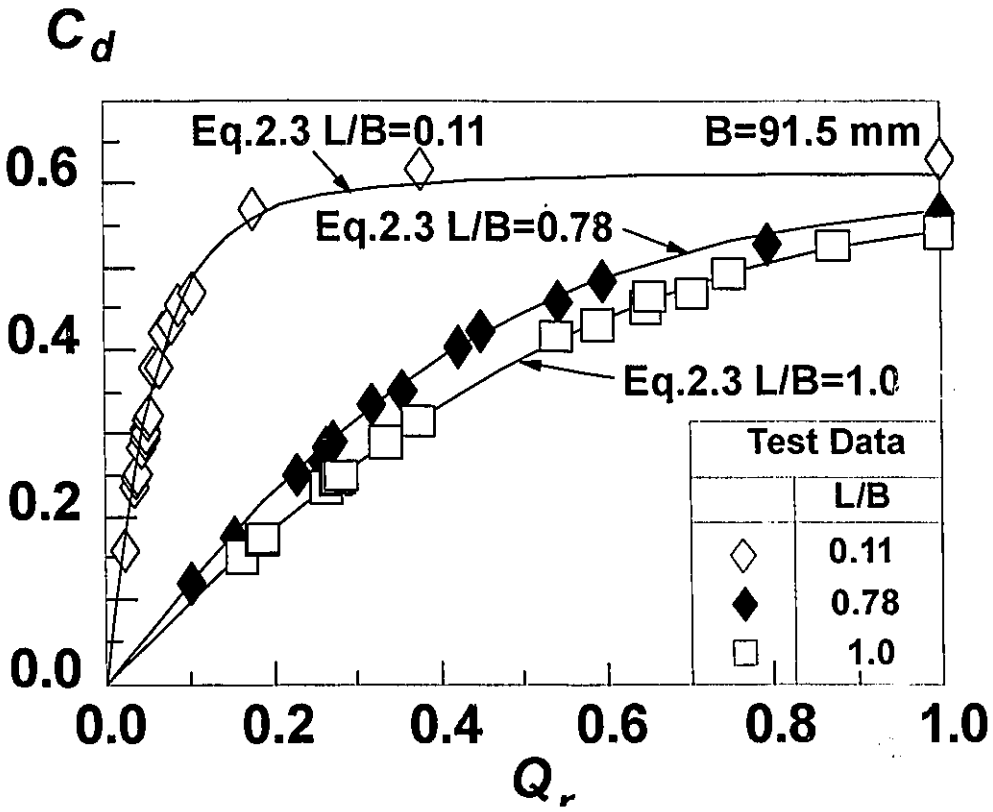

Fig. 2.6 Variation of C_d with Q_r (= Q_3 /Q_1)

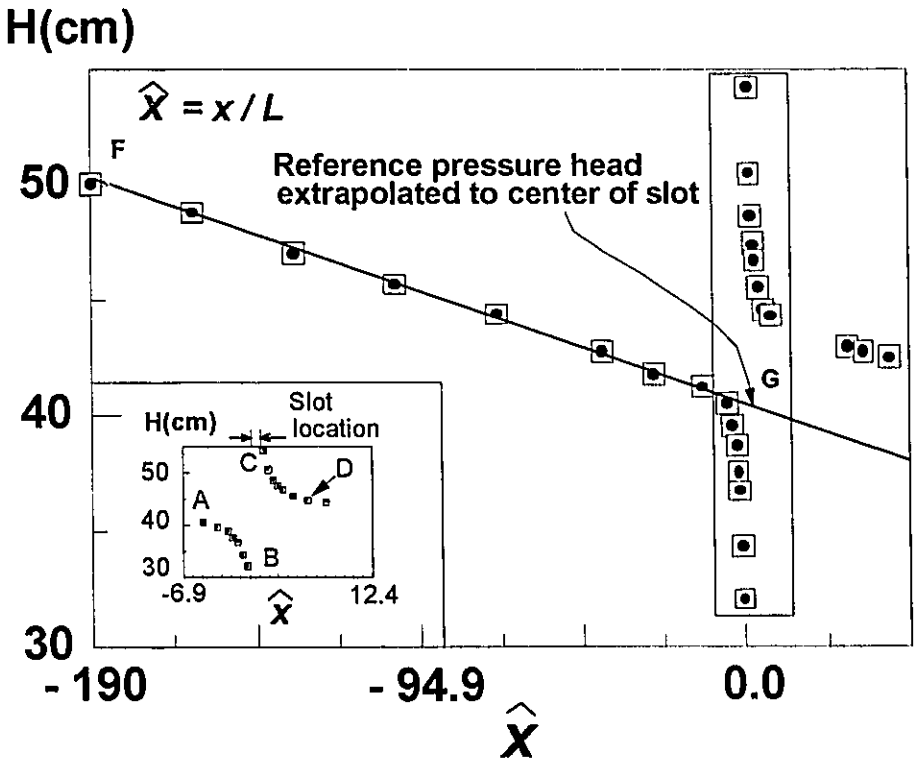

Fig. 2.7 Typical Pressure Head Distribution
(Insert shows details of pressure head)

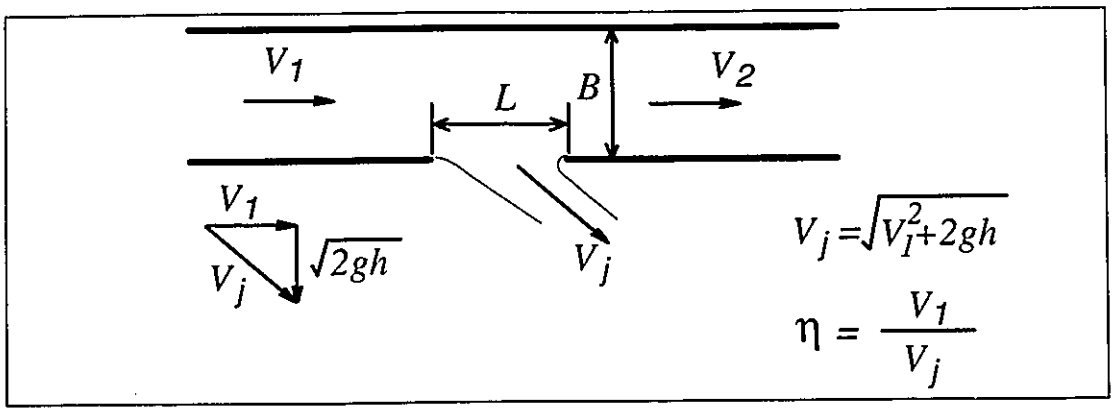

Fig. 3.1 Two-Dimensional Conduit Outlet Model

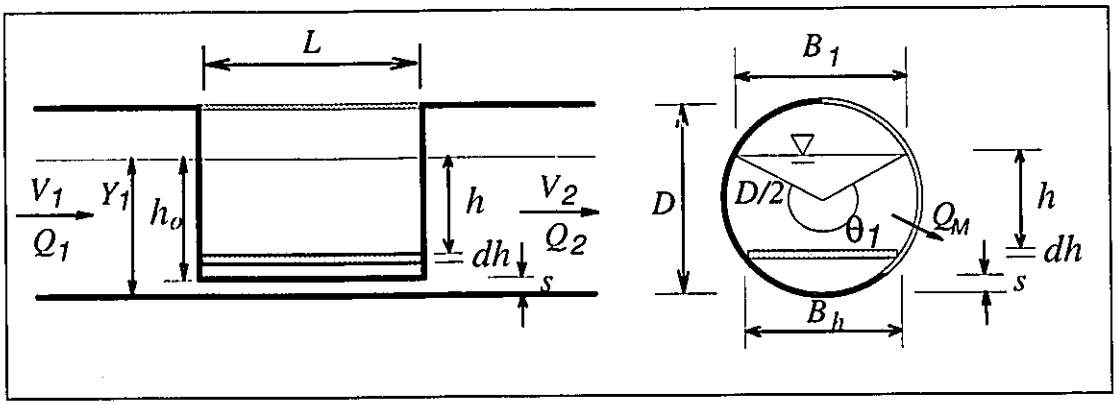

Fig. 3.2 A Rectangular Lateral Weir in A Circular Channel

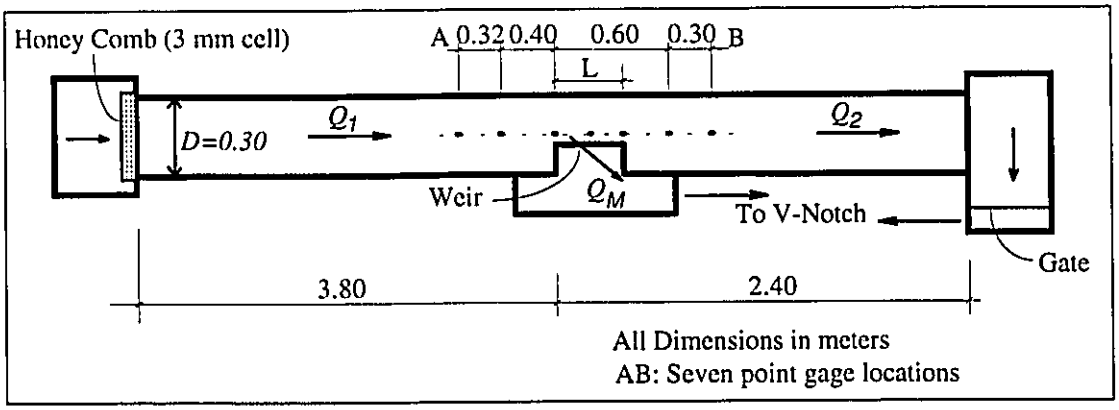

Fig. 3.3 Experimental setup

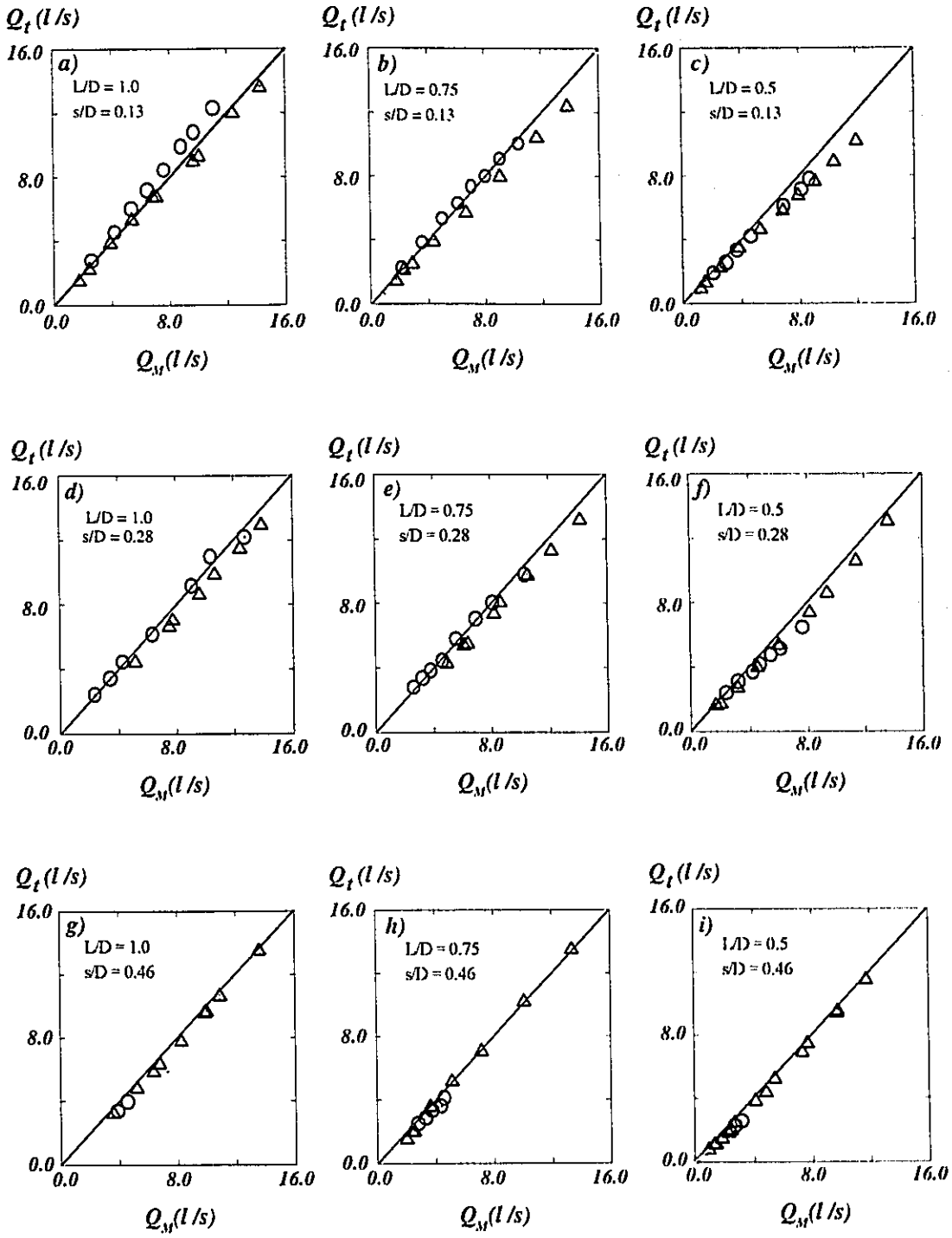

Fig. 3.4 Measured weir discharge Q_M vs theoretical discharge Q_t

(o — $F_1 > 1.0$, △ — $F_1 < 1.0$)

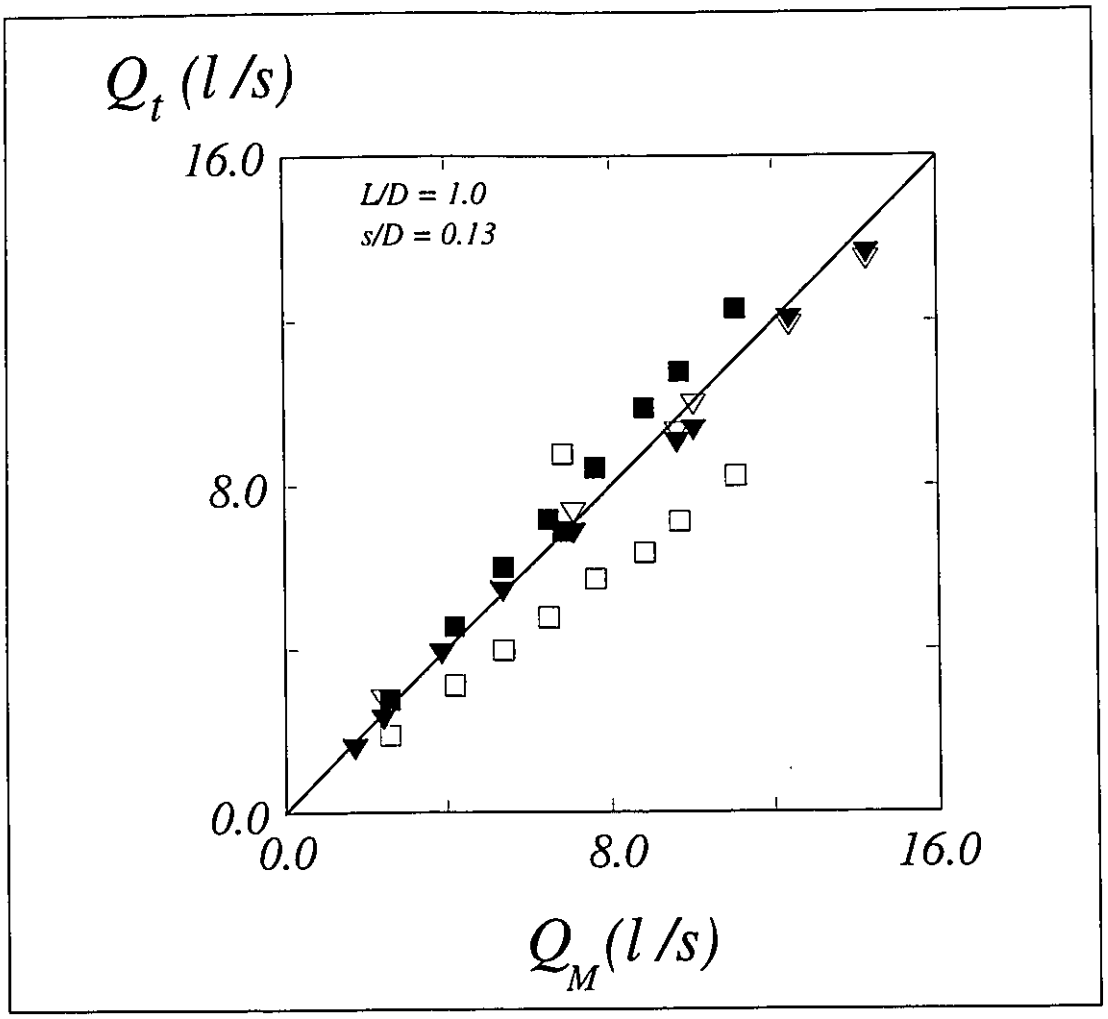

Fig. 3.5 Comparison of present model with Uyumaz's model (1985)

▽ (□) —Eq. 55 to Eq. 70, Uyumaz (1987) for F1 < 1 (F1 > 1)
▼ (■) —Present model for F1 < 1 (F1 > 1)

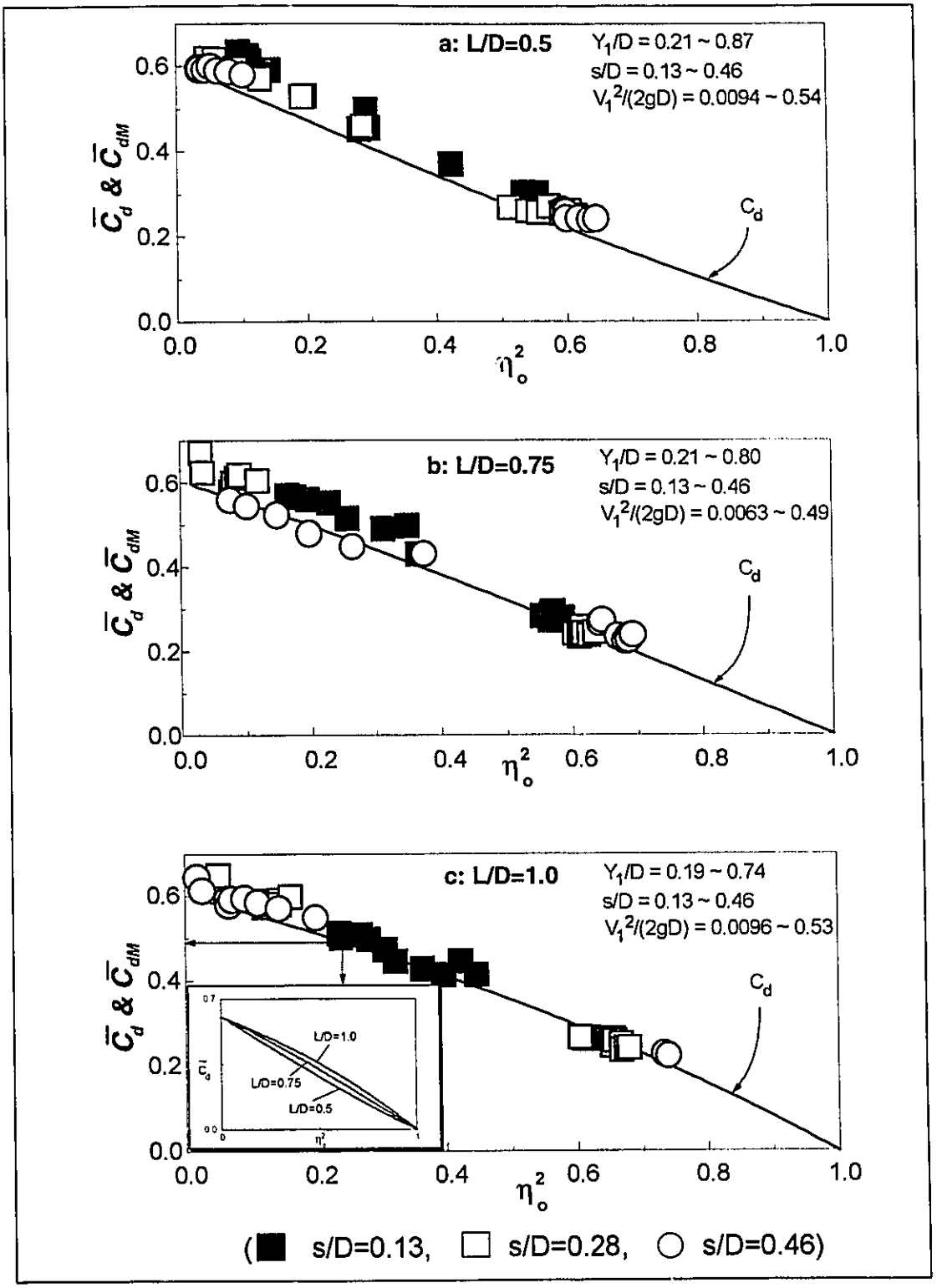

Fig. 3.6 Variation of $\bar{C}_d$ and $\bar{C}_{dM}$ with η_o^2

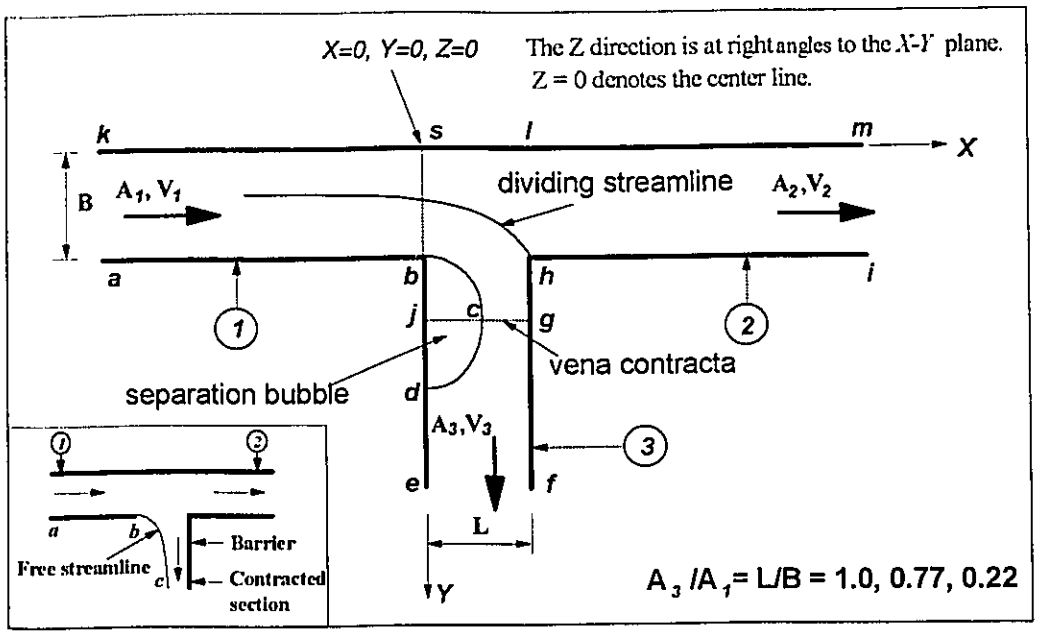

Fig.4.1 Dividing Rectangular Conduit Flow

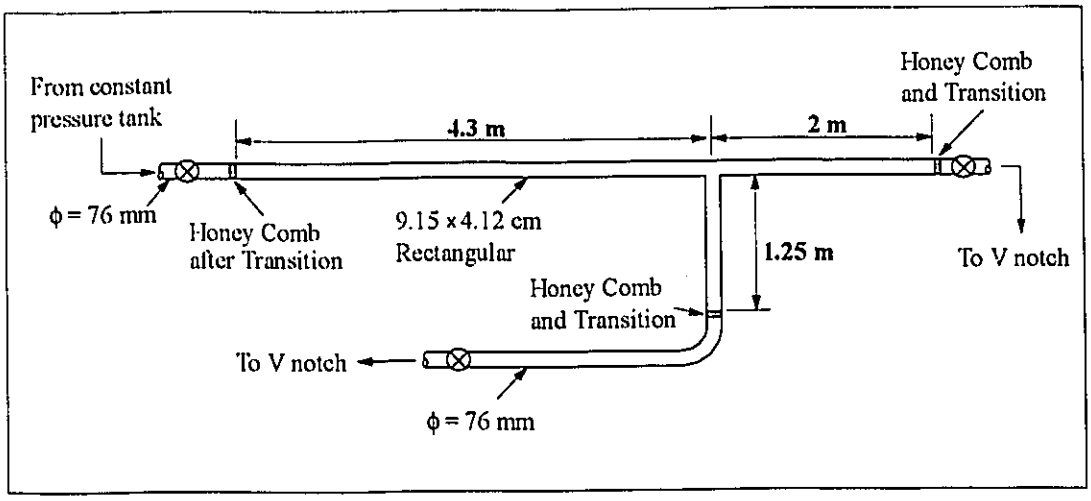

Fig.4.2 Dividing Rectangular Conduit Flow Test Set-up

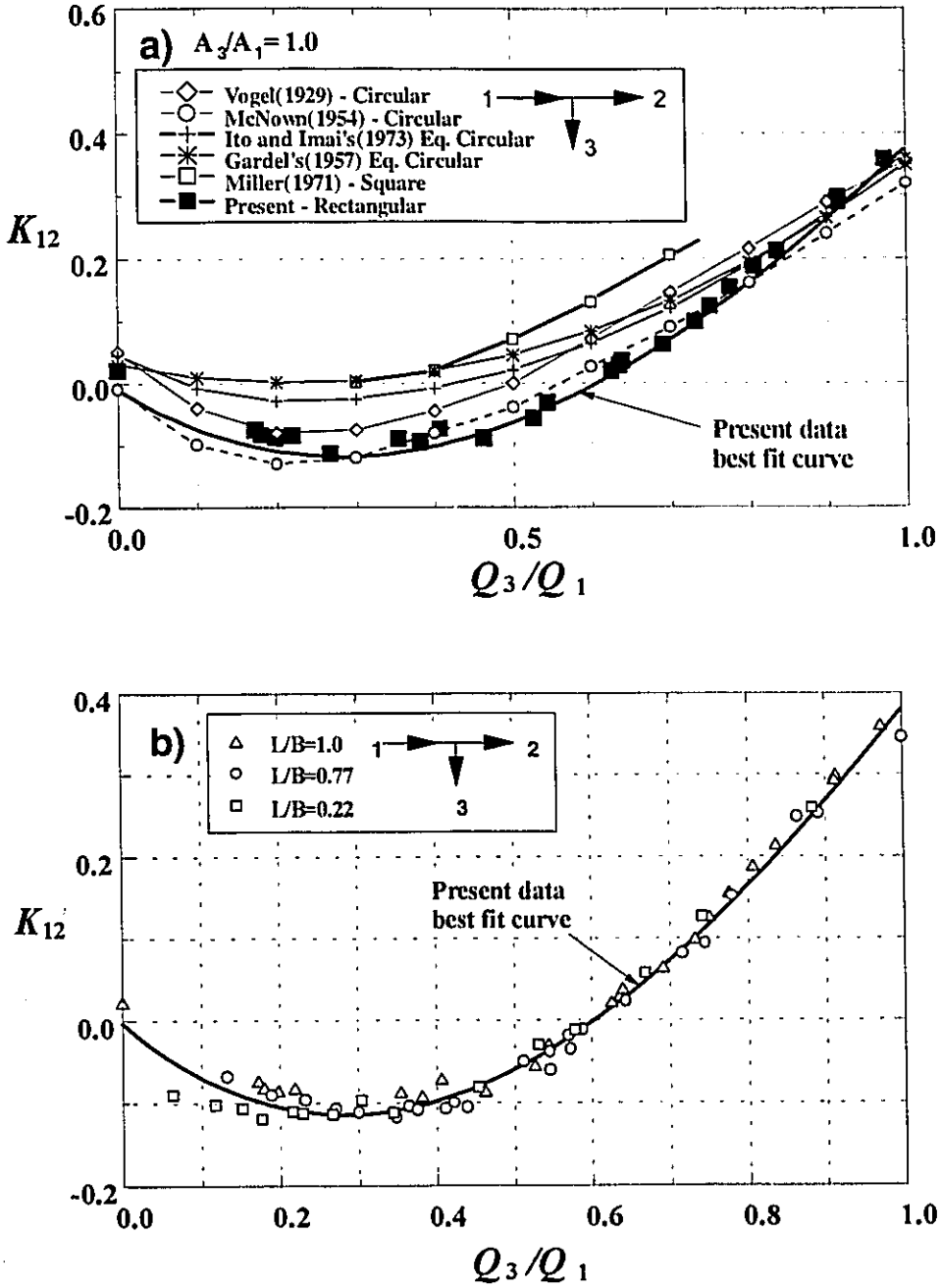

Fig. 4.3 Energy Loss Coefficient K_{12} for Dividing Closed Conduit Flow

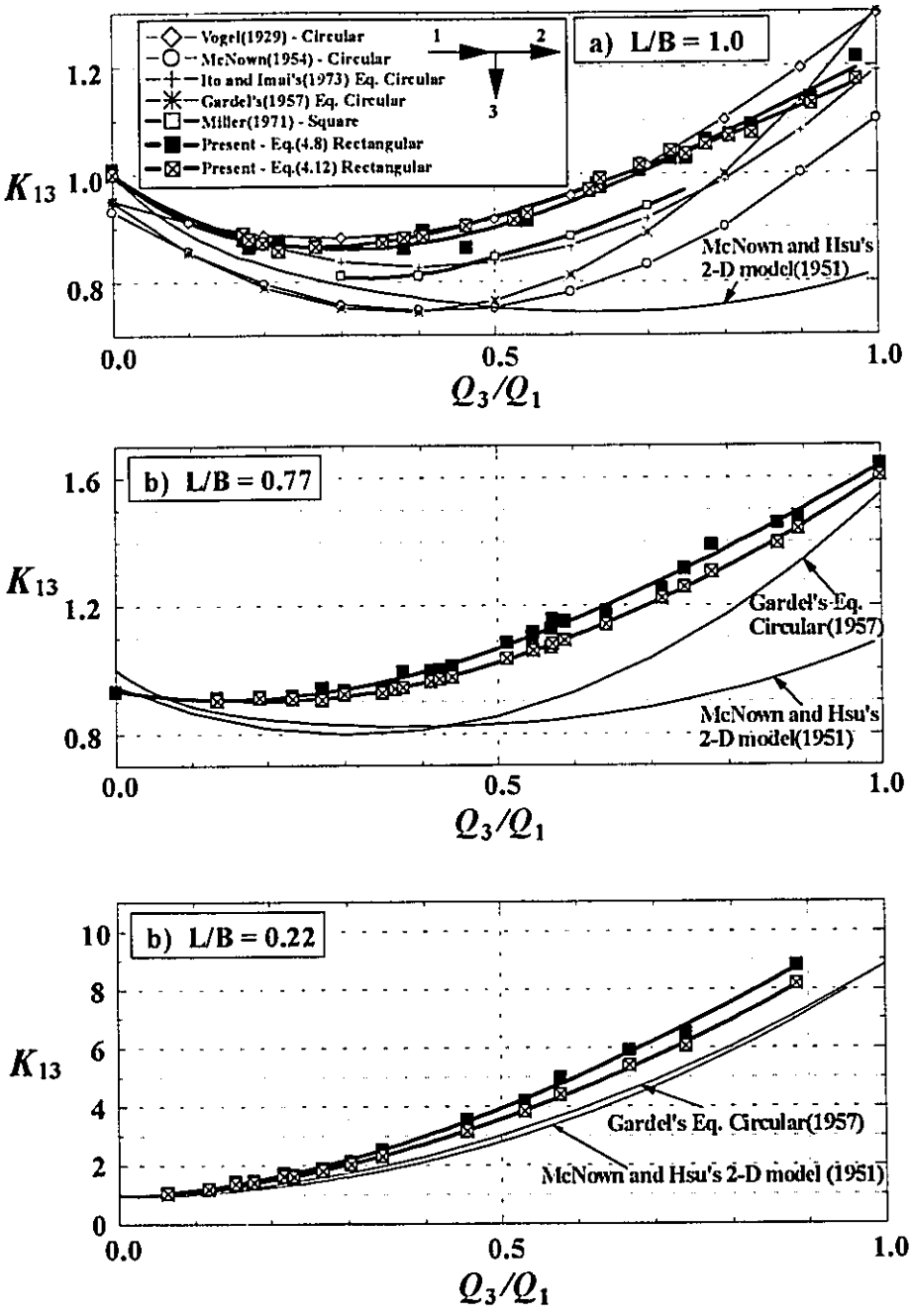

Fig.4.4 Energy Loss Coefficient K_{13} for Dividing Closed Conduit Flow

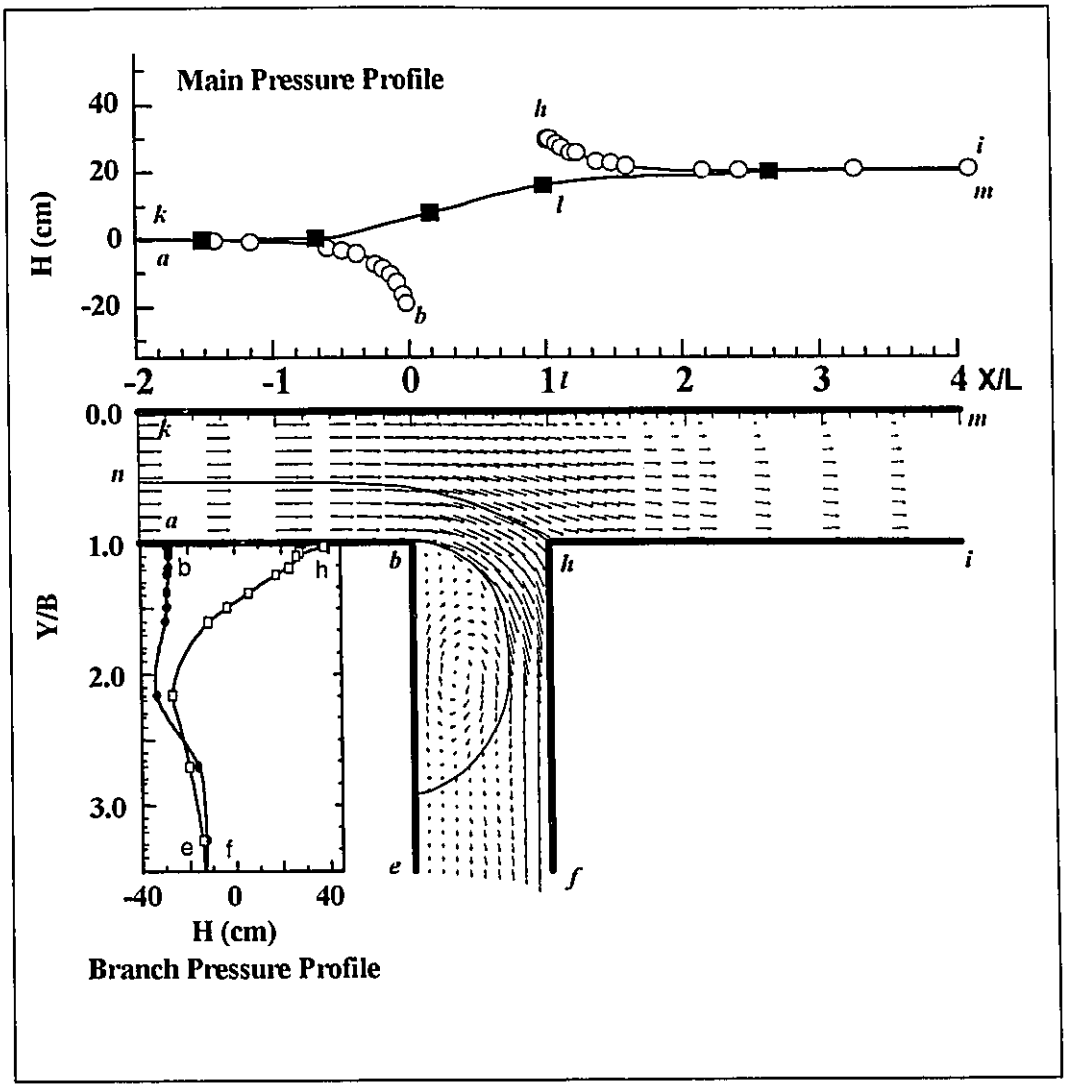

Fig.4.5a Flow Field and Pressure Profiles for Dividing Conduit Flow
L/B = 1.0, Q_3/Q_1 = 0.46

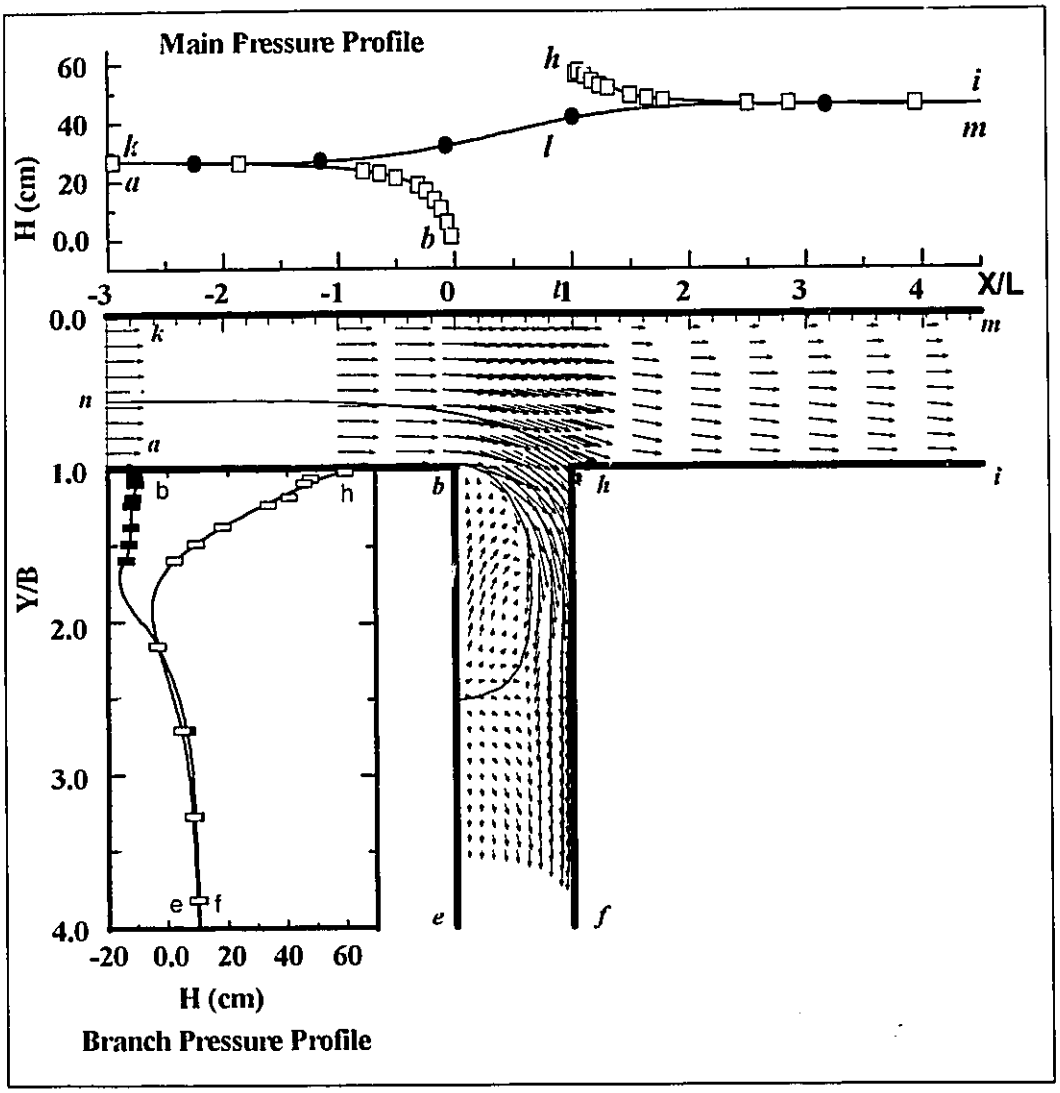

Fig.4.5b Flow Field and Pressure Profiles for Dividing Conduit Flow
$L/B = 0.77$, $Q_3/Q_1 = 0.42$

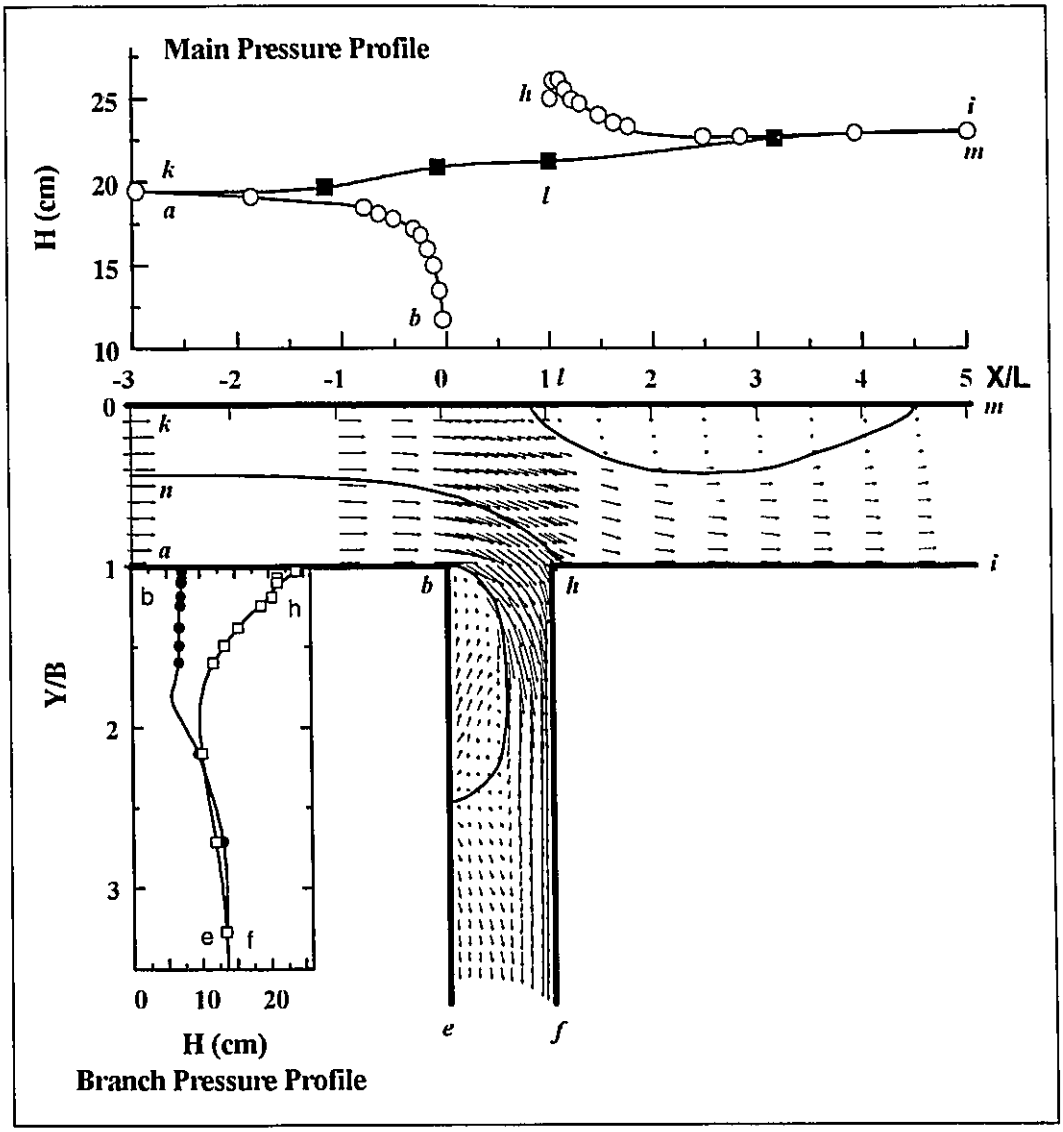

Fig.4.5c Flow Field and Pressure Profiles for Dividing Conduit Flow
$L/B = 0.77$, $Q_3/Q_1 = 0.57$

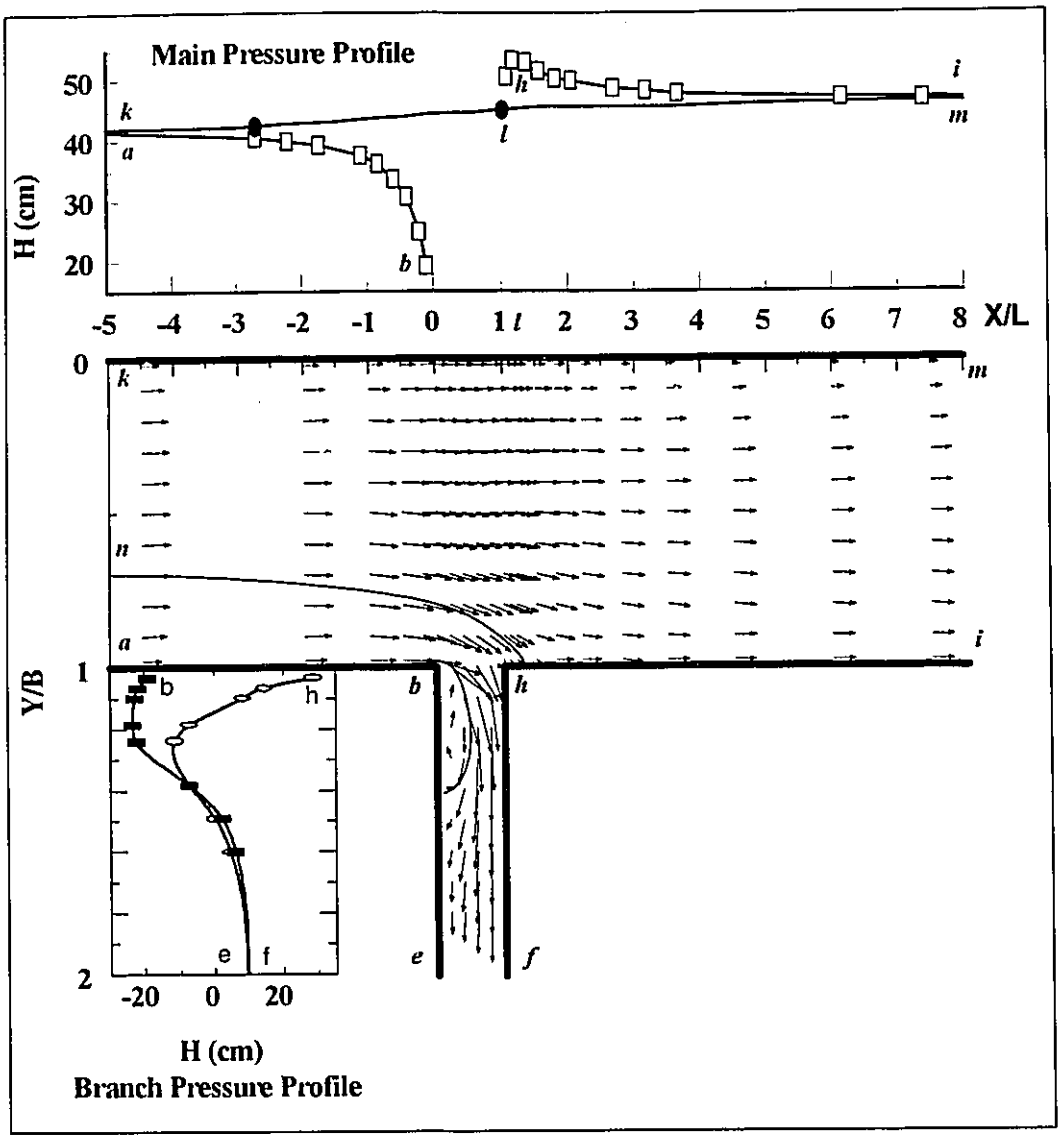

Fig.4.5d Flow Field and Pressure Profiles for Dividing Conduit Flow
$L/B = 0.22$, $Q_3/Q_1 = 0.30$

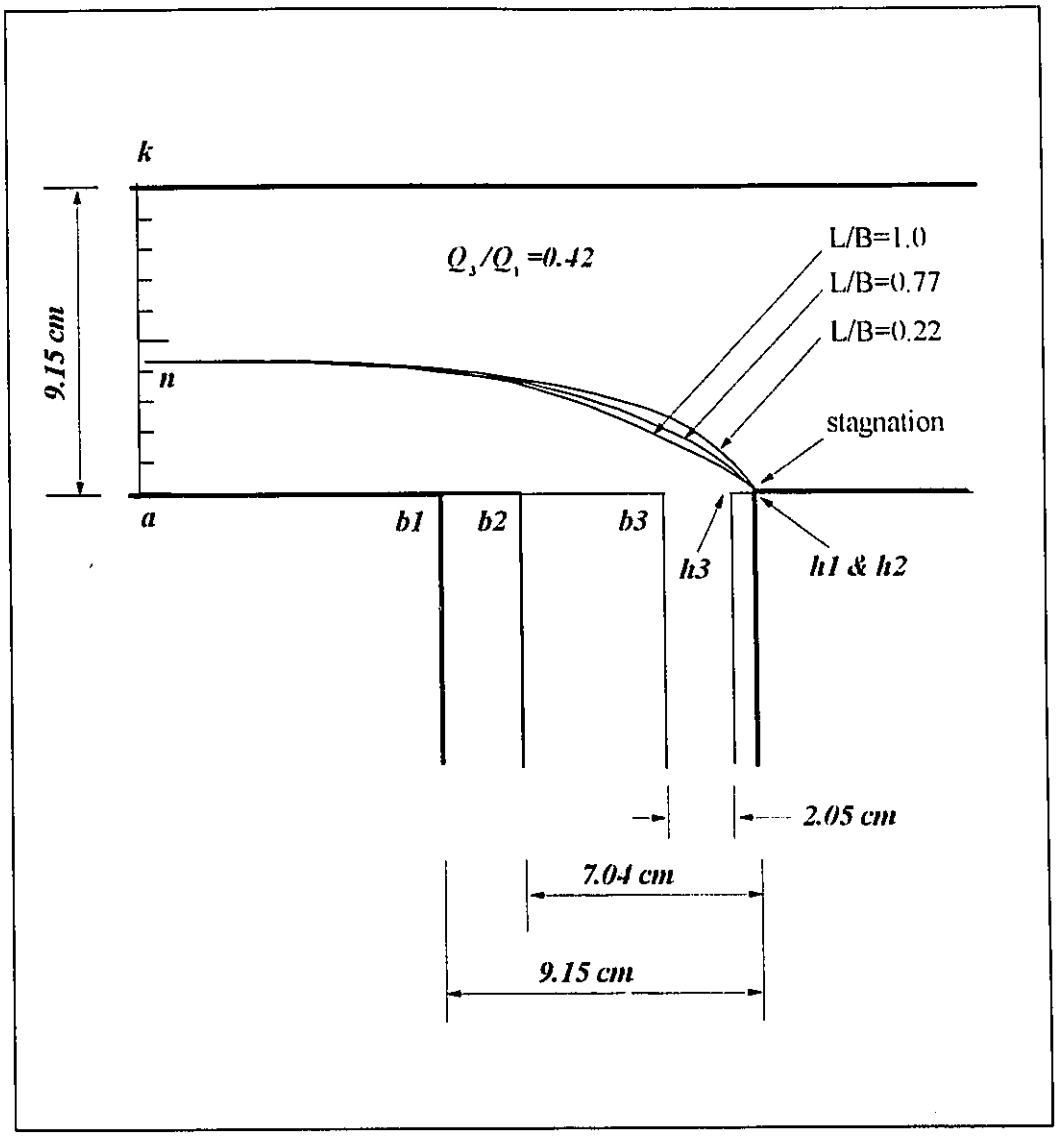

Fig.4.6 Dividing Streamline Pattern

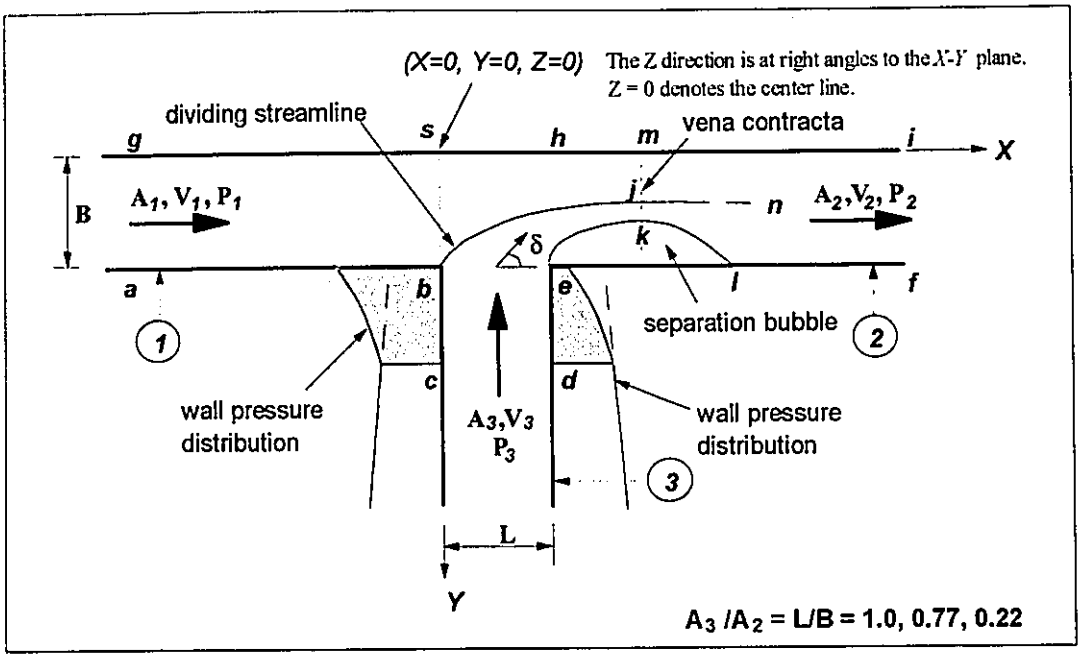

Fig.5.1 Combining Rectangular Conduit Flow Junction

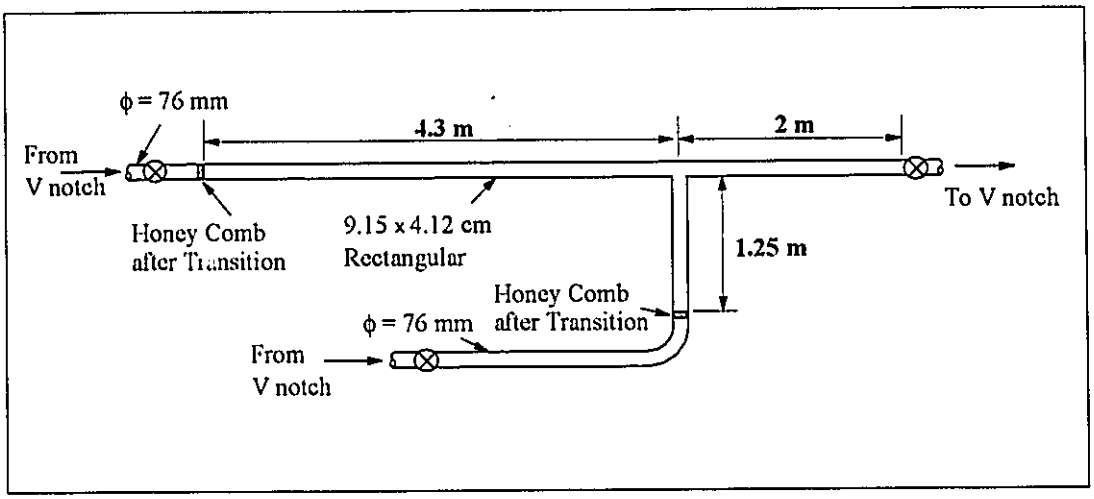

Fig.5.2 Combining Rectangular Conduit Flow Test Set-up

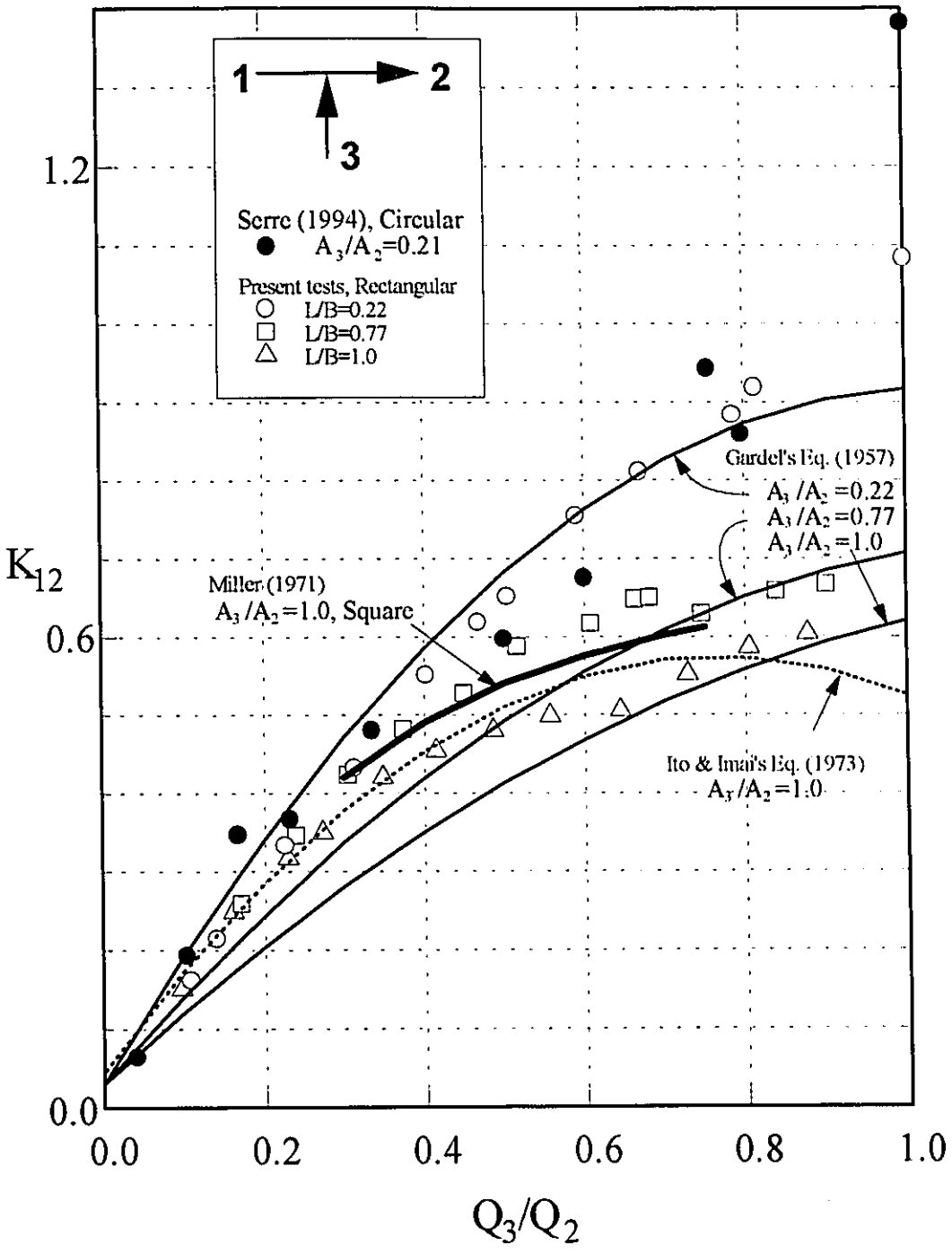

Fig.5.3a Combining Conduit Flow K_{12} vs Q_3/Q_2

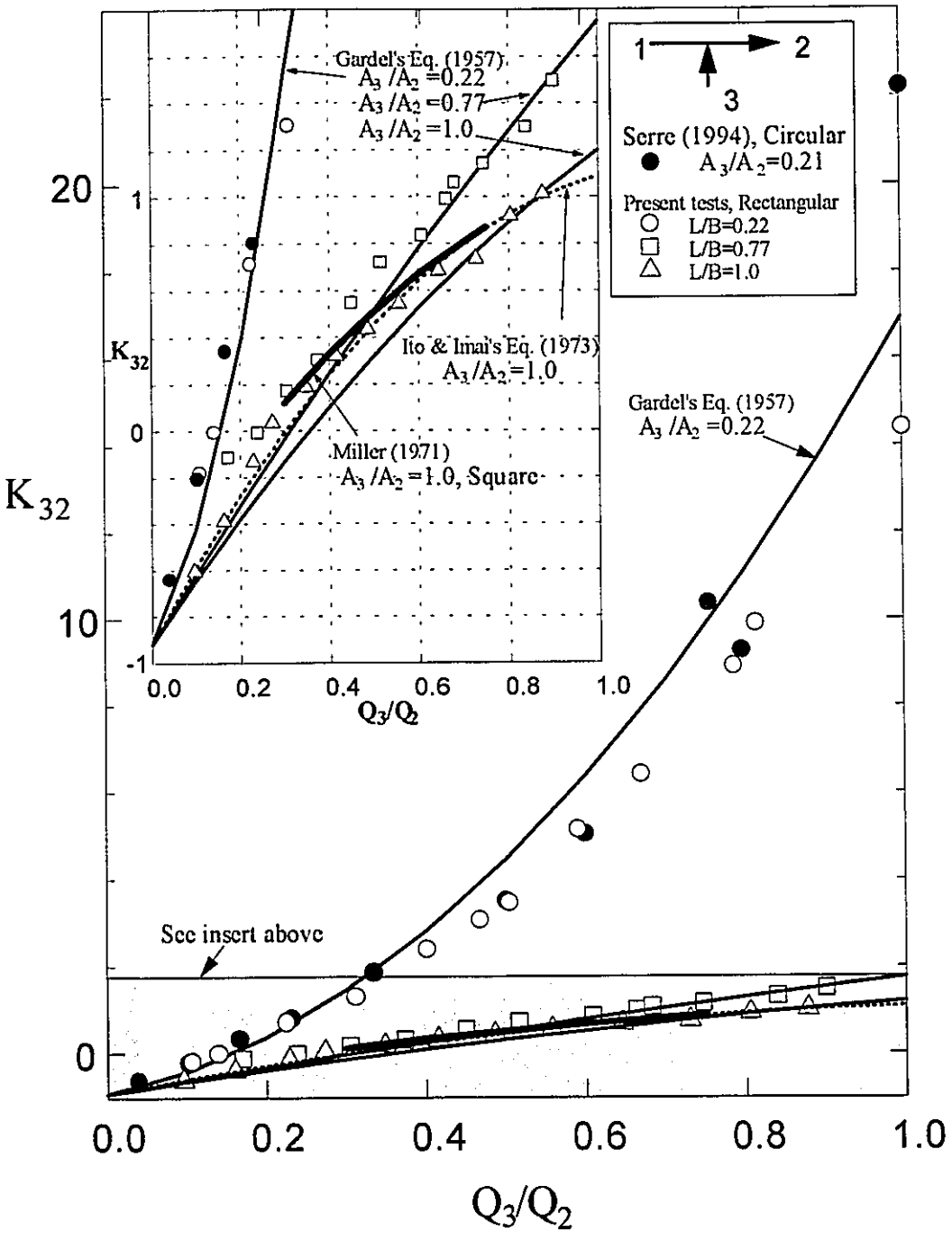

Fig.5.3b Combining Conduit Flow K_{32} vs Q_3/Q_2
Insert: Expanded Scale for Shaded Region of Fig.5.3b

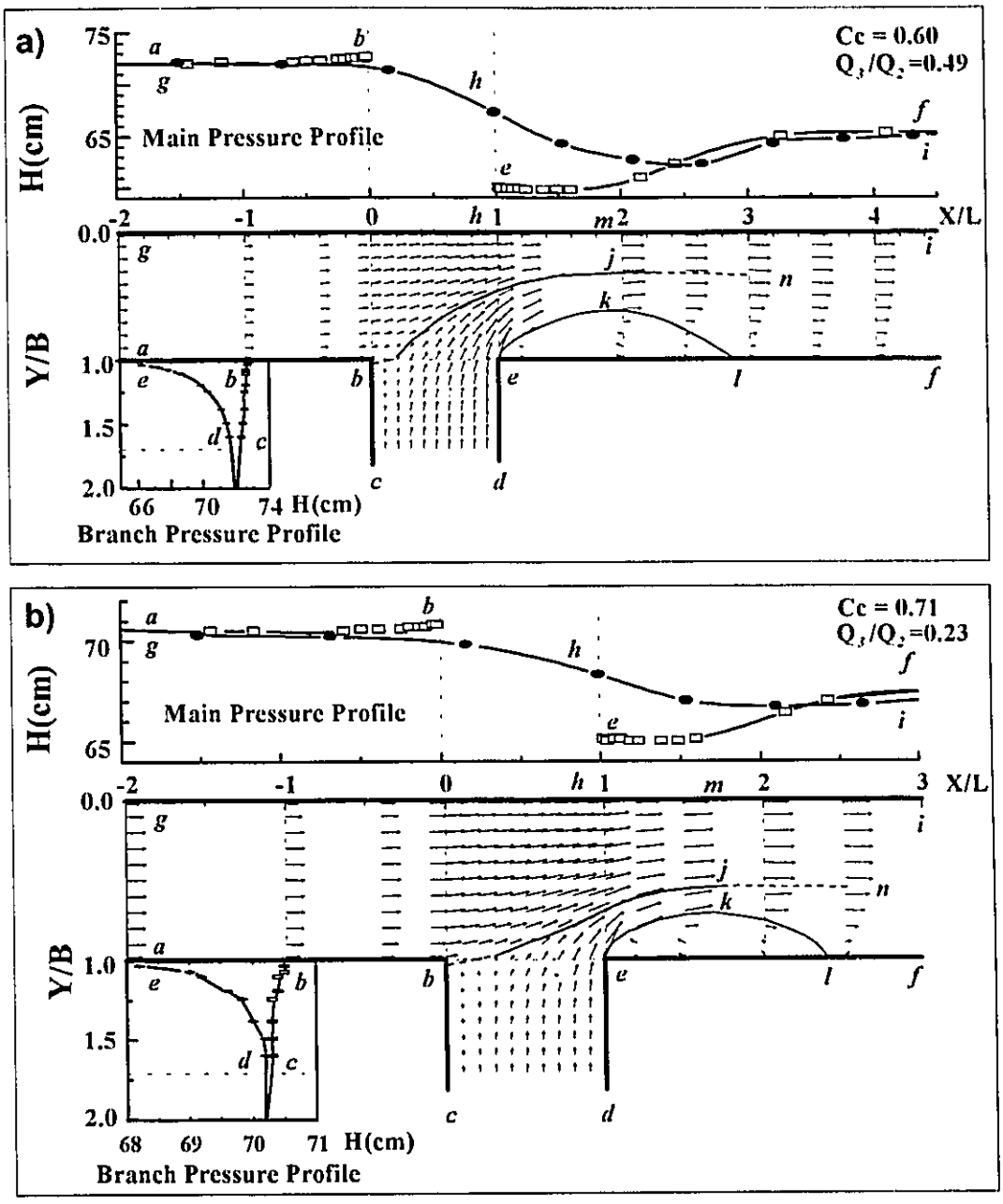

Fig.5.4 Flow Pattern and Pressure Profiles in Combining Conduit Flow L/B=1.0

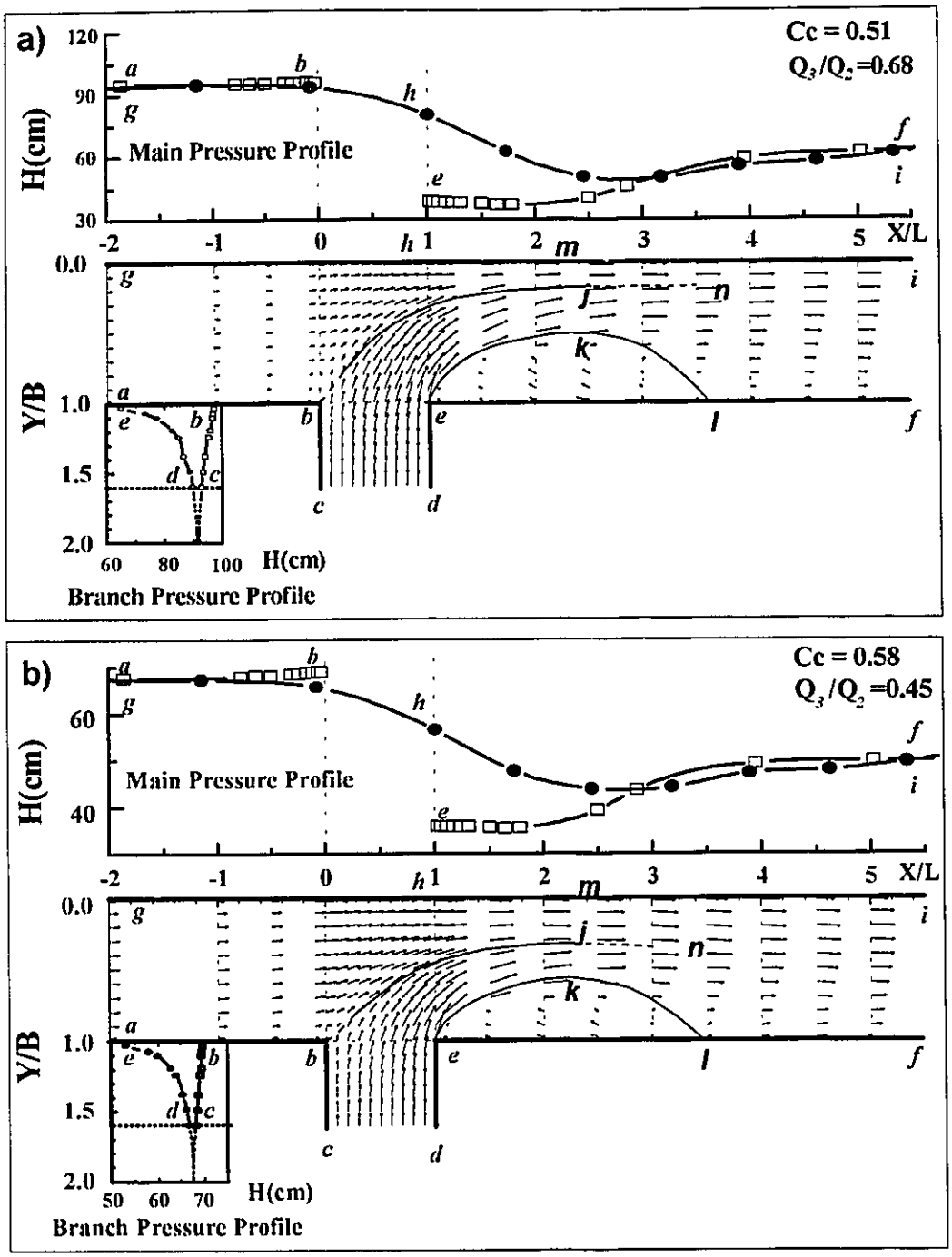

Fig. 5.5 Flow Pattern and Pressure Profiles in Combining Conduit Flow L/B = 0.77

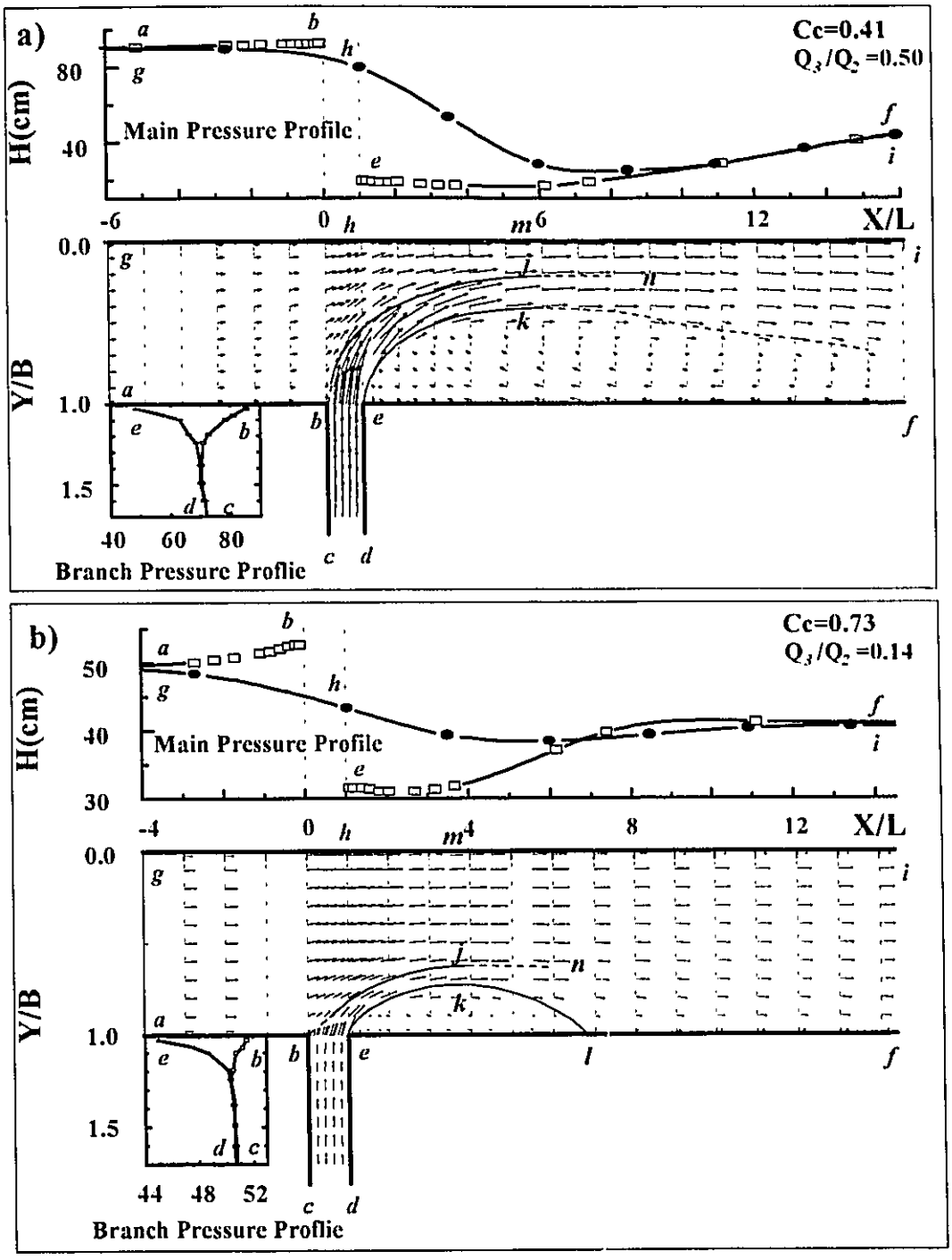

Fig.5.6 Flow Pattern and Pressure Profiles in Combining Conduit Flow L/B=0.22

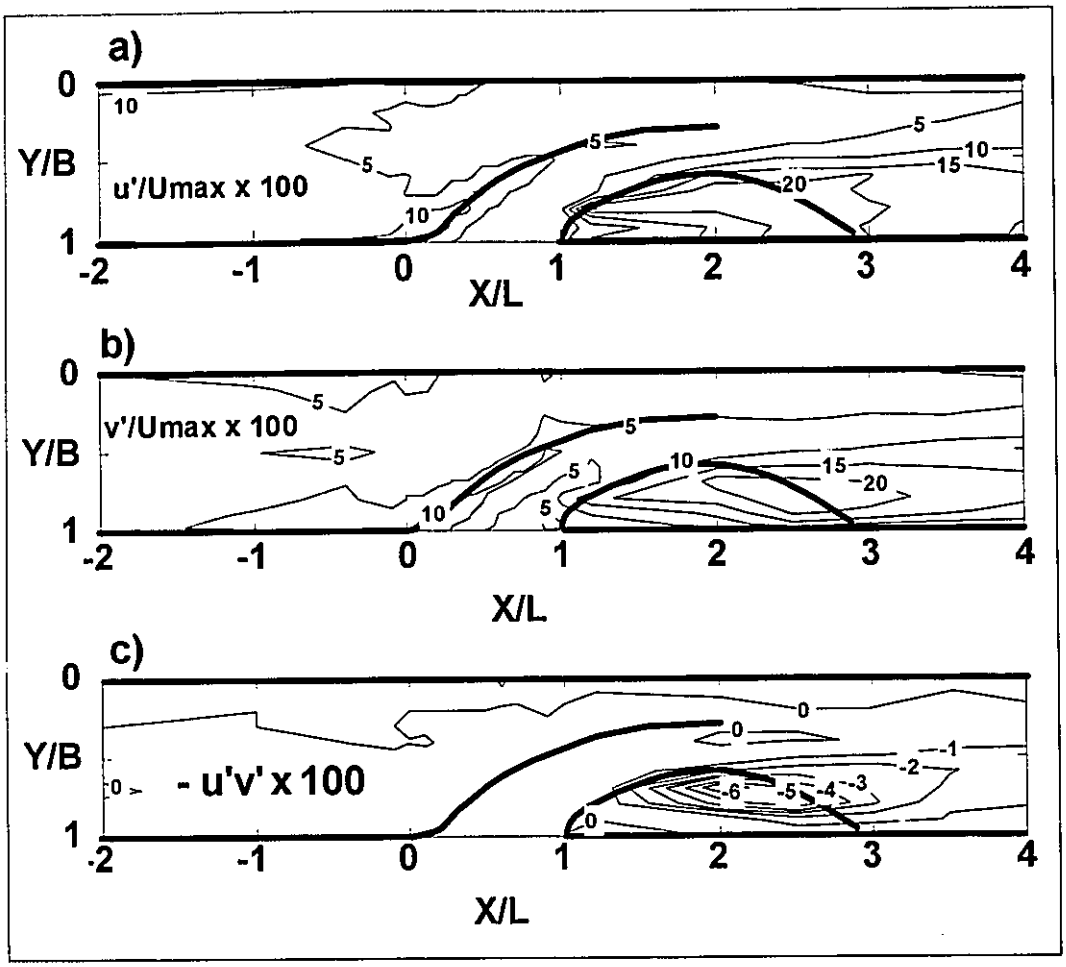

Fig.5.7 Turbulent Intensity and Shear in Main Conduit
of Rectangular Combining Flow, L/B = 1.0, $Q_3/Q_2 = 0.49$

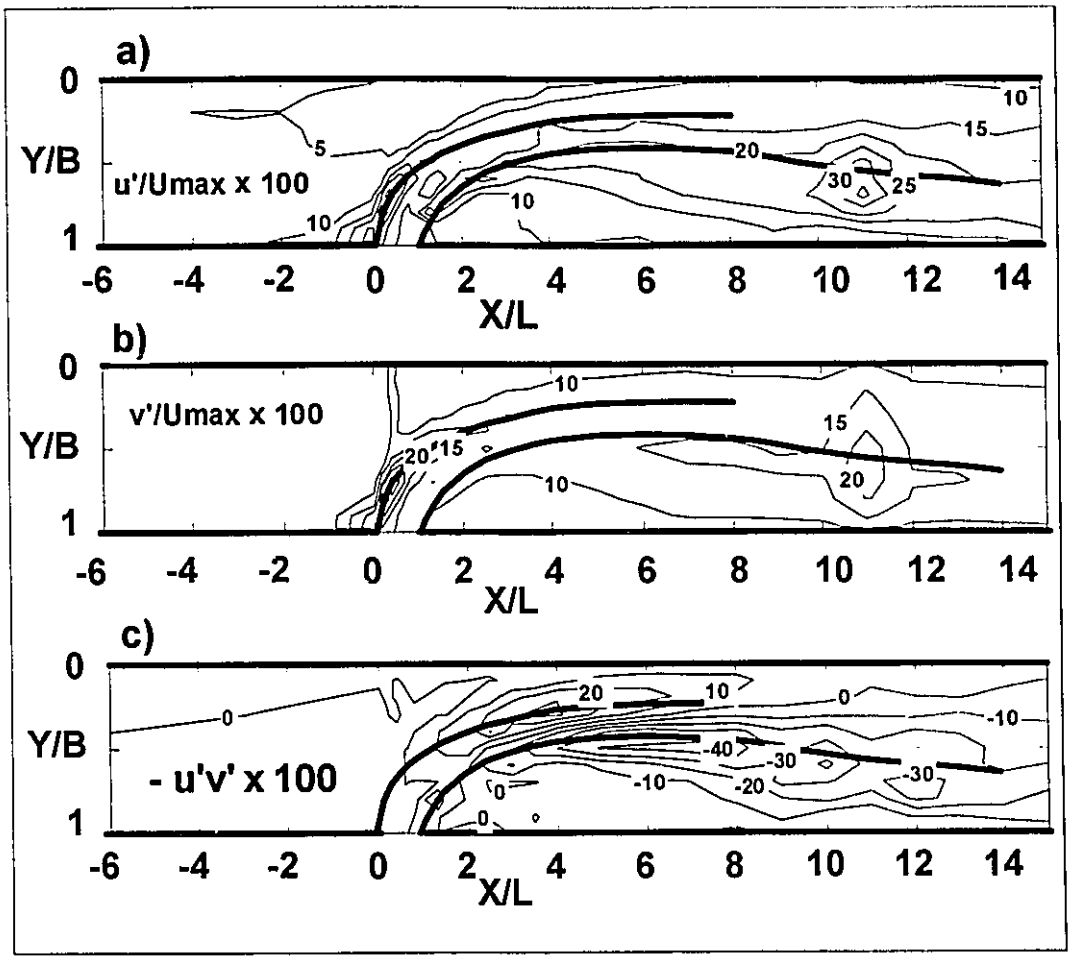

Fig.5.8 Turbulent Intensity and Shear in Main Conduit
of Rectangular Combining Flow, L/B = 0.22, $Q_3/Q_2 = 0.50$

Table 2.1 Experimental data of two-dimensional slot flow *L/B = 1.0*

tap No.	distance X(cm)	pressure head H (cm)								
1	-197.12	43.4	35.7	23.9	33.3	38.9	27.4	17.8	22	24.6
2	-166.38	42.1	34.2	22.3	30.3	35.8	24.9	17.2	21.1	23.5
3	-135.9	40.1	32	20.2	25.5	31.4	21.2	16.5	19.8	21.7
4	-105.42	38.1	30.1	18.1	21	26.9	17.6	15.8	18.5	20.3
5	-74.94	36.3	28.2	16.3	17.1	23	14.5	15.2	17.3	18.7
6	-43.1	34	25.9	13.9	12.6	18.5	10.9	14.45	16	17.2
7	-27.86	33.4	25.2	13.1	10.7	16.6	9.4	14.2	15.4	16.6
8	-12.62	31.8	23.9	11.7	8.2	14.4	7.4	13.5	14.5	15.9
9	-5	28.9	21.3	9.8	6.5	12	5.8	12.6	13	13.9
10	-3.5	26.6	19.4	8.5	5.6	10.6	5.1	11.7	12.2	13
11	-2.35	24.3	17.4	7.3	4.7	9.4	4.5	10.8	11	11.6
12	-1.85	22.6	16	6.4	4.3	8.7	4.1	10.2	10.3	11
13	-1.35	20.2	14	5.2	3.7	7.3	3.5	9.3	9.2	9.8
14	-0.85	16.7	11.2	3.6	2.9	6	2.6	8.2	7.8	8.3
15	-0.35	10.5	6.3	0.8	1.7	3.6	1.7	5.7	5.2	5.3
16	9.5	55.2	51	38.7	38.7	55.8	33.7	17.5	27.9	31.8
17	10	52.4	48	33.8	32.6	49.6	29.3	18.2	29	31.8
18	10.5	50	46.1	32.3	29.6	46.2	26.1	18.3	27.2	30.7
19	11	47.4	43.7	30.5	27.8	43.7	25.9	18.5	26.9	29.6
20	11.5	46	41.9	29.6	26.4	42.4	24.6	17.2	24.6	28.7
21	12.65	44.4	39.4	28.4	24.3	39.8	23.3	17.6	24.8	27.3
22	14.15	43.2	37	27	23.1	38.5	22.4	17.5	23.4	25.7
23	16.15	42.5	35.6	25.8	22.3	37.1	22.2	17	21.7	24.8
24	30.95	42.6	35.2	25	19.8	35.1	18.2	16.85	21.2	24.2
25	36.03	43.1	35.5	25.2	19.5	34.85	17.8	16.85	21.4	24.3
26	43.65	43.6	36.2	25.4	18.7	34.5	17.5	16.85	21.8	25.2
Discharge, discharge ratio, velocity parameter, discharge coefficient, and Reynolds numbers										
Q_1 (*l/s*)		7.38	7.47	7.61	11.4	11.31	9.96	3.95	5.6	6.34
Q_2 (*l/s*)		6.44	5.59	4.11	1.85	3.18	1.87	3.95	3.94	4.11
Q_r		0.87	0.75	0.54	0.16	0.28	0.19	1	0.7	0.65
η_1^2		0.36	0.44	0.6	0.89	0.79	0.86	0.3	0.44	0.49
C_d		0.52	0.49	0.42	0.15	0.25	0.17	0.54	0.47	0.45
$Re_1 \times 10^{-5}$		1.13	1.14	1.16	1.74	1.73	1.52	0.6	0.86	0.97
$Re_2 \times 10^{-5}$		0.14	0.29	0.54	1.46	1.24	1.24	0	0.25	0.34

Table 2.1 (continued)

tap No.	distance X(cm)	pressure head H (cm)							
1	-197.12	24.8	33	32.2	24.7	12.9	13.9	33.4	38.3
2	-166.38	22.9	30	29.9	23.5	12.1	12.6	30.8	35.2
3	-135.9	19.9	25.2	26.3	22.7	11	10.7	26.5	30.5
4	-105.42	17.4	20.9	23.2	18.8	10.2	9.1	22.6	26.2
5	-74.94	15.1	17.2	20.3	17.3	9.4	7.6	19.3	22.5
6	-43.1	12.3	12.7	17.2	16.5	8.3	6	15.4	18
7	-27.86	11.2	11	15.8	15.7	7.9	5.2	13.8	16.1
8	-12.62	9.9	8.7	14	13.8	7.5	4.4	11.7	13.7
9	-5	8	6.5	11.7	13.1	6.3	3.4	9.4	11.1
10	-3.5	7.4	5.9	10.8	12.6	5.9	3	8.5	10.1
11	-2.35	6.3	4.9	9.5	11.6	5.2	2.6	7.3	8.6
12	-1.85	5.8	4.5	8.8	10.9	4.9	2.4	6.9	7.9
13	-1.35	5	3.8	7.6	9.8	4.3	2	5.8	6.9
14	-0.85	4	3.1	6.1	8.2	3.6	1.6	4.6	5.5
15	-0.35	2.2	1.6	3.6	5.3	2.2	0.8	2.6	3.1
16	9.5	35.9	41	47.4	31.9	16.9	18.4	47.1	55
17	10	32.6	34.8	43.6	31.8	16.7	16.2	41.8	48.9
18	10.5	30.7	31.6	41	30.8	16	14.9	38.7	45.5
19	11	29.2	29.6	39.3	29.6	15.3	14.1	36.8	43.1
20	11.5	28.3	28.3	38.2	28.8	14.8	13.6	35.5	41.6
21	12.65	26.7	26.2	36.2	27.3	14.1	12.6	33.4	39.2
22	14.15	25.7	25	35	26	13.5	12.1	32.1	37.6
23	16.15	24.9	23.5	33.8	24.6	12.8	11.8	31	36.3
24	30.95	23.9	21.7	33.6	24.3	12.6	11.1	29.3	34.5
25	36.03	23.1	21.1	32.4	24.3	12.8	10.8	28.8	34
26	43.65	23.7	20.8	32.5	25.2	13	10.9	29	33.8
Discharge, discharge ratio, velocity parameter, discharge coefficient, and Reynolds numbers									
Q_1 (*l/s*)		8.53	11.09	9.39	6.24	4.72	6.45	10.4	11.26
Q_2 (*l/s*)		2.85	2.06	3.5	4.07	2.79	1.7	2.86	3.13
Q_r		0.33	0.19	0.37	0.65	0.59	0.26	0.28	0.28
η_1^2		0.75	0.87	0.72	0.51	0.53	0.81	0.8	0.8
C_d		0.29	0.17	0.32	0.47	0.43	0.24	0.25	0.25
$Re_1 \times 10^{-5}$		1.3	1.7	1.44	0.95	0.72	0.99	1.59	1.72
$Re_2 \times 10^{-5}$		0.87	1.38	0.9	0.33	0.3	0.73	1.15	1.24

Table 2.2 Experimental data of two-dimensional slot flow $L/B = 0.78$

tap No.	distance X(cm)	pressure head H (cm)							
1	-197.12	40	27.2	26.2	47.4	50.2	34.9	20	48.9
2	-166.38	38.3	25.8	24.9	46.8	49.5	33.6	18.6	44.4
3	-135.9	36.3	23.8	22.8	46.1	48.2	31.4	16.3	37.5
4	-105.42	34.1	21.8	20.8	45	47	29.1	14.2	30.7
5	-74.94	32.3	20	19	44	45.5	28.1	12.3	24.9
6	-43.1	29.9	17.5	16.4	42.7	43.5	26.2	9.8	16.9
7	-27.86	29.3	16.8	15.6	42.3	43	25.5	9.1	15.2
8	-12.62	28	15.4	13.6	40.5	40.8	23.1	7.6	11.7
9	-5	25.4	13.5	11.8	38.1	37.9	20.6	6.1	8.7
10	-3.5	23.3	11.8	10.2	36.1	35.4	18.8	4.8	7.3
11	-2.35	21.7	10.5	9.1	34	33	17	4.1	5.9
12	-1.85	20	9.6	8.2	32.2	31.2	15.7	3.5	4.9
13	-1.35	17.9	8.2	6.9	29.8	28.5	14.1	2.5	3.7
14	-0.85	14.8	6.2	5.1	26	24.5	12.4	1.2	2.4
15	-0.35	9	2.8	1.9	18.6	16.8	6.7	-0.9	0.5
16	7.49	55.6	42.1	39.9	46.8	63.9	50.8	31.2	
17	7.99	51.6	37.7	35.3	47.8	62.5	46.4	27.2	
18	8.49	49.8	35.9	33.6	48	60.5	44.8	25.4	
19	8.99	48.2	34.2	32	47.5	58.1	42.8	23.3	
20	9.49	46.2	33	30.9	47	55.9	41.1	22.3	
21	10.64	45.3	32.2	30	46.9	53.9	40.3	21.9	
22	12.14	43.6	31.1	28.9	46.5	51.8	38.7	20.9	
23	14.14	41.7	30.2	28	46	50.4	37.5	20.1	
24	30.95	40.9	29.3	27	46.7	50.6	36.6	19	
25	36.03	41.2	29.1	27	46.7	50.9	36.7	18.9	
26	43.65	41.6	29.1	26.9	46.7	51.4	37.1	18.7	
Discharge, discharge ratio, velocity parameter, discharge coefficient, and Reynolds numbers									
Q_1 (*l/s*)		7.58	7.76	7.72	5.48	6.82	7.61	7.8	6.87
Q_2 (*l/s*)		4.51	3.47	3.25	5.48	5.41	4.12	2.47	1.77
Q_r		0.6	0.45	0.42	1	0.79	0.54	0.32	0.26
η_1^2		0.41	0.55	0.56	0.2	0.27	0.44	0.69	0.66
C_d		0.48	0.42	0.4	0.57	0.53	0.46	0.34	0.27
$Re_1 \times 10^{-5}$		1.16	1.19	1.18	0.84	1.04	1.16	1.19	1.05
$Re_2 \times 10^{-5}$		0.47	0.66	0.68	0	0.22	0.53	0.81	0.78

Table 2.2 (continued)

tap No.	distance X(cm)	pressure head H (cm)							
1	-197.12	32.8	28.8	23.5	20.1	22.4	17.2	28.9	38.6
2	-166.38	29.8	26.3	21.7	18.9	22	16	26.9	35.8
3	-135.9	25	22.6	19	17	21.4	14	23.8	31.8
4	-105.42	20.5	18.9	16.4	15.4	20.8	12.3	20.8	28
5	-74.94	16.6	15.8	14.3	14	20.2	10.8	18.2	24.8
6	-43.1	12.1	12.2	11.7	12.2	19.6	9	15.45	21.1
7	-27.86	10.2	10.7	10.6	11.6	19.4	8.2	14.1	19.3
8	-12.62	7.8	8.8	9.2	10.4	19	7.3	12.5	17.3
9	-5	5.9	7	7.8	9	17.1	6	10.6	14.6
10	-3.5	5.2	6.35	7	8.5	17	5.5	9.6	13.4
11	-2.35	4.4	5.5	6.2	7.7	15.9	4.8	8.4	11.8
12	-1.85	4	5	5.7	7.1	15.1	4.5	7.8	11
13	-1.35	3.4	4.4	4.9	6.3	14.1	3.8	6.9	9.6
14	-0.85	2.8	3.5	4.1	5.3	12.5	3.1	5.8	8
15	-0.35	1.7	2.2	2.6	3.6	9.4	1.9	3.5	4.9
16	7.49	30.6	32.9	30.4	26.8	21.5	22.7	38.5	53.25
17	7.99	27.8	29.2	27.7	25.9	23.1	20.4	34.6	47.65
18	8.49	23.3	25.9	24.9	24.7	22.7	19	32.3	44.6
19	8.99	21.8	24.6	24	23.8	22.8	18.1	30.8	42.4
20	9.49	21.9	23.7	22.7	23	22	17.5	29.8	41
21	10.64	19	21.4	21.8	21.9	22.4	16.3	28	38.6
22	12.14	18.2	20.6	21	21	22	15.9	27	37.2
23	14.14	16.9	19.8	20.4	20.6	21.6	15.2	26.1	36
24	30.95	13.2	17.1	18.3	19.3	21.5	14.6	25	34.5
25	36.03	12.7	16.6	18.2	19.2	21.55	14.4	24.4	34.05
26	43.65	11.9	16	17.9	19.1	21.55	14.5	24.6	33.8
Discharge, discharge ratio, velocity parameter, discharge coefficient, and Reynolds numbers									
Q_1 (*l/s*)		11.41	10.04	8.27	6.55	3.49	6.66	8.83	10.29
Q_2 (*l/s*)		1.14	1.52	1.88	2.32	3.49	1.8	2.33	2.79
Q_r		0.1	0.15	0.23	0.35	1	0.27	0.26	0.27
η_1^2		0.89	0.83	0.75	0.61	0.19	0.71	0.71	0.71
C_d		0.12	0.18	0.25	0.35	0.55	0.29	0.28	0.29
$Re_1 \times 10^{-5}$		1.74	1.53	1.27	1	0.53	1.02	1.35	1.57
$Re_2 \times 10^{-5}$		1.57	1.3	0.98	0.65	0	0.74	0.99	1.15

Table 2.3 Experimental data of two-dimensional slot flow $L/B = 0.11$

tap No.	distance X(cm)	pressure head H (cm)									
1	-197.12	49.2	41.8	22	31.7	34.8	43.7	48	39.7	45.4	40.8
2	-166.38	47.8	41.2	20.9	30.7	31.9	40.7	45.2	36.8	42.8	
3	-135.9	45.9	39.6	19.3	28.9	27.1	36.1	40.7	32.5	38.6	
4	-105.42	44	38.2	17.8	27.2	22.6	31.6	36.4	28.3	34.8	
5	-74.94	42.1	36.8	16.4	25.6	18.9	28	32.6	24.9	31.7	
6	-43.1	39.8	35.1	14.6	23.7	14.3	23.5	28.3	20.5	27.9	
7	-27.86	39.2	34.4	14.1	23.1	12.5	21.6	26.4	18.9	26.2	40.6
8	-12.62	37.9	33	12.9	22	10.1	19.3	24.2	16.5	24	40.45
9	-5	35.5	32.2	12.1	21	8.5	17.5	22.2	14.8	22.1	40.3
10	-3.5	35.4	31.1	11.5	20.1	7.9	16.6	21	14.1	21.3	40.2
11	-2.35	34.5	30.6	11	19.4	7.1	15.4	19.9	12.9	20.1	40
12	-1.85	33.7	30	10.5	18.8	6.6	14.9	19.1	12.5	19.3	39.7
13	-1.35	32.5	28.7	9.9	17.9	5.9	13.7	17.7	11.4	17.9	39.4
14	-0.85	30.2	26.9	8.7	16.3	4.8	11.9	15.9	10.1	16.1	38.6
15	-0.35	24.6	22	6.1	12.5	2.7	8.3	11.1	6.6	11.5	35.8
16	1.4	54.6	46.6	22.6	34.6	18.7	32.9	40.3	28.9	39.8	38.7
17	1.9	47.9	41.6	18.4	29	14.7	27.3	33.9	23.9	33.8	
18	2.4	46	39.7	17.2	27.5	13.1	25.2	31.3	21.8	32.1	
19	2.9	43.6	37.9	15.9	26.1	12.3	23.9	30.1	21	29.9	
20	3.4	42.7	37.2	15.3	25.2	12	23.4	28.9	20.2	29.3	
21	4.55	42.5	37	15.2	25	11.3	22.1	27.9	19.2	27.7	40.4
22	6.05	41.8	36.6	14.8	24.5	10.8	21.5	27.1	18.6	27	40.3
23	8.05	41.5	36.2	14.6	24.2	10.1	20.9	26.1	18	26.3	40.3
24	30.95	39.2	34.4	13.2	22.5	6.3	17.2	22.6	14.5	23.1	
25	36.03	38.9	34.2	12.8	22.2	5.7	16.5	22.2	13.7	22.5	
26	43.65	38.5	34.1	12.5	21.8	4.7	15.5	21.3	12.9	21.8	40.3
Discharge, discharge ratio, velocity parameter, discharge coefficient, and Reynolds numbers											
Q_1 (*l/s*)		7.49	6.51	6.6	6.97	11.34	11.22	11.13	10.89	10.42	0.79
Q_2 (*l/s*)		0.58	0.56	0.36	0.47	0.23	0.38	0.45	0.35	0.47	0.79
Q_r		0.08	0.09	0.06	0.07	0.02	0.03	0.04	0.03	0.05	1
η_1^2		0.33	0.3	0.51	0.42	0.81	0.69	0.64	0.71	0.61	0.01
C_d		0.43	0.46	0.38	0.42	0.16	0.25	0.28	0.24	0.31	0.63
$Re_1 \times 10^{-5}$		1.15	1	1.01	1.07	1.73	1.72	1.7	1.66	1.59	0.12
$Re_2 \times 10^{-5}$		1.06	0.91	0.95	1	1.7	1.66	1.63	1.61	1.52	0

Table 2.3 (continued)

tap No.	distance X(cm)	pressure head H (cm)									
1	-197.12	43.3	25.3	21.5	35.7	21.9	50	50	13.4	22	36
2	-166.38	43.15	23.6	20.4	35.7		47	48.8	12.6	20.7	34.2
3	-135.9		21.5	18.5	33.9	21.85	42.2	47	11.3	18.8	31.4
4	-105.42		19.3	17.3			38.3	45.7	10.5	17.2	29.1
5	-74.94		17.4	15.8			34.4	44.4	9.5	15.6	26.8
6	-43.1	42.3	15.2	14.2			30.1	42.7	8.3	14	24.2
7	-27.86	42.2	14.3	13.6	32.5	21.75	28.2	41.8	7.9	13.2	23.2
8	-12.62	41.8	13	12.7	31.9	21.7	26.3	41.2	7.4	12.2	21.9
9	-5	41.5	11.9	11.9	31.5	21.6	24.1	40.5	6.8	11.3	20.4
10	-3.5	41.2	11.5	11.1	31	21.5	23.3	39.5	6.6	10.9	19.9
11	-2.35	40.8	10.9	10.7	29.8	21.4	22.1	38.7	6.2	10.3	18.7
12	-1.85	40.4	10.3	10.4	29.4	21.3	21.1	37.5	6	10.2	18.3
13	-1.35	39.8	9.8	9.7	28.9	21.1	19.8	36.7	5.5	9.5	17.1
14	-0.85	38.65	8.5	8.8	26.9	20.6	17.9	34.3	5.1	8.6	15.9
15	-0.35	34.9	5.7	6.3	23.5	19.2	13.3	32	3.7	6.3	11.9
16	1.4	43.3	22.2	18	36	20.4	42.6	54.2	11.5	19.1	33.9
17	1.9	43.8	18.7	15.7	34.4	21.2	36.1	50.5	10	16.6	29.6
18	2.4	43.6	17.3	14.7	34.2	21.4	33.8	48.6	9.4	15.6	27.8
19	2.9	43.2	16.8	14.1	33.7	21.4	32.3	47.4	9	15	26.7
20	3.4	43.1	16.5	13.5	33.5		31.4	46.7	8.7	14.6	26
21	4.55	43.1	15.6	12.9	32.4	21.5	30	45.5	8.3	13.8	25
22	6.05	43.1	15	12.4	32.2	21.3	29.3	44.6	8.15	13.5	24.4
23	8.05	42.75	14.6	12.8	32.4	21.4	28.4	44.3	7.8	13	23.8
24	30.95	42.5	12.6	12.5	32.9	21.6	24.8	43	7.1	12	22
25	36.03	42.5	12.1	12.3	32.7		23.9	42.7	6.9	11.7	21.4
26	43.65	42.5	11.9	12.2	32.3		23.2	42.5	6.8	11.6	21.2
Discharge, discharge ratio, velocity parameter, discharge coefficient, and Reynolds numbers											
Q_1 (*l/s*)		2.13	7.58	6.24	3.89	0.59	11.12	6.46	5	6.54	8.21
Q_2 (*l/s*)		0.8	0.36	0.39	0.69	0.59	0.4	0.67	0.23	0.29	0.41
Q_r		0.38	0.05	0.06	0.18	1	0.04	0.1	0.05	0.05	0.05
η_1^2		0.04	0.58	0.49	0.14	0.01	0.64	0.27	0.56	0.57	0.54
C_d		0.62	0.32	0.38	0.57	0.63	0.25	0.47	0.3	0.3	0.32
$Re_1 \times 10^{-5}$		0.33	1.16	0.95	0.6	0.09	1.7	0.99	0.76	1	1.26
$Re_2 \times 10^{-5}$		0.2	1.1	0.9	0.49	0	1.64	0.89	0.73	0.96	1.19

Table 3.1 Range of geometric variables: Lateral weirs in circular channels

Test	sill heights (mm)	ratio of weir width to channel diameter L/D	ratio of sill heights to diameter s/D
a	38.1	0.5	0.13
b		0.75	
c		1	
d	84.6	0.5	0.28
e		0.75	
f		1	
g	137.5	0.5	0.46
h		0.75	
i		1	

Table 3.2 Experimental Data of Rectangular Side Weir in a Circular Channel
D = 30 cm, L = 30 cm, s = 3.81 cm

depth of the water Y at each location X (cm)							weir discharge	downstream discharge	upstream discharge	calculated weir discharge	upstream Froude number	discharge coefficient		velocity coef.
-72	-40	0	15	30	60	90	Q_M (l/s)	Q_2 (l/s)	Q_1 (l/s)	Q_t(l/s)	F_1	$\bar{C}_d$	$\bar{C}_{dM}$	η_o^2
11.95	11.59	11.26	12.15	12.71	13.56	13.78	14.3	4.64	18.9	13.7	0.754	0.489	0.511	0.238
11.45	11.11	10.65	11.44	12.13	12.62	12.74	12.4	4.56	17.0	12.1	0.753	0.488	0.501	0.240
10.77	10.3	9.87	10.08	10.94	11.28	11.55	10.1	4.45	14.5	9.39	0.798	0.474	0.508	0.271
10.71	10.36	9.54	9.98	10.85	11.22	11.52	9.63	4.83	14.5	9.09	0.819	0.469	0.497	0.283
10.34	10.17	8.37	8.9	9.79	10.67	11	6.83	7.64	14.5	6.88	1.03	0.415	0.412	0.397
9.61	9.29	8.66	8.85	9.73	10.06	7.47	7.09	4.89	12.0	6.88	0.845	0.458	0.472	0.309
8.92	8.54	7.73	8.18	8.89	9.24	9.39	5.36	4.78	10.1	5.46	0.848	0.452	0.444	0.324
8.23	7.88	6.93	7.29	7.98	8.32	8.5	3.88	4.61	8.49	3.95	0.885	0.434	0.427	0.365
7.36	6.99	6.01	6.14	7.03	7.35	7.47	2.44	4.32	6.75	2.34	0.954	0.396	0.413	0.447
6.45	6.12	5.41	5.68	6.21	6.49	6.55	1.73	3.22	4.96	1.60	0.841	0.41	0.444	0.424
9.58	9.37	7.68	6.67	5.79	7.47	8.56	2.61	9.51	12.1	2.76	1.52	0.277	0.261	0.655
11.33	10.91	9.03	7.88	6.5	6.22	6.46	4.2	13.1	17.3	4.55	1.6	0.283	0.261	0.639
12.52	12.03	9.84	8.79	7.05	6.37	6.77	5.39	15.7	21.1	6	1.61	0.29	0.261	0.623
13.52	13.06	10.56	9.38	7.71	6.74	7.32	6.47	18.3	24.7	7.17	1.64	0.289	0.261	0.622
14.28	14.02	11.44	9.95	8.27	7.04	7.71	7.62	20.7	28.4	8.42	1.65	0.29	0.262	0.618
15.05	14.68	12.08	10.7	8.78	7.32	8.26	8.83	22.9	31.7	9.88	1.63	0.297	0.266	0.603
16.05	15.07	12.5	11.08	9.34	7.53	8.81	9.7	25.2	34.9	10.8	1.66	0.293	0.264	0.608
16.88	16.83	13.32	11.76	9.97	8.11	9.57	11.09	28.7	39.8	12.3	1.68	0.291	0.262	0.611

Table 3.3 Experimental Data of Rectangular Side Weir in a Circular Channel
D = 30 cm, L = 22.5 cm, s = 3.81 cm

depth of the water Y at each location X (cm)							weir discharge	downstream discharge	upstream discharge	calculated weir discharge	upstream Froude number	discharge coefficient		velocity coef.
-72	-40	0	11.25	22.5	60	90	Q_M (l/s)	Q_2 (l/s)	Q_1 (l/s)	Q_t(l/s)	F_1	$\bar{C}_d$	$\bar{C}_{dM}$	η_o^2
13.34	13.25	13.17	13.41	13.89	14.57	14.84	13.8	4.92	18.7	12.5	0.607	0.515	0.568	0.164
12.15	11.96	12.09	12.37	12.76	13.29	13.5	11.7	4.81	16.5	10.5	0.625	0.509	0.565	0.175
10.98	10.92	10.47	11	11.5	11.83	11.92	9.07	4.67	13.7	8.08	0.656	0.499	0.56	0.196
9.7	9.59	9.18	9.5	10.12	10.36	10.52	6.65	4.56	11.2	5.81	0.701	0.483	0.552	0.229
8.44	8.21	7.87	8.29	8.71	8.87	9.05	4.40	4.37	8.76	4.02	0.723	0.47	0.514	0.257
7.56	7.26	6.76	7.12	7.68	7.86	7.89	2.89	4.18	7.07	2.6	0.776	0.442	0.49	0.313
7.14	6.92	6.41	6.89	7.08	7.47	7.5	2.31	4.76	7.08	2.22	0.851	0.413	0.43	0.366
6.44	6.24	6.04	6.1	6.43	6.64	6.74	1.79	3.40	5.19	1.53	0.766	0.424	0.496	0.350
9.41	9.17	7.58	6.97	6.49	8.99	8.93	2.17	9.55	11.7	2.22	1.35	0.285	0.279	0.586
11.63	11.36	9.16	8.52	7.36	10.27	11	3.63	14.5	18.2	3.81	1.46	0.283	0.27	0.581
13.24	12.92	10.34	9.68	8.49	8.66	7.96	5.01	18.6	23.6	5.33	1.47	0.289	0.272	0.566
14.15	13.73	11.07	10.36	9.19	8.75	8.26	6.10	21.3	27.4	6.3	1.5	0.288	0.279	0.566
14.96	14.87	11.86	11.05	9.75	8.63	8.6	7.06	23.8	30.9	7.33	1.49	0.293	0.282	0.556
15.97	15.08	12.43	11.44	10.34	8.81	5.94	8.04	26.6	34.7	7.97	1.54	0.283	0.286	0.570
16.33	16.5	13.24	12.18	10.81	9.08	9.69	9.08	30.2	39.2	9.06	1.55	0.282	0.283	0.569
17.53	16.95	13.98	12.69	11.47	9.48	10.24	10.4	32.9	43.39	9.99	1.57	0.28	0.293	0.571

Table 3.4 Experimental Data of Rectangular Side Weir in a Circular Channel
D = 30 cm, L = 15 cm, s = 3.81 cm

depth of the water Y at each location X (cm)							weir discharge	downstream discharge	upstream discharge	calculated weir discharge	upstream Froude number	discharge coefficient		velocity coef.
-72	-40	0	7.5	15	60	90	Q_M (l/s)	Q_2 (l/s)	Q_1 (l/s)	Q_t(l/s)	F_1	$\bar{C}_d$	$\bar{C}_{dM}$	η_o^2
14.71	14.86	14.98	15.07	15.43	15.73	15.91	12.0	5.24	17.2	10.3	0.447	0.541	0.632	0.095
14.11	13.92	14	14.13	14.44	14.69	14.81	10.4	5.15	15.6	9	0.458	0.538	0.624	0.100
13.14	13.2	13.02	13.13	13.46	13.84	13.87	9.07	5.06	14.1	7.74	0.477	0.532	0.624	0.109
12.41	12.33	12.4	12.41	12.71	12.95	13.08	7.93	4.98	12.9	6.88	0.484	0.53	0.611	0.113
11.51	11.42	11.46	11.59	12.11	12.34	12.5	6.85	6.01	12.9	5.93	0.548	0.51	0.59	0.142
10.68	10.47	10.08	10.68	11.03	11.49	11.55	5.30	7.57	12.9	4.75	0.655	0.474	0.529	0.197
9.74	9.47	9.24	9.51	9.92	10.27	10.61	3.83	9.01	12.8	3.58	0.807	0.422	0.451	0.282
9.78	9.6	8.08	8.25	8.7	10.12	10.03	2.58	10.2	12.8	2.35	1.05	0.337	0.369	0.424
7.27	7.03	6.68	6.9	7.08	7.22	7.38	1.55	4.64	6.19	1.42	0.731	0.418	0.454	0.296
6.65	6.48	6.21	6.28	6.6	6.8	6.83	1.24	3.66	4.90	1.06	0.684	0.422	0.496	0.292
12.87	12.39	10.24	9.85	9.01	9.81	13.02	3.70	19.5	23.2	3.3	1.4	0.267	0.299	0.537
11.72	11.24	9.44	8.78	8.3	10.67	11.37	2.95	16.2	19.1	2.53	1.4	0.258	0.302	0.555
10.28	9.97	8.25	7.83	7.62	9.63	9.75	2.10	12.1	14.2	1.88	1.3	0.27	0.302	0.538
13.91	13.79	11.34	10.87	10	10.18	9.11	4.68	24.0	28.7	4.18	1.42	0.267	0.299	0.534
21.11	18.39	15.56	14.48	13.43	12.07	11.98	8.74	44.1	52.8	7.77	1.49	0.261	0.293	0.539
20.44	17.39	14.76	13.84	13.21	11.83	11.7	8.19	40.8	49.0	7.13	1.49	0.26	0.298	0.541
17.28	15.7	13.66	12.82	11.94	11.7	10.64	6.96	34.0	41.0	6.07	1.46	0.265	0.303	0.534

Table 3.5 Experimental Data of Rectangular Side Weir in a Circular Channel
D = 30 cm, L = 30 cm, s = 8.46 cm

depth of the water Y at each location X (cm)							weir discharge	downstream discharge	upstream discharge	calculated weir discharge	upstream Froude number	discharge coefficient		velocity coef.
-72	-40	0	15	30	60	90	Q_M (l/s)	Q_2 (l/s)	Q_1 (l/s)	Q_t(l/s)	F_1	$\bar{C}_d$	$\bar{C}_{dM}$	η_o^2
17.3	17.23	17.37	17.71	17.86	18.37	18.4	16.5	5.09	21.6	15.8	0.416	0.548	0.574	0.121
16.22	16.33	16.22	16.6	16.89	17.06	17.15	13.9	5.01	18.9	13.0	0.411	0.547	0.582	0.122
15.83	15.74	15.74	15.93	16.25	16.45	16.51	12.4	4.92	17.4	11.6	0.406	0.546	0.587	0.123
14.95	14.93	14.88	15.29	15.49	15.62	15.62	10.7	4.86	15.6	9.97	0.397	0.547	0.587	0.123
14.59	14.52	14.44	14.6	15.05	15.23	15.23	9.63	5.95	15.6	8.75	0.429	0.535	0.59	0.145
13.57	13.63	13.62	13.87	14.16	14.28	14.31	7.76	5.82	13.6	7.15	0.415	0.536	0.581	0.145
12.35	12.32	12.23	12.46	12.66	12.82	12.85	5.14	5.66	10.8	4.54	0.406	0.527	0.597	0.162
13.82	13.66	13.71	13.77	13.84	13.92	13.92	7.52	0	7.51	6.76	0.233	0.583	0.648	0.051
13.82	13.48	11.7	11.43	10.55	13.18	13.56	2.42	23.6	26.0	2.40	1.18	0.238	0.24	0.675
15.17	14.87	12.81	12.22	10.91	15.71	14.48	3.47	28.8	32.3	3.39	1.30	0.234	0.24	0.680
16.51	15.48	13.59	12.8	11.57	11.32	15.52	4.32	32.6	36.9	4.43	1.33	0.24	0.235	0.668
18.02	17.22	15.09	13.8	12.38	11.3	11.83	6.40	39.4	45.8	6.17	1.42	0.24	0.249	0.667
20.57	19.87	16.9	15.27	14.04	12.15	13.11	9.11	49.2	58.3	9.16	1.47	0.247	0.245	0.655
20.86	20.66	17.57	16.06	14.51	12.36	13.87	10.4	47.7	58.1	11.0	1.34	0.278	0.264	0.605
21.13	21.43	18.75	16.9	14.64	13.24	14.75	12.8	59.5	72.3	12.2	1.53	0.244	0.257	0.657

Table 3.6 Experimental Data of Rectangular Side Weir in a Circular Channel
D = 30 cm, L = 22.5 cm, s = 8.46 cm

depth of the water Y at each location X (cm)							weir discharge	downstream discharge	upstream discharge	calculated weir discharge	upstream Froude number	discharge coefficient		velocity coef.
-72	-40	0	11.25	22.5	60	90	Q_M (l/s)	Q_2 (l/s)	Q_1 (l/s)	Q_t(l/s)	F_1	$\bar{C}_d$	$\bar{C}_{dM}$	η_o^2
19.98	19.99	20.23	20.34	20.62	20.77	20.99	17.4	5.21	22.7	17	0.331	0.563	0.578	0.078
18.39	18.35	18.32	18.58	18.78	18.94	19.16	14.2	5.06	19.2	13.3	0.337	0.561	0.598	0.081
17.39	17.36	17.36	17.56	17.81	17.91	18.06	12.2	4.98	17.2	11.4	0.334	0.561	0.601	0.082
16.65	16.54	16.48	16.74	16.93	17.06	17.15	10.5	4.89	15.4	9.82	0.33	0.56	0.601	0.082
15.25	15.21	15.14	15.35	15.55	15.65	15.65	8.19	4.81	13.0	7.48	0.327	0.558	0.611	0.086
13.93	13.82	13.88	14.07	14.21	14.28	14.37	6.10	4.67	10.8	5.49	0.321	0.555	0.618	0.091
13.12	13.09	13.09	13.28	13.47	13.43	13.64	4.93	5.82	10.7	4.39	0.357	0.539	0.605	0.118
15.73	15.68	15.7	15.83	15.86	15.93	15.9	8.65	0	8.65	8.17	0.206	0.588	0.624	0.035
14.21	14.21	14.11	14.18	14.19	14.25	14.34	6.35	0	6.35	5.58	0.186	0.59	0.671	0.032
14.97	15.05	12.58	12.44	12.29	14.68	14.86	2.64	27.9	30.6	2.76	1.15	0.245	0.233	0.611
16.14	15.3	13.35	12.98	12.55	15.44	16.2	3.24	31.4	34.6	3.32	1.21	0.243	0.237	0.614
17.18	16.54	14.03	13.39	12.92	16.9	17.42	3.83	35.1	39.0	3.79	1.27	0.235	0.237	0.626
17.82	17.34	14.65	13.96	13.27	17.09	17.94	4.64	39.4	44.0	4.38	1.33	0.229	0.243	0.635
19.04	18.33	15.8	14.95	14.16	16.32	20.04	5.59	43.5	49.0	5.78	1.3	0.247	0.239	0.604
20.47	20.14	16.77	15.96	14.68	13.55	14.16	6.96	50.2	57.1	6.99	1.35	0.243	0.242	0.610
20.8	21.05	17.77	16.64	15.45	13.98	14.49	8.13	56.5	64.6	8.04	1.4	0.238	0.241	0.617
21.58	22.04	18.99	17.82	16.25	14.8	15.04	10.4	63.8	74.2	9.74	1.42	0.239	0.255	0.615

Table 3.7 Experimental Data of Rectangular Side Weir in a Circular Channel
D = 30 cm, L = 15 cm, s = 8.46 cm

depth of the water Y at each location X (cm)							weir discharge	downstream discharge	upstream discharge	calculated weir discharge	upstream Froude number	discharge coefficient		velocity coef.
-72	-40	0	7.5	15	60	90	Q_M (l/s)	Q_2 (l/s)	Q_1 (l/s)	Q_t(l/s)	F_1	$\bar{C}_d$	$\bar{C}_{dM}$	η_o^2
21.57	21.53	21.54	21.78	21.95	22.05	22.15	13.6	5.42	19.0	13.2	0.244	0.577	0.598	0.044
20.06	20.02	19.96	20.04	20.2	20.13	20.53	11.4	5.30	16.7	10.7	0.252	0.575	0.613	0.046
18.58	18.49	18.47	18.56	18.74	18.82	18.94	9.38	5.15	14.5	8.71	0.254	0.574	0.618	0.048
17.64	17.58	17.46	17.62	17.77	17.97	17.94	8.16	6.37	14.5	7.49	0.281	0.565	0.615	0.059
15.87	15.8	15.74	15.87	16.08	16.32	16.32	5.99	8.53	14.5	5.45	0.342	0.542	0.595	0.091
14.51	14.37	14.36	14.64	14.85	14.98	15.04	4.54	9.90	14.4	4.09	0.399	0.515	0.571	0.128
13.28	13.29	13.18	13.29	13.61	13.67	13.67	3.17	11.3	14.5	2.83	0.477	0.47	0.528	0.192
12.19	12.22	11.95	12.17	12.25	12.36	12.51	2.02	12.5	14.5	1.79	0.571	0.408	0.458	0.287
13.69	13.44	11.96	12.42	12.68	14.25	13.92	1.71	23.0	24.7	1.72	0.941	0.269	0.268	0.513
15.32	15.38	13.26	13.36	13.52	15.38	15.01	2.42	30.0	32.4	2.35	1.06	0.252	0.26	0.541
17.56	16.98	14.44	14.38	14.31	16.87	17.3	3.24	37.2	40.4	3.06	1.15	0.243	0.257	0.557
19.17	17.88	15.72	15.11	14.95	18.43	18.82	4.24	43.6	47.8	3.66	1.23	0.233	0.27	0.573
20.14	19.32	16.43	15.86	15.16	20.26	21.9	4.70	50.1	54.8	4.11	1.3	0.222	0.254	0.592
20.73	20.6	17.25	16.52	15.96	21.17	19.86	5.50	55.8	61.3	4.7	1.34	0.219	0.257	0.597
21.51	21.32	17.75	17.05	16.33	16.42	16.39	6.15	60.5	66.7	5.09	1.38	0.214	0.259	0.606
22.1	20.84	19.19	18.58	17.88	18.21	16.29	7.68	74.0	81.6	6.43	1.43	0.209	0.249	0.614

Table 3.8 Experimental Data of Rectangular Side Weir in a Circular Channel
D = 30 cm, L = 30 cm, s = 13.75 cm

depth of the water Y at each location X (cm)							weir discharge	downstream discharge	upstream discharge	calculated weir discharge	upstream Froude number	discharge coefficient		velocity coef.
-72	-40	0	15	30	60	90	Q_M (l/s)	Q_2 (l/s)	Q_1 (l/s)	Q_t(l/s)	F_1	$\bar{C}_d$	$\bar{C}_{dM}$	η_o^2
22.01	21.97	21.92	22.19	22.37	22.5	22.47	13.6	5.70	19.3	13.6	0.239	0.576	0.577	0.067
20.83	20.76	20.81	20.92	21.11	21.1	21.16	11.0	5.57	16.5	10.7	0.229	0.576	0.59	0.065
20.42	20.21	20.31	20.48	20.65	20.67	20.76	10.0	6.47	16.5	9.72	0.239	0.573	0.59	0.072
19.52	19.45	19.44	19.52	19.83	19.82	19.94	8.27	8.25	16.5	7.86	0.261	0.563	0.593	0.091
18.72	18.72	18.58	18.82	19.04	19.05	19.11	6.78	9.72	16.5	6.42	0.282	0.553	0.583	0.112
17.88	17.92	17.83	17.96	18.09	18.23	18.29	5.21	11.3	16.5	4.89	0.307	0.536	0.57	0.144
16.86	16.89	16.84	16.99	17.18	17.29	17.29	3.61	12.9	16.5	3.34	0.343	0.506	0.547	0.201
20.51	20.49	20.52	20.51	20.62	20.64	20.7	9.92	0	9.92	9.66	0.143	0.595	0.611	0.027
18.64	18.62	18.62	18.68	18.68	18.75	18.75	6.37	0	6.37	5.94	0.11	0.599	0.642	0.019
21.64	21.18	18.31	17.56	16.88	23.57	19.91	3.96	57.1	61.1	3.37	1.2	0.193	0.226	0.733
22.2	21.97	18.97	17.85	17.49	24.05	21.46	4.60	62.9	67.5	3.93	1.26	0.189	0.221	0.740

Table 3.9 Experimental Data of Rectangular Side Weir in a Circular Channel
D = 30 cm, L = 22.5 cm, s = 13.75 cm

depth of the water Y at each location X (cm)							weir discharge	downstream discharge	upstream discharge	calculated weir discharge	upstream Froude number	discharge coefficient		velocity coef.
-72	-40	0	11.25	22.5	60	90	Q_{Mf} (l/s)	Q_2 (l/s)	Q_1 (l/s)	Q_t(l/s)	F_1	$\bar{C}_d$	$\bar{C}_{dMf}$	η_o^2
22.06	21.84	21.95	22.25	22.54	22.68	22.62	10.1	14.2	24.4	10.3	0.299	0.55	0.543	0.101
23.81	23.66	23.79	23.95	24.32	24.33	24.42	13.4	11.2	24.5	13.6	0.257	0.566	0.558	0.076
20.44	20.03	20.07	20.41	20.82	20.82	20.79	7.17	17.3	24.4	7.15	0.355	0.521	0.522	0.148
18.89	18.64	18.95	19.19	19.45	19.42	19.39	5.12	19.4	24.5	5.24	0.403	0.489	0.478	0.198
18.18	17.67	17.75	18.11	18.23	18.05	18.35	3.65	20.9	24.6	3.65	0.453	0.448	0.447	0.265
17.01	16.68	16.64	16.77	17.12	17.29	17.07	2.38	22.1	24.5	2.11	0.518	0.38	0.429	0.375
17.55	17.27	15.94	16.68	17.15	16.37	18.17	2.00	38.9	40.9	1.61	0.884	0.218	0.271	0.647
18.45	18.44	16.66	17.12	17.75	14.54	19.42	2.52	43.5	46.0	2.09	0.936	0.22	0.265	0.644
19.89	19.17	17.47	17.63	17.81	19.57	18.78	2.81	50.8	53.6	2.46	1.04	0.204	0.233	0.670
21.2	20.52	18.18	18	17.98	20.94	19.42	3.34	56.6	60.0	2.8	1.11	0.195	0.232	0.686
22.1	21.39	18.73	18.54	18.3	23.08	19.97	3.79	61.7	65.5	3.29	1.15	0.194	0.224	0.687
22.41	22.49	19.19	18.83	18.31	24.39	20.67	4.40	65.0	69.4	3.54	1.19	0.191	0.237	0.693
22.75	23.07	19.86	19.25	18.63	25.12	21.46	4.60	67.9	72.5	4.09	1.19	0.198	0.222	0.682

Table 3.10 Experimental Data of Rectangular Side Weir in a Circular Channel
D = 30 cm, L = 15 cm, s = 13.75 cm

depth of the water Y at each location X (cm)							weir discharge	downstream discharge	upstream discharge	calculated weir discharge	upstream Froude number	discharge coefficient		velocity coef.
-72	-40	0	7.5	15	60	90	Q_M (l/s)	Q_2 (l/s)	Q_1 (l/s)	Q_t(l/s)	F_1	$\bar{C}_d$	$\bar{C}_{dM}$	η_o^2
18.25	18.2	18.16	18.23	18.29	18.32	18.29	2.72	9.72	12.5	2.55	0.226	0.549	0.586	0.080
19.71	19.64	19.63	19.68	19.76	19.82	19.82	4.11	8.41	12.5	3.91	0.196	0.57	0.598	0.053
20.97	20.98	20.96	21.02	21.11	21.13	21.16	5.43	7.03	12.5	5.32	0.171	0.582	0.594	0.037
22.96	22.99	22.87	22.94	23.05	23.11	23.14	7.68	7.20	14.9	7.57	0.172	0.584	0.593	0.035
24.55	24.52	24.48	24.51	24.68	24.75	24.78	9.79	7.38	17.2	9.62	0.171	0.585	0.595	0.035
25.97	25.94	25.75	25.97	26.08	26.16	26.19	11.8	7.49	19.3	11.6	0.168	0.585	0.594	0.035
24.45	24.43	24.29	24.44	24.61	24.69	24.75	9.70	9.55	19.3	9.49	0.194	0.578	0.59	0.044
22.55	22.51	22.46	22.48	22.67	22.86	22.89	7.33	12.0	19.3	7.02	0.231	0.563	0.588	0.062
20.32	20.28	20.18	20.2	20.49	20.58	20.67	4.82	14.4	19.3	4.45	0.285	0.534	0.578	0.101
16.53	16.28	15.97	16.48	16.42	16.49	15.94	0.957	33.7	34.6	0.855	0.771	0.215	0.241	0.600
17.98	17.08	16.71	17.04	17.24	16.86	17.68	1.41	39.1	40.5	1.19	0.837	0.216	0.256	0.599
18.49	18.41	17.15	17.6	18.21	17.62	19.15	1.82	43.9	45.7	1.55	0.883	0.218	0.257	0.595
19.66	19.63	17.91	18.16	18.64	18.6	20.67	2.27	48.5	50.7	1.91	0.923	0.219	0.261	0.594
20.65	19.96	18.34	18.53	18.92	19.36	19.51	2.46	54.4	56.9	2.09	0.996	0.205	0.241	0.619
21.94	20.85	18.85	18.88	19.02	20.73	19.85	2.77	59.5	62.3	2.27	1.05	0.196	0.239	0.636
22.59	21.46	19.32	19.3	19.29	22.1	20.36	3.17	64.5	67.6	2.51	1.1	0.19	0.241	0.646

Table 4.1 Experimental data of dividing closed conduit flow *L/B = 1.0*

tap No.	distance (cm)	pressure head H (cm)							
		test1	test2	test3	test4	test5	test6	test7	test8
1	-152.24	7.1	21.7	23.2	34.4	47.4	45.3	40.9	36.1
2	-117.26	4.25	18.85	20.45	31.55	44.5	42.5	38.1	33.2
3	-94.4	1.6	16.5	18	29.3	42.2	40.1	35.6	30.8
4	-63.92	-1.24	13.56	15.16	26.56	39.3	37.3	32.8	27.8
5	-41.06	-3.38	11.62	13.22	24.72	37.5	35.3	30.9	25.9
6	-20.74	-5.53	9.57	11.27	22.87	35.2	33.4	28.9	23.9
7	-13.12	-6.37	8.43	10.03	21.63	34.5	32.4	27.7	22.9
8	-10.58	-6.62	8.18	9.58	21.18	34.4	32.2	27.6	22.7
9	-5.5	-8.07	7.03	7.63	18.33	33.4	31.3	26.5	21.3
10	-4.5	-8.71	6.19	6.89	17.09	33.2	31	26.1	21
11	-3.5	-9.66	5.34	5.54	15.14	32.7	30.5	25.6	20.3
12	-2.2	-11.2	3.9	2.9	11.3	32.1	30	24.9	19.5
13	-1.7	-12.65	2.55	1.05	8.55	31.4	29.6	24.2	18.9
14	-1.2	-13.79	1.11	-1.19	4.91	31.1	29	23.7	18.3
15	-0.8	-15.34	-0.44	-3.94	0.36	30.5	28.3	23.1	17.6
16	-0.4	-17.58	-2.78	-8.28	-6.48	29.5	27.4	21.9	16.4
17	-0.2	-18.93	-4.33	-11.33	-11.23	29.2	27	21.3	15.8
18	9.35	18.32	33.72	38.72	51.92	37.7	36.7	35.1	33.2
19	9.55	18.98	33.88	39.38	54.18	41.9	41.3	39.2	36.9
20	9.95	17.53	32.53	38.33	52.93	46.9	45.7	42.7	39.3
21	10.35	16.14	31.34	36.64	50.54	46.7	45.3	42	38
22	10.85	15.4	30.2	35.3	48.2	46.1	44.5	41	37.1
23	11.35	14.95	29.95	34.55	46.55	45.5	43.9	40.5	36.7
24	12.65	13.3	28.4	32.2	42.2	44.5	42.9	39.5	35.5
25	13.65	12.56	27.76	31.06	40.26	44.3	42.7	39	35.1
26	14.65	12.11	27.11	30.21	38.71	43.7	42.2	38.6	34.6
27	19.73	11.17	26.27	28.57	37.27	43	41.5	37.8	34
28	22.27	10.92	26.12	28.42	37.32	42.7	41.1	37.4	33.7
29	29.89	10.97	25.87	29.17	38.07	42.4	40.7	37.1	33.3
30	37.51	10.73	25.73	29.43	38.83	41.9	40.3	36.8	32.9
31	45.13	10.48	25.78	29.78	39.58	41.6	40	36.4	32.6
32	52.75	10.14	25.44	29.84	40.14	40.9	39.5	35.9	32.3
33	60.37	9.89	25.19	29.89	40.59	40.6	39.1	35.5	31.9
34	67.99	9.45	24.85	29.95	40.95	40.2	38.7	35.1	31.4
35	75.61	9.2	24.4	29.9	41.6	39.4	40	34.3	30.8
36	83.23	8.86	24.26	29.96	41.66	39.1	37.7	34.1	30.6

Table 4.1 (continued)

tap No.	distance (cm)	pressure head H (cm)							
		test1	test2	test3	test4	test5	test6	test7	test8
37	104.47	7.81	23.41	29.61	41.81	37.7	36	32.6	29
38	119.71	7.07	22.77	29.47	41.97	36.7	35	31.6	28
39	142.57	5.92	21.72	29.02	41.82	35.1	33.5	30.2	26.5
40	165.43	4.87	20.67	28.27	41.27	33.4	31.8	28.7	25.1
41	188.29	4.33	20.33	28.23	41.33	32.6	31.1	27.8	24.1
42	-13.82	-6.42	8.68	10.58	22.08	34.5	32.4	27.6	22.5
43	-6.2	-6.26	9.14	11.24	23.84	34.2	32.2	27.4	22.4
44	1.42	-1.31	14.19	19.19	33.49	36.1	34.2	30	25.1
45	9.04	7.05	22.45	25.15	35.75	41.2	38.9	35.5	31.3
46	24.28	10.5	25.6	28.3	36.7	42.4	40.5	37.2	33.3
47	39.52	10.3	25.3	29.5	38.3	41.5	39.9	36.3	32.5
48	54.76	9.7	24.9	29.7	39.5	40.6	39	35.6	31.8
49	70	8.9	24.3	29.7	40.6	39.6	38	34.6	30.9
50	9.45	-24.5	-10.3	-22.1	-31.1	26.9	24.4	18.7	12.8
51	9.75	-24.5	-10.4	-22.1	-31	26.9	24.4	18.7	12.8
52	10.05	-24.6	-10.5	-22.2	-31.3	26.8	24.3	18.6	12.7
53	10.85	-24.8	-10.6	-22.6	-31.9	26.7	24.2	18.5	12.5
54	11.35	-25	-10.7	-22.7	-32.3	26.6	24.1	18.5	12.4
55	12.65	-25.1	-11	-23.1	-32.7	26.5	24	18.4	12.4
56	13.65	-25.6	-11.4	-23.7	-33.2	26.5	23.9	18.3	12.2
57	14.65	-26.6	-12.3	-24.3	-33.3	26.3	23.8	18.2	12.1
58	19.73	-27.8	-14.3	-26.2	-36.8	26	23.6	18	12
59	24.81	-16.1	-1.9	-9	-17	26.9	24.9	20.9	16.2
60	29.89	-14.4	0	-5.2	-5.3	29.4	27.4	22.8	17.9
61	34.97	-13.8	0.6	-4	-3.2	30.2	28.1	23	18.1
62	40.05	-13.3	1.1	-3.6	-2.3	30.5	28.5	23.4	18.3
63	45.13	-13.1	1.6	-3.2	-1.7	30.9	28.8	23.6	18.5
64	50.21	-12.8	1.9	-2.8	-1.5	31.4	29.2	24.3	19
65	55.29	-12.4	2.3	-2.4	-1.4	32.1	29.9	24.9	19.5
66	60.37	-12	2.6	-2.1	-1.5	32.7	30.4	25.4	20
67	65.45	-11.7	2.8	-1.9	-1.6	33.5	31	26	20.4
68	9.45	31.9	45	42.8	43.8	69.7	68.7	64.7	60.7
69	9.75	22.9	36	32.6	33	62.7	61.2	57.1	52.4
70	10.05	21.8	35.2	32	32	61.7	60.1	56.2	51.5
71	10.85	18.6	32.1	28.5	29.6	51.7	51.2	48.2	45
72	11.35	13	26.8	23.6	24.2	45.7	44.4	42.6	38.3

Table 4.1 (continued)

tap No.	distance (cm)	pressure head H (cm)							
		test1	test2	test3	test4	test5	test6	test7	test8
73	12.65	0.1	14.7	11.9	11.8	33.9	32.2	28.6	24.8
74	13.65	-8.5	6.6	3.6	2.9	29.6	27.5	22.9	18.1
75	14.65	-15.7	0	-3.8	-4.8	27.5	25.2	19.7	14.1
76	19.73	-25	-10.5	-20.8	-24	24.2	21.7	16.2	13.5
77	24.81	-18.9	-4.5	-13.5	-18.9	26.7	24.6	20.2	15.3
78	29.89	-15.2	-0.8	-7.2	-9.9	29.5	27.4	22.7	17.5
79	34.97	-14.3	0.4	-4.9	-5.3	30.2	28.2	23.5	18.2
80	40.05	-13.4	1	-3.8	-3.1	30.6	28.4	23.7	18.3
81	45.13	-12.9	1.6	-2.9	-2	30.9	28.8	24.1	18.6
82	50.21	-12.5	2	-2.5	-1.7	31.4	29.5	24.5	19
83	55.29	-12.2	2.5	-2.1	-1.5	32.1	30.2	25	19.6
84	60.37	-11.7	2.7	-2	-1.3	32.6	30.5	25.5	20.1
85	65.45	-11.5	3.2	-1.7	-1.1	33.3	31.4	26.2	21
86	80.45	-10.7	3.6	-1.5	-1	34.5	32	27	21.8
87	95.69	-10.2	4	-1.3	-1.3	34.9	32.6	27.7	22.3
88	110.93	-10	4.4	-1.2	-2	35	33.1	28.1	22.6
89	126.17	-10	4.6	-1.1	-2.5	35	33	28	22.5
discharges, discharge ratio, Reynolds number, and energy loss coefficients									
Q_1 (*l/s*)		9.11	8.89	8.89	8.73	8.83	8.9	8.94	9.01
Q_2 (*l/s*)		5.89	5.5	4.05	2.18	7.3	7.3	7.17	7.03
Q_3 (*l/s*)		3.22	3.39	4.84	6.55	1.53	1.6	1.77	1.97
Q_3/Q_1		0.35	0.38	0.54	0.75	0.17	0.18	0.2	0.22
$Re_1 \times 10^{-5}$		1.36	1.33	1.32	1.3	1.32	1.33	1.33	1.34
$Re_2 \times 10^{-5}$		0.88	0.82	0.6	0.33	1.09	1.09	1.07	1.05
$Re_3 \times 10^{-5}$		0.48	0.51	0.72	0.98	0.23	0.24	0.26	0.29
K_{12} Eq.(4.6)		-0.09	-0.09	-0.03	0.12	-0.08	-0.08	-0.09	-0.08
K_{13} Eq.(4.8)		0.87	0.86	0.91	1.03	0.88	0.86	0.87	0.88
K_{13} Eq.(4.12)		0.87	0.88	0.93	1.04	0.89	0.88	0.87	0.86

Notes:

1. Pressure taps 1 to 41 located on the center of the branch side wall of main conduit, taps 42 to 49 on the opposite wall of the main. The distances equate to X.
2. Pressure taps 50 to 67 located on the center of upstream side wall of branch conduit, taps 68 to 89 on the downstream side wall of the branch. The distances equate to Y.

Table 4.1 (continued)

tap No.	distance (cm)	pressure head H (cm)							
		test9	test10	test11	test12	test13	test14	test15	test16
1	-152.24	23.9	9.7	44.5	51.1	43.4	40.9	39.6	35.3
2	-117.26	20.9	6.4	41.9	48.5	40.5	38.2	36.8	32.5
3	-94.4	18.3	3.9	39.3	46.2	38.3	35.8	34.3	30
4	-63.92	15.1	0.6	36.3	43.4	35.4	32.9	31.4	27.2
5	-41.06	13.2	-1.4	34.4	41.5	33.5	30.9	29.4	25.5
6	-20.74	11.2	-3.7	32.5	39.5	31.5	28.9	27.5	23.3
7	-13.12	10.1	-4.8	31.4	38.3	30.2	27.7	26.2	22.1
8	-10.58	10	-5	30.7	37.9	30	27	25.8	21.7
9	-5.5	8.5	-7.4	27.1	34.5	26.7	24	22.5	18.6
10	-4.5	8.2	-8.4	25.7	32.8	25	22.7	21.2	17.4
11	-3.5	7.5	-9.5	23.1	30.4	22.8	20.4	19.1	15.2
12	-2.2	6.4	-11.5	18	24.1	18.2	15.9	14.9	11.1
13	-1.7	5.5	-13.1	14.2	21.4	14.7	12.4	11.7	8.2
14	-1.2	4.7	-14.9	9.2	16.6	10.3	8.1	7.8	4.5
15	-0.8	3.4	-16.2	3	11	4.9	3.3	1.8	0.1
16	-0.4	2.1	-19	-6.4	1.7	-3.1	-4.4	-4.4	-6.7
17	-0.2	1.1	-20.6	-13.9	-5.5	-9.6	-10.6	-10.2	-12
18	9.35	27.9	24.4	60.7	66.5	63.7	61.1	59.1	53.2
19	9.55	30.3	24.5	59.9	65.9	64.7	62.9	60.9	56
20	9.95	30.5	22.6	56.4	62.2	61.6	60.5	59.1	55.2
21	10.35	29	21.2	53.9	60.2	58.3	56.7	56.4	52.7
22	10.85	27.9	20.4	52.9	59	55.5	53.8	53.5	50.4
23	11.35	27.4	19.8	51.9	58.4	53.7	52	52	48.8
24	12.65	26.2	18	48.8	55.4	49.3	47.4	47.2	44.4
25	13.65	26	17	47.6	54.3	47.6	45.7	45.1	42.2
26	14.65	25.3	16.6	47.1	53.7	46.6	44.6	43.7	40.7
27	19.73	24.4	15.9	46.3	53.4	45.7	43.2	42.1	38.6
28	22.27	24.2	15.6	46.2	53.4	45.6	43.2	42	38.6
29	29.89	23.9	15.5	47.2	54.5	46.4	44.1	43	39.4
30	37.51	23.6	15.3	48.1	55.5	47.2	44.9	43.8	40
31	45.13	23.5	14.7	49	56	48.1	45.8	44.6	40.8
32	52.75	23.2	14.5	49.4	56.1	48.7	46.3	45.1	41.4
33	60.37	22.7	14.3	49.6	56.2	49.2	46.8	45.8	42.3
34	67.99	22.2	13.9	49.7	56.2	49.8	47.5	46.5	42.5
35	75.61	21.5	13.4	49.5	56.1	49.8	47.7	46.7	42.8
36	83.23	21.3	13.3	49.5	56.1	49.9	47.8	46.8	43.1

Table 4.1 (continued)

tap No.	distance (cm)	pressure head H (cm)							
		test9	test10	test11	test12	test13	test14	test15	test16
37	104.47	19.8	12.4	49.4	56	49.8	47.8	46.9	43.4
38	119.71	19	11.7	49.4	56	49.8	47.8	46.9	43.3
39	142.57	17.7	10.8	49.3	55.9	49.7	47.6	46.7	43.1
40	165.43	16.7	9.9	49.3	55.9	49.7	47.5	46.6	43
41	188.29	15.9	9.2	49.2	55.8	49.6	47.4	46.4	42.7
42	-13.82	10.8	-5.5	32	38.8	30.8	28	26.8	22.3
43	-6.2	10.7	-5.1	33.8	40.4	32.4	29.7	28.4	23.9
44	1.42	14	1	44.1	51.2	42.9	40.3	38.7	34.2
45	9.04	21.4	10.4	45.8	52.7	45	42.5	41.2	37.1
46	24.28	24.2	14.4	46.5	53.3	45.6	43.2	41.9	38.3
47	39.52	23	14.2	47.7	55.3	47	44.9	43.7	40.4
48	54.76	22.4	13.7	48.9	55.7	48.5	46	44.9	41.5
49	70	21.7	13.1	48.9	55.7	49.6	47.2	46.1	42.5
50	9.45	-2	-28.7	-44.6	-34.7	-35.3	-34.8	-32.7	-32.5
51	9.75	-2.1	-28.7	-44.4	-34.4	-35.2	-34.7	-32.8	-32.4
52	10.05	-2.2	-28.9	-44.9	-34.8	-35.5	-35.1	-33.1	-32.6
53	10.85	-2.3	-29.3	-45.8	-35.7	-36.4	-35.6	-33.7	-33.1
54	11.35	-2.4	-29.5	-46.1	-36.1	-36.8	-36	-34	-33.5
55	12.65	-2.6	-29.8	-47	-36.8	-37.4	-36.7	-34.8	-34.1
56	13.65	-3.5	-30.2	-47.4	-37.3	-37.8	-37.2	-35.1	-34.5
57	14.65	-4.5	-31.2	-47.8	-37.7	-38.4	-37.6	-35.6	-34.8
58	19.73	-4.7	-32.9	-48.6	-38.2	-41.4	-41.1	-39.5	-39.4
59	24.81	3.1	-18.2	-25.2	-16.1	-19.5	-18.9	-17.4	-17.1
60	29.89	4.2	-15.9	-11.3	-3.5	-6.3	-6.3	-5	-5.9
61	34.97	4.4	-15.2	-8.3	0.4	-2.8	-3.1	-2.2	-3.7
62	40.05	4.7	-14.6	-6.5	1.8	-1.4	-2.1	-1.4	-2.8
63	45.13	5	-14.1	-6	2.3	-0.9	-1.6	-0.9	-2.3
64	50.21	5.5	-13.8	-5.7	2.7	-0.2	-1	-0.5	-1.9
65	55.29	5.9	-13.3	-5.8	2.7	-0.3	-1	-0.5	-1.9
66	60.37	6.5	-12.9	-5.5	-6.1	-0.2	-0.9	-0.3	-1.8
67	65.45	6.9	-12	-5.4	2.8	-0.1	-0.8	-0.2	-1.7
68	9.45	49.7	35.4	39.3	47.1	48.7	47.6	47.5	45.6
69	9.75	40.7	25	33.4	41.5	38.7	37.6	36.9	34
70	10.05	40	23.7	32.1	39.4	36.9	35.9	35.7	33.7
71	10.85	35.3	20.1	26.4	34.1	32.1	31.7	32.2	30.8
72	11.35	28.9	14.5	20.7	28.5	26.3	26	26.5	25.1

Table 4.1 (continued)

tap No.	distance (cm)	pressure head H (cm)							
		test9	test10	test11	test12	test13	test14	test15	test16
73	12.65	14.7	1.2	7.8	15.7	13.1	12.7	13.2	12
74	13.65	6.2	-7.9	-1.9	6.2	3.6	3.5	3	2.9
75	14.65	0.7	-15.5	-10.3	-2.2	-5	-4.9	-4.1	-5.2
76	19.73	-3.9	-29.3	-30.7	-22.1	-25.3	-25.5	-24.9	-25.3
77	24.81	1.5	-21.9	-25.6	-17.3	-20	-20.6	-19.1	-19.9
78	29.89	3.9	-17.2	-15.3	-6.9	-10.2	-10.6	-9.4	-10.2
79	34.97	4.2	-15.7	-10.1	-2.1	-4.9	-5.8	-5	-5.5
80	40.05	4.7	-14.6	-7.1	1.1	-2.2	-2.6	-2.1	-3.5
81	45.13	5.1	-14.1	-5.9	2.4	-1	-1.3	-1	-2.4
82	50.21	5.5	-13.4	-5.5	3	-0.3	-0.8	-0.4	-2
83	55.29	5.9	-13	-5.1	3.2	0	-0.5	-0.2	-1.7
84	60.37	6.5	-12.7	-5.3	3.2	0.1	-0.4	-0.1	-1.7
85	65.45	7.3	-12.3	-5.2	3.1	0	-0.4	-0.1	-1.6
86	80.45	8	-11.2	-5.1	3.1	0.1	-0.4	-0.1	-1.6
87	95.69	8.7	-11.5	-5.5	2.6	-0.4	-0.9	-0.4	-1.9
88	110.93	9.1	-10.8	-6.2	1.9	-0.9	-1.6	-0.9	-2.1
89	126.17	9	-11	-7.2	0.8	-1.7	-2.2	-1.6	-2.7
discharges, discharge ratio, Reynolds number, and energy loss coefficients									
Q_1 (*l/s*)		9.21	9.42	8.86	8.74	8.87	8.92	8.95	9.01
Q_2 (*l/s*)		6.75	5.59	0.76	0.76	1.45	1.73	2	2.42
Q_3 (*l/s*)		2.46	3.83	8.1	7.98	7.42	7.19	6.94	6.59
Q_3/Q_1		0.27	0.41	0.91	0.91	0.84	0.81	0.78	0.73
Re_1 x 10^{-5}		1.37	1.4	1.32	1.3	1.32	1.33	1.33	1.34
Re_2 x 10^{-5}		1.01	0.83	0.11	0.11	0.22	0.26	0.3	0.36
Pe_3 x 10^{-5}		0.37	0.57	1.21	1.19	1.11	1.07	1.04	0.98
K_{12} Eq.(4.6)		-0.11	-0.07	0.3	0.29	0.21	0.19	0.15	0.1
K_{13} Eq.(4.8)		0.87	0.89	1.14	1.14	1.09	1.07	1.06	1.03
K_{13} Eq.(4.12)		0.86	0.88	1.13	1.13	1.07	1.07	1.05	1.04

Table 4.1 (continued)

tap No.	distance (cm)	pressure head H (cm)							
		test17	test18	test19	test20	test21	test22	test23	test24
1	-152.24	34.4	30.8	54.5	36.7	26.8	69.5	13.8	54.4
2	-117.26	31.6	27.7	51.7	34	23.8	67	10.5	52.5
3	-94.4	29.2	25.2	49.4	31.6	21.4	64.8	8.2	49.2
4	-63.92	26.3	22.2	46.5	28.8	18.2	62.3	4.9	48
5	-41.06	24.3	20.1	44.5	27	16.3	60.1	2.2	47.7
6	-20.74	22.1	18.2	42.6	25.3	14.3	58.6	0.6	45.7
7	-13.12	21	17	41.6	24.1	13.1	57.4	-0.4	44.5
8	-10.58	20.7	16.7	41.4	23.7	12.7	56.7	-0.7	44.9
9	-5.5	17.7	14	39	21.2	10.6	53.3	-2.7	44.6
10	-4.5	16.7	13.2	38	20.1	9.7	51.7	-3.5	44.7
11	-3.5	14.9	11.2	36.4	18.5	8.4	49.4	-4.5	44.2
12	-2.2	11.1	7.9	33.4	15.2	5.6	43.5	-7.6	44.6
13	-1.7	8.4	5.3	31.2	13.1	3.6	40.3	-8.9	44.2
14	-1.2	4.9	2.1	28.3	10.4	1.3	35.5	-10.7	44.6
15	-0.8	1	-1.4	24.9	7.1	-1.4	29.6	-13	44.5
16	-0.4	-5.4	-6.9	19.6	2	-5.6	19.7	-16.7	44.4
17	-0.2	-10.5	-11	15.8	-1.7	-8.7	11.9	-19.4	43.3
18	9.35	50.7	46.4	65.9	51.6	42.9	78.5	29.5	38.3
19	9.55	53.6	48.7	71.1	53.3	43.6	78	29.7	41.2
20	9.95	53	48.3	70.8	52.7	42.5	75.4	28.4	41.6
21	10.35	50.8	45.9	68.7	51	40.8	74.5	27.1	42
22	10.85	48.7	44.1	66.8	49.1	39.2	73.9	25.7	42.3
23	11.35	47.5	43.4	66.3	48.4	38.7	73.7	25.6	42.4
24	12.65	43.7	40.2	63.3	45.5	36.3	71.7	23.2	42.2
25	13.65	41.8	38.9	61.9	44.2	35.3	71.2	22.6	42.5
26	14.65	40.2	37.4	60.6	43.2	34.3	70.6	21.8	42.5
27	19.73	37.9	35.2	58.4	40.8	32.8	70.3	20.4	42.1
28	22.27	37.7	34.7	58.2	40.6	32.7	70.5	20.4	41.9
29	29.89	38.6	35.7	58.9	41.3	33.3	71.9	20.7	41.2
30	37.51	39.8	36.5	59.8	42.2	33.7	72.3	20.8	40.9
31	45.13	40.5	37.2	60.3	42.8	34	72.4	20.9	41.2
32	52.75	40.9	37.7	60.7	43.2	34	72.4	20.7	40.2
33	60.37	41.6	38	61.1	43.5	34	72.5	20.4	39.7
34	67.99	42	38.3	61.3	43.8	34.1	72.5	20.2	39.3
35	75.61	42.1	38.3	61.4	43.8	33.9	72.6	19.9	38.5
36	83.23	42.3	38.4	61.5	43.9	33.9	72.6	19.8	37.6

Table 4.1 (continued)

tap No.	distance (cm)	pressure head H (cm)							
		test17	test18	test19	test20	test21	test22	test23	test24
37	104.47	42.5	38.4	61.5	43.9	33.4	72.5	19.2	37
38	119.71	42.5	38.4	61.6	43.8	33.1	72.5	18.7	35.4
39	142.57	42.3	38.1	61.3	43.5	32.7	72.4	18	34
40	165.43	42.1	37.9	60.8	43.2	32.2	72.5	17.5	32.9
41	188.29	41.8	37.5	60.4	42.8	31.6	72.4	16.6	31.7
42	-13.82	21.2	17.3	40.7	24	13.3	57.9	-0.2	44.7
43	-6.2	22.3	18.1	43	25.1	14	59.7	0.3	44.4
44	1.42	32.7	28	52.1	34.1	22.1	69	7.8	43.9
45	9.04	36.1	32.3	56	38.5	28.8	70.3	16.1	43.3
46	24.28	37.4	34.4	57.6	40.4	32.3	70.9	20.1	41.9
47	39.52	39.4	36.4	61.2	41.9	33.3	71.7	20.6	41
48	54.76	40.7	37.7	60.4	42.8	33.6	71.5	20.4	40.1
49	70	41.6	37.9	59.7	43.3	33.6	70.9	20	39.1
50	9.45	-28.6	-26.6	1.3	-16	-19.8	-19.4	-27.9	43.2
51	9.75	-28.6	-26.5	1.3	-16.1	-19.9	-19.5	-27.9	43.2
52	10.05	-28.8	-26.7	1.3	-16.2	-20	-19.7	-28	43.2
53	10.85	-29.3	-27.3	0.9	-16.5	-20.2	-20.6	-28.2	43.1
54	11.35	-29.7	-27.4	0.6	-16.7	-20.4	-21.1	-28.4	43.1
55	12.65	-30.1	-27.7	0.2	-17	-20.8	-22	-28.8	43
56	13.65	-30.8	-28.1	-0.5	-17.7	-21.2	-22.2	-29.1	43
57	14.65	-31.3	-28.6	-0.7	-18.1	-22	-22.5	-29.7	42.9
58	19.73	-35.6	-32.4	-4.2	-20.6	-23.4	-24.8	-33.4	43.1
59	24.81	-12.9	-11.9	15	-1.8	-7.1	1.3	-15.8	43.6
60	29.89	-3.7	-4.5	22	4.6	-2.9	13.1	-12.8	43.6
61	34.97	-2	-3.1	23.2	5.7	-1.7	16.3	-12	43.6
62	40.05	-1.3	-2.4	24.2	6.4	-1	17.5	-11.2	43.6
63	45.13	-0.9	-1.8	24.6	6.8	-0.4	18.1	-10.6	43.6
64	50.21	-0.5	-1.4	25	7.2	0.2	18.5	-10.1	43.6
65	55.29	-0.5	-1.3	25.1	7.3	0.4	18.5	-9.8	43.6
66	60.37	-0.3	-1.1	25.2	7.6	0.9	18.6	-9.4	43.6
67	65.45	-0.3	-1	25.2	7.7	1.1	18.5	-9.1	43.6
68	9.45	47	46.7	67.7	52.2	48.4	48.3	37.6	47.8
69	9.75	35.1	34.7	58.7	41.4	37.5	49.2	27.4	46.5
70	10.05	34.6	34.5	57.9	41.3	36.6	49	26.2	45.6
71	10.85	32.1	31.7	55.4	38.2	33.1	46.5	23	43.9
72	11.35	26.7	26.3	50.3	33	27.7	41.9	17.5	43.6

Table 4.1 (continued)

tap No.	distance (cm)	pressure head H (cm)							
		test17	test18	test19	test20	test21	test22	test23	test24
73	12.65	13	16.7	38.7	21.3	15.4	30	5.5	43.2
74	13.65	4.9	4.7	30.4	12.9	6.6	21.5	-3.5	43.1
75	14.65	-3	-3	23.2	5.7	-0.8	12.8	-11.5	42.8
76	19.73	-23.3	-22.7	4.9	-12.4	-18.1	-5.6	-26.7	43.2
77	24.81	-16.9	-16.1	11.1	-6.8	-11	0.3	-19.8	43.5
78	29.89	-7.6	-16.6	19	1.8	-4.4	9.8	-14.2	43.6
79	34.97	-3.7	-14.3	22.1	4.6	-2.1	14.8	-12.4	43.7
80	40.05	-1.6	-2.4	23.8	6.3	-0.7	17.1	-11.1	43.8
81	45.13	-0.9	-1.7	24.4	7	-0.2	18.3	-10.5	43.8
82	50.21	-0.6	-1.3	24.6	7.3	0.6	18.7	-10.1	43.8
83	55.29	-0.3	-1	25	7.7	0.9	19.2	-9.7	43.8
84	60.37	-0.1	-0.8	25.2	7.9	1.1	19.1	-9.3	43.8
85	65.45	0	-0.7	25.5	8.1	1.5	19.2	-9.1	43.8
86	80.45	0.1	-0.5	25.9	8.5	2.2	19.2	-8.3	43.8
87	95.69	-0.1	-0.5	25.8	8.4	2.4	18.7	-7.7	43.8
88	110.93	-0.3	-0.7	25.8	8.3	2.5	18	-7.5	43.8
89	126.17	-0.8	-1.1	25.2	7.9	2.1	16.8	-7.7	43.8
discharges, discharge ratio, Reynolds number, and energy loss coefficients									
Q_1 (*l/s*)		9.04	9.09	8.7	8.77	9.09	8.43	9.32	7.22
Q_2 (*l/s*)		2.8	3.32	3.14	3.29	4.31	0.23	5	7.22
Q_3 (*l/s*)		6.24	5.77	5.56	5.48	4.78	8.2	4.32	0
Q_3/Q_1		0.69	0.63	0.64	0.63	0.53	0.97	0.46	0
$Re_1 \times 10^{-5}$		1.35	1.36	1.3	1.31	1.35	1.26	1.39	1.08
$Re_2 \times 10^{-5}$		0.42	0.5	0.47	0.49	0.64	0.03	0.75	1.08
$Re_3 \times 10^{-5}$		0.93	0.86	0.83	0.82	0.71	1.22	0.64	0
K_{12} Eq.(4.6)		0.06	0.03	0.04	0.02	-0.06	0.36	-0.09	0.02
K_{13} Eq.(4.8)		1.01	0.98	0.97	0.97	0.92	1.21	0.86	1.01
K_{13} Eq.(4.12)		1.02	0.98	0.99	0.97	0.91	1.17	0.9	1

Table 4.2 Experimental data of dividing closed conduit flow $L/B = 0.77$

tap No.	distance (cm)	pressure head H (cm)							
		test1	test2	test3	test4	test5	test6	test7	test8
1	-154.36	75.5	61.8	51.7	42.3	34.6	29.5	36.3	43.3
2	-119.38	72.7	59	49	39.3	31.4	26.7	33.4	40.5
3	-96.52	70.8	56.9	46.6	37	29.1	24.7	31.5	38.6
4	-66.04	68.2	53.9	44	33.9	26.2	21.8	28.7	35.9
5	-43.18	66.6	52.2	41.9	32.1	24.3	20.1	27.1	34.2
6	-20.74	64.5	50.1	39.9	29.8	21.8	17.8	24.9	32.1
7	-13.12	63.9	49.4	39.1	29.1	21	17.2	24.2	31.4
8	-5.5	62.7	47.9	37.5	27	18.9	14.8	21.6	28.5
9	-4.5	62.5	47.8	37.1	26.8	18.3	14.3	21	27.4
10	-3.5	62.2	47.2	36.4	25.8	17.3	13.1	19.8	25.9
11	-2.2	61.4	46.1	35.1	24.3	15.7	11	17.1	22.9
12	-1.7	61	45.5	34.3	23.5	14.2	9.5	15.1	20.8
13	-1.2	60.3	44.4	32.9	21.6	12.5	7.4	12.5	17.7
14	-0.8	59.7	43.5	31.6	19.8	10.5	5.1	9.4	13.9
15	-0.4	58.9	42	29.9	17.6	7.7	1.8	5.2	8.5
16	-0.2	58.3	41.1	28.4	16	5.3	-0.9	1.4	3.9
17	7.24	66.3	61.3	56.6	51	45.7	42.8	51.2	57.9
18	7.44	71.9	64.4	58.1	51.4	45.5	42.6	51.9	59.6
19	7.84	73.8	64.1	56.8	49.4	43.7	40.9	50.3	58.8
20	8.24	72.9	62.7	55.4	48	42.5	39.5	48.6	56.7
21	8.74	72.3	61.8	54.3	46.9	41.3	38.3	47.2	55
22	9.24	72	61.4	53.8	46.5	40.8	37.8	46.7	54.5
23	10.54	71	60.4	52.4	45	39.1	35.9	44.4	51.8
24	11.54	70.7	59.8	51.9	44.5	38.4	35.1	43.7	50.8
25	12.54	70.4	59.5	51.5	43.9	38.2	34.6	43.3	50.1
26	17.62	69.7	58.8	51	43	37.2	33.7	42.3	48.6
27	20.16	69.6	58.5	50.1	42.9	37	33.6	42.4	48.7
28	27.78	68.9	58.1	49.7	42.7	36.7	33.5	42.3	49
29	35.4	68.5	57.7	49.4	42.4	36.4	33.3	42	49.1
30	43.02	68	57.2	49.1	41.9	36.1	33	42	49.2
31	50.64	67.5	56.8	48.6	41.7	35.7	32.7	41.8	49.3
32	58.26	67.3	56.4	48.3	41.3	35.4	32.4	41.6	49.2
33	65.88	66.8	56	47.9	40.9	35	32.1	41.2	49.1
34	73.5	66.2	55.4	47.4	40.3	34.6	31.7	41	49
35	81.12	65.7	54.9	46.9	39.8	34.2	31.3	40.9	48.7
36	102.36	64.3	53.6	45.6	38.6	33.1	30.7	40.2	48.5

Table 4.2 (continued)

tap No.	distance (cm)	pressure head H (cm)							
		test1	test2	test3	test4	test5	test6	test7	test8
37	117.6	63.1	52.5	44.8	37.7	32.3	30.4	39.8	48.4
38	140.46	61.6	50.7	43.6	36.6	31	29.3	39	47.9
39	163.31	60.2	49.8	42.4	35.4	30	28.3	38.5	47.4
40	186.18	58.8	48.5	41.1	34.2	28.8	27.5	38.3	46.8
41	201.42	57.8	47.9	40.3	33.5	28.2	26.9	38	46.6
42	-15.74	64.2	49.7	39.1	29.5	21.9	17.6	25.3	31.7
43	-8.12	63.7	49.2	38.8	29.2	21.4	17.4	25.4	31.9
44	-0.5	64.6	50.9	41.1	32	24.5	21.2	29.5	37.5
45	7.12	67.8	56.1	47.2	39.2	32.6	29.3	37.8	44.8
46	22.36	69	58.1	50	42.3	36.3	33.2	41.6	47.8
47	37.6	68.2	57.3	49.5	41.9	35.7	33.7	41.8	48.9
48	52.84	67.3	56.5	48.7	41.2	35.1	33.1	41.4	49
49	68.08	66.2	55.7	48	40.5	34.4	32.7	41.1	48.9
50	9.45	58.8	38.1	24.2	10.4	-0.9	-8	-10.1	-11.6
51	9.75	56.9	38.1	24.2	10.4	-0.8	-7.9	-10	-11.4
52	10.05	56.7	38	24	10.3	-1	-8.1	-10.2	-11.5
53	10.85	56.6	37.8	23.7	10.1	-1.4	-8.4	-10.5	-12
54	11.35	56.5	37.6	23.6	10	-1.7	-8.6	-10.9	-12.1
55	12.65	56.5	37.3	23.3	9.4	-1.8	-8.7	-11.4	-12.8
56	13.65	56.4	37.1	22.7	9.1	-2.1	-9.3	-11.8	-13.2
57	14.65	56.1	36.5	22	8.2	-2.8	-9.9	-12.3	-13.8
58	19.73	56	38.8	26.3	13.7	3.4	-2.8	-3	-2.6
59	24.81	58.4	42.6	30.4	18.7	9.5	4	6.1	8.6
60	29.89	59.3	43.4	31.4	20	11.3	6	8.5	11.2
61	34.97	60	44	32	20.8	12.3	7.2	9.8	12.4
62	40.05	60.9	44.8	32.8	21.7	13.3	8.1	10.5	13
63	45.13	61.8	45.6	33.6	22.4	14	8.7	11	13.5
64	50.21	62.8	46.4	34.5	23.1	14.7	9	11.4	13.7
65	55.29	63.3	47.2	35	23.9	15	9.3	11.6	13.9
66	60.37	63.6	47.8	35.7	24.3	15.6	9.7	11.8	14
67	65.45	63.8	48	36.1	24.7	16	10	11.8	13.9
68	9.45	94.8	84.1	73.3	66.3	59.4	50.6	53	55.8
69	9.75	88.6	75.8	65.6	55.5	48	36.8	42.2	44.3
70	10.05	86	74.3	64.1	54.3	46.7	38.1	41.1	43.7
71	10.85	73.6	64.8	56.3	47.7	40.5	33.1	36.4	38.6
72	11.35	67.2	57.6	49.2	38.3	33.4	26.8	30.3	32.7

Table 4.2 (continued)

tap No.	distance (cm)	pressure head H (cm)							
		test1	test2	test3	test4	test5	test6	test7	test8
73	12.65	59.2	45.1	35.2	24.8	18.2	13.6	16.5	18.6
74	13.65	57.3	43.2	28.6	17.9	9.1	5.6	8.2	10.3
75	14.65	56.5	38.1	24.9	13.3	4.6	-0.1	1.8	4
76	19.73	55.9	38.8	25.6	12.8	3.1	-3.5	-3.3	-2.2
77	24.81	58.2	42.3	29.7	17.7	8.6	2.6	4.3	6.4
78	29.89	59.3	43.4	31.2	19.6	10.9	5.4	8.4	10.4
79	34.97	59.9	44.1	31.7	20.3	12	6.7	9.4	11.8
80	40.05	60.7	45	32.8	21.5	13	7.6	10.3	12.6
81	45.13	61.6	45.6	33.7	22.2	13.8	8.3	10.9	13.2
82	50.21	62.5	46.5	34.6	22.9	14.5	8.8	11.2	13.5
83	55.29	63	47.1	35.2	23.4	15.1	9.2	11.4	13.6
84	60.37	63.3	47.7	35.6	23.9	15.5	9.5	11.6	13.8
85	65.45	63.6	48.2	36.1	24.3	15.8	9.8	11.7	13.7
86	80.55	63.7	48.6	36.7	24.9	16.5	10.4	11.9	13.8
87	95.79	63.6	48.4	36.5	24.8	16.4	10.3	11.7	13.5
88	111.03	63.5	48.3	36.3	24.6	16	10.1	11.4	12.9
89	126.27	63.4	48.2	36.1	24.3	15.7	9.7	10.9	12.2
discharges, discharge ratio, Reynolds number, and energy loss coefficients									
Q_1 (*l/s*)		8.44	8.61	8.82	8.95	9.1	8.72	8.62	8.5
Q_2 (*l/s*)		7.33	6.98	6.77	6.52	6.37	5.54	4.82	4.14
Q_3 (*l/s*)		1.12	1.63	2.05	2.43	2.73	3.18	3.79	4.35
Q_3/Q_1		0.13	0.19	0.23	0.27	0.3	0.37	0.44	0.51
Re_1 x 10^{-5}		1.26	1.28	1.32	1.33	1.36	1.3	1.28	1.27
Re_2 x 10^{-5}		1.09	1.04	1.01	0.97	0.95	0.83	0.72	0.62
Re_3 x 10^{-5}		0.2	0.29	0.36	0.43	0.48	0.56	0.67	0.77
K_{12} Eq.(4.6)		-0.07	-0.09	-0.1	-0.11	-0.11	-0.1	-0.11	-0.05
K_{13} Eq.(4.8)		0.91	0.92	0.92	0.94	0.93	0.95	1.01	1.08
K_{13} Eq.(4.12)		0.9	0.91	0.91	0.91	0.92	0.94	0.98	1.04

Notes:

1. Pressure taps 1 to 41 located on the center of the branch side wall of main conduit, taps 42 to 49 on the opposite wall of the main. The distances equate to X.
2. Pressure taps 50 to 67 located on the center of upstream side wall of branch conduit, taps 68 to 89 on the downstream side wall of the branch. The distances equate to Y.

Table 4.2 (continued)

tap No.	distance (cm)	pressure head H (cm)							
		test9	test10	test11	test12	test13	test14	test15	test16
1	-154.36	48.8	41.9	36.4	103.9	85.9	69.2	37	47.5
2	-119.38	46.2	39.1	33.3	101.4	83.2	66.6	33.7	44.5
3	-96.52	44.3	37.2	31.2	100	81.5	64.6	31.8	42.2
4	-66.04	41.8	34.4	28.1	97.7	78.9	61.7	28.6	39.2
5	-43.18	40	32.6	26.2	96.1	77.5	60.1	26.6	37.4
6	-20.74	37.9	30.5	23.9	94.4	75.4	58	24.1	35
7	-13.12	36.9	29.6	23.1	93.2	74.7	57.1	23.4	34.1
8	-5.5	34.7	26.3	21.1	88.8	70.1	52.9	20.5	30.9
9	-4.5	32.9	25.4	20.7	87.1	68.6	51.5	19.8	29.9
10	-3.5	31.3	23.5	19.5	84.2	65.9	49	18.8	28.1
11	-2.2	28	19.8	17.5	78	60	43.6	16.2	24.4
12	-1.7	25.4	17.2	16.1	73.5	55.9	39.9	14.1	21.7
13	-1.2	21.7	13.5	14	66.8	49.7	34.1	11.3	18.1
14	-0.8	17.6	8.9	11.6	58.4	42.4	27.4	8.5	13.6
15	-0.4	11.5	2.2	8.4	44.9	30.3	17.1	4.5	7
16	-0.2	5.9	-3.6	5.6	32.8	19.4	7.8	0.1	1.2
17	7.24	62.6	55.4	49.9	106.4	96.9	83.2	52.7	63.2
18	7.44	65.9	59.2	49.7	108.8	101.4	89.4	53.2	66.2
19	7.84	65.2	59	47.9	109.2	100.5	90.3	51.5	65.5
20	8.24	63.2	56.7	46.4	109.3	98.3	87.3	49.7	62.8
21	8.74	61.3	54.7	45.3	109.4	96.1	84	48.4	60.9
22	9.24	60.8	54.1	44.7	109.2	94.8	82.5	48	60.3
23	10.54	57.8	51.2	42.9	106.7	91.2	77.2	46	57.4
24	11.54	56.6	49.7	42.1	105.8	89.7	74.8	44.8	55.9
25	12.54	55.6	48.5	41.7	105.6	89	73.5	44.2	55.1
26	17.62	53.5	46.2	40.8	105.1	88.1	71.3	43	52.9
27	20.16	53.4	46.1	40.6	105.9	88.2	71.5	42.9	52.8
28	27.78	53.7	46.7	40.4	106.8	88.9	72.1	42.8	53.4
29	35.4	54.2	47.3	40.2	106.9	89.3	72.8	42.5	53.9
30	43.02	54.7	47.8	39.9	106.9	90	73.6	42.4	54.1
31	50.64	54.9	48.2	39.8	106.9	90.5	74.1	42.2	54.2
32	58.26	55	48.4	39.5	106.9	90.7	74.6	42	54.4
33	65.88	55.1	48.4	39.3	106.9	90.9	75	41.7	54.4
34	73.5	55.1	48.5	38.7	106.9	91	75.4	41.3	54.5
35	81.12	55.1	48.4	38.4	106.9	90.9	75.6	41.1	54.3
36	102.36	55	48.3	37.4	106.9	90.9	75.7	40.3	54.2

Table 4.2 (continued)

tap No.	distance (cm)	pressure head H (cm)							
		test9	test10	test11	test12	test13	test14	test15	test16
37	117.6	54.9	48.2	36.7	106.9	90.8	75.6	39.9	53.9
38	140.46	54.7	47.9	35.6	106.9	90.8	75.5	39.1	53.3
39	163.31	54.2	47.6	34.5	106.9	90.8	75.4	38.3	52.9
40	186.18	53.7	47.3	33.8	106.9	90.8	75.3	37.5	52.5
41	201.42	53.5	47	33.2	106.9	90.7	75.3	37.1	52.2
42	-15.74	37.6	30.3	24.2	95.1	76.1	58	23.7	34.8
43	-8.12	37.8	30.8	24.1	96.2	77.1	58.7	23.8	35.1
44	-0.5	44.3	37.5	27.8	104.2	85.4	67.3	28.7	41.7
45	7.12	50.5	43.1	36.4	105.9	87.9	70.4	38.4	49
46	22.36	53	45.6	40.2	106.6	88.6	71.2	42.8	52.4
47	37.6	54.3	47.7	39.9	107	90.3	73	42.4	53.8
48	52.84	54.9	48.3	39.5	107	91.2	74.2	42	54.3
49	68.08	55	48.5	39	107	91.4	74.7	41.6	54.4
50	9.45	-13.4	-24.6	-2.5	-18.4	-24.6	-28.8	-11.8	-18.3
51	9.75	-13.3	-24.5	-2.4	-18.4	-24.6	-28.7	-11.7	-18.2
52	10.05	-13.4	-24.6	-2.5	-18.5	-24.8	-29	-11.8	-18.4
53	10.85	-13.9	-25.1	-2.9	-19.6	-25.5	-29.8	-12.5	-19
54	11.35	-14.1	-25.3	-3.1	-20.1	-25.7	-30.1	-12.7	-19.2
55	12.65	-14.7	-26	-4.1	-21	-26.6	-30.9	-13.1	-19.8
56	13.65	-15.1	-26.4	-4.7	-21.1	-27.1	-31.3	-13.5	-20.4
57	14.65	-15.6	-26.8	-5.2	-22.5	-28	-32.4	-14.1	-21
58	19.73	-2.3	-13.2	2	7.4	-3	-10.9	-4.5	-7.2
59	24.81	10.4	0.8	8.8	31.8	20.3	10	4.7	6.4
60	29.89	13	3.6	11	34.6	23.5	13.4	7.9	9.1
61	34.97	14.1	4.7	12.2	35.1	24.6	14.4	9	10.4
62	40.05	15	5.3	13.1	35.3	24.9	14.8	9.7	11.3
63	45.13	15.3	5.7	13.8	35.2	24.9	14.9	10.5	11.7
64	50.21	15.1	6	14.6	34.9	24.7	14.8	11.4	11.8
65	55.29	15.3	6	15.1	34.5	24.3	14.5	11.8	11.9
66	60.37	15.4	5.9	15.4	34	24	14.2	11.9	11.8
67	65.45	15.3	5.8	15.6	33.2	23.2	13.9	12.1	11.7
68	9.45	57.2	49.2	58.4	35.8	50.3	56	57.4	58.7
69	9.75	45.4	36.9	47.4	50	51.6	44.4	45.1	45.7
70	10.05	45.2	37	46	56.8	55.8	46	43.2	45.3
71	10.85	40.2	32	40.9	55.8	49.4	41.1	38	39.5
72	11.35	33.9	25.1	34.1	49.6	42.3	34.1	31.2	32.7

Table 4.2 (continued)

tap No.	distance (cm)	pressure head H (cm)							
		test9	test10	test11	test12	test13	test14	test15	test16
73	12.65	19.9	10.6	19.3	34.7	26.3	17.6	16.3	17.2
74	13.65	11.4	1.6	11	25	16	7.7	7.5	7.8
75	14.65	4.8	-5.1	5.1	17.6	8.3	-0.1	0.6	0.4
76	19.73	-1.8	-11.7	2	13.8	3	-6.4	-4.4	-6.6
77	24.81	7.3	-2.2	8.3	26.7	15.3	5.1	3.2	3.5
78	29.89	11.7	2.4	11.1	32.9	21.6	11.4	6.7	8.1
79	34.97	13.2	4.1	12.3	34.8	23.5	13.6	8.6	9.8
80	40.05	14.4	4.9	13.5	35.5	24.7	14.5	10.2	10.9
81	45.13	14.8	5.4	14.2	35.4	24.9	14.7	10.8	11.5
82	50.21	15	5.8	14.6	35.2	24.6	14.6	11.4	11.7
83	55.29	15.2	5.9	15.2	34.8	24.4	14.4	11.3	11.8
84	60.37	15.2	5.9	15.5	34.2	23.7	14.1	11.5	11.9
85	65.45	15.1	5.7	15.7	33.7	23.3	13.6	11.7	11.8
86	80.55	15	5.5	16.1	32.4	22.1	12.7	12.1	11.7
87	95.79	14.6	5	16.1	31	21	11.7	12	11.4
88	111.03	14	4.3	15.9	29.3	19.5	10.3	11.6	10.8
89	126.27	13.1	3.3	15.5	27.1	17.9	8.8	11.1	10
discharges, discharge ratio, Reynolds number, and energy loss coefficients									
Q_1 (*l/s*)		8.45	8.52	8.98	7.81	8.14	8.47	9.01	8.96
Q_2 (*l/s*)		3.63	3.51	5.84	0	0.88	1.87	5.3	4.07
Q_3 (*l/s*)		4.82	5.01	3.14	7.81	7.26	6.6	3.72	4.89
Q_3/Q_1		0.57	0.59	0.35	1	0.89	0.78	0.41	0.55
$Re_1 \times 10^{-5}$		1.26	1.27	1.34	1.16	1.21	1.26	1.34	1.34
$Re_2 \times 10^{-5}$		0.54	0.52	0.87	0	0.13	0.28	0.79	0.61
$Re_3 \times 10^{-5}$		0.85	0.89	0.56	1.38	1.29	1.17	0.66	0.87
K_{12} Eq.(4.6)		-0.02	-0.01	-0.12	0.35	0.25	0.15	-0.11	-0.04
K_{13} Eq.(4.8)		1.13	1.15	0.94	1.64	1.48	1.39	0.99	1.1
K_{13} Eq.(4.12)		1.07	1.09	0.93	1.61	1.44	1.31	0.96	1.07

Table 4.2 (continued)

tap No.	distance (cm)	pressure head H (cm)							
		test17	test18	test19	test20	test21	test22	test23	test24
1	-154.36	40	20.1	24.9	22.4	43.4	21.2	25.2	21
2	-119.38	36.4	18.6	23.3	21.6	42.2	20	24	19.7
3	-96.52	34.4	17.6	22.4	21.1	41.7	19.4	23.5	19.1
4	-66.04	31.1	16.4	21	20.4	40.7	18.4	22.4	18.1
5	-43.18	29.1	15.7	20.1	19.9	39.9	17.8	22.1	17.3
6	-20.74	26.7	14.4	18.9	19.3	39.4	16.7	21.1	16.5
7	-13.12	26.1	14	18.5	19.1	38.9	16.5	20.7	16.2
8	-5.5	23.2	12.8	17.1	18.4	37.4	15.4	19.5	15
9	-4.5	22.4	12.5	16.6	18	36.4	14.8	18.7	14.4
10	-3.5	20.8	11.9	15.8	17.7	35.6	14	17.7	13.5
11	-2.2	18.4	11.2	14.4	17.1	33.9	12.8	16.3	12.2
12	-1.7	16.3	10.6	13.2	16.7	32.6	11.8	15	11
13	-1.2	13.3	9.1	11.4	15.9	30.1	10	12.9	9
14	-0.8	10.3	8.1	9.5	14.9	27.7	8.3	10.9	7.1
15	-0.4	5.6	6.2	6.3	13.4	23.7	5.6	7.5	4
16	-0.2	0.9	4.5	3.3	11.7	19.2	2.4	3.6	0.5
17	7.24	56.7	26	31.2	25	46	24.3	28.9	24.4
18	7.44	57.4	26.1	32.6	26	48	26.4	31	26.6
19	7.84	55.8	25.4	32.3	26.1	48.2	26.6	31.5	27
20	8.24	54.1	24.6	31.1	25.5	47.1	25.9	30.7	26.3
21	8.74	52.6	24	30.4	24.9	46.1	24.9	29.5	25.2
22	9.24	51.9	23.8	30.1	24.7	45.4	24.7	29	24.8
23	10.54	49.3	22.8	28.7	24	44	23.6	27.4	23.5
24	11.54	48.3	22.5	28.1	23.5	43.3	22.9	26.4	22.7
25	12.54	47.5	22.2	27.6	23.3	43.2	22.5	26	22.2
26	17.62	46.4	21.8	26.8	22.7	42.8	21.4	25.2	21.1
27	20.16	46.3	21.7	26.5	22.7	42.9	21.5	25.2	21.1
28	27.78	46.2	21.6	26.7	22.9	43.2	21.7	25.4	21.3
29	35.4	45.8	21.5	26.9	23	43.4	22	25.5	21.6
30	43.02	45.8	21.5	27.1	23.1	43.6	22.4	26	21.9
31	50.64	45.8	21.3	27.2	23.2	43.8	22.5	26.2	22.2
32	58.26	45.6	21.2	27.3	23.4	43.9	22.7	26.4	22.3
33	65.88	45.4	21	27.4	23.5	44	22.8	26.5	22.4
34	73.5	45.2	20.9	27.3	23.5	44.1	22.9	26.6	22.5
35	81.12	44.7	20.7	27.3	23.4	44	22.9	26.6	22.6
36	102.36	44.5	20.5	27.2	23.3	44	22.9	26.7	22.7

Table 4.2 (continued)

tap No.	distance (cm)	pressure head H (cm)							
		test17	test18	test19	test20	test21	test22	test23	test24
37	117.6	43.8	20.2	27	23.3	44	22.8	26.7	22.6
38	140.46	42.9	19.8	26.8	23.2	44	22.8	26.6	22.6
39	163.31	42	19.4	26.7	23.2	44	22.7	26.6	22.5
40	186.18	41.1	18.9	26.4	23	44	22.6	26.6	22.4
41	201.42	40.7	18.7	26.2	22.9	44	22.5	26.5	22.3
42	-15.74	26.3	14	18.7	19.6	38.7	18	21.1	16.6
43	-8.12	26.6	14.1	18.9	19.8	39	18.3	21.3	16.8
44	-0.5	31.7	15.9	21.9	21	41.7	20.7	24	19.4
45	7.12	41.5	19.8	25.3	21.4	42.7	21.6	24.8	20.4
46	22.36	45.8	21.5	26.4	22.8	43	22.2	24.9	21.2
47	37.6	45.8	21.6	27.1	23.3	43.1	23.2	26	21.8
48	52.84	45.3	21.4	27.3	23.5	43.6	23.6	26.4	22.2
49	68.08	44.9	21.1	27.4	23.5	43.9	23.8	26.6	22.4
50	9.45	-11	1	-4.3	8.1	7	-3	-5.7	-7.8
51	9.75	-10.9	1.1	-4.3	8.2	6.9	-2.9	-5.7	-7.8
52	10.05	-10.8	1	-4.3	8.1	6.8	-3	-5.8	-7.8
53	10.85	-11.6	0.9	-4.5	8	6.8	-3.2	-5.9	-8.1
54	11.35	-12	0.7	-4.7	7.8	6.6	-3.2	-6	-8
55	12.65	-12.3	0.6	-4.9	7.7	6.4	-3.4	-6.1	-8.4
56	13.65	-12.9	0.3	-5.1	7.3	6.2	-3.6	-6.5	-8.7
57	14.65	-13.8	0	-5.6	7	6	-3.9	-6.6	-9
58	19.73	-3.5	3.4	0.3	10.4	13.5	1.2	-0.7	-2.8
59	24.81	6.2	7.1	6.5	13.8	21.2	6.9	6.4	3.4
60	29.89	8.9	8.1	7.9	14.3	22.2	7.8	7.5	4.4
61	34.97	10.2	8.6	8.4	14.6	22.5	8.2	7.8	4.7
62	40.05	11.1	8.8	8.5	14.7	22.4	8.4	7.9	4.8
63	45.13	11.9	9.1	8.7	14.8	22.4	8.4	7.8	4.8
64	50.21	12.3	9.3	8.8	14.8	22.3	8.4	7.8	4.7
65	55.29	12.7	9.5	8.7	14.6	22.2	8.3	7.7	4.6
66	60.37	13	9.6	8.6	14.5	22	8.2	7.6	4.5
67	65.45	13.3	9.8	8.5	14.4	21.7	8	7.4	4.3
68	9.45	59.9	29.4	29.3	24	33.8	23	22.4	19.4
69	9.75	48	24.2	23.6	21.2	32.1	18.3	17.4	14.4
70	10.05	45.8	23.3	23.3	21.2	33.3	18.3	17.8	14.6
71	10.85	40.5	21.4	21.1	20.4	32.3	17.5	16.8	14
72	11.35	33.6	18.3	18.1	18.8	29.4	14.9	14.2	11.2

Table 4.2 (continued)

tap No.	distance (cm)	pressure head H (cm)							
		test17	test18	test19	test20	test21	test22	test23	test24
73	12.65	18.2	11.8	11.2	15.4	23.9	10.2	9.1	6.4
74	13.65	9.4	8.1	7.4	13.4	20.2	7.1	5.8	3.1
75	14.65	2.3	5	4.3	11.8	17.3	4.8	3.3	0.8
76	19.73	-3.3	2.9	0.9	10.1	15	2.3	1.1	-1.7
77	24.81	4.5	6.2	5.2	12	18.6	5.5	4.4	1.4
78	29.89	8.2	7.8	7.3	13.4	21.3	7.5	6.5	3.5
79	34.97	9.8	8.3	8	13.5	21.6	7.9	6.9	4.1
80	40.05	11	8.9	8.4	13.8	22.4	8.5	7.6	4.7
81	45.13	11.8	9.2	8.6	14	22.6	8.7	7.8	4.9
82	50.21	12.3	9.4	8.8	14	22.4	8.6	7.7	4.8
83	55.29	12.7	9.6	8.8	14	22.3	8.5	7.6	4.7
84	60.37	12.9	9.7	8.7	13.9	22	8.4	7.4	4.5
85	65.45	13	9.7	8.6	13.8	21.6	8.3	7.2	4.3
86	80.55	13.2	9.8	8.5	13.7	21.2	8.2	7	4.1
87	95.79	13.1	9.7	8.3	13.5	20.8	7.8	6.5	3.7
88	111.03	12.8	9.5	8	13.3	20.2	7.5	6.2	3.4
89	126.27	12.2	9.3	7.5	13	19.5	7	5.5	2.8
discharges, discharge ratio, Reynolds number, and energy loss coefficients									
Q_1 (*l/s*)		9.22	5.88	5.84	4	4.62	4.73	4.73	4.95
Q_2 (*l/s*)		5.32	3.67	2.64	1.72	0.63	1.69	1.21	1.41
Q_3 (*l/s*)		3.9	2.21	3.19	2.29	4	3.04	3.52	3.54
Q_2/Q_1		0.42	0.38	0.55	0.57	0.86	0.64	0.74	0.72
$Re_1 \times 10^{-5}$		1.37	0.88	0.87	0.6	0.69	0.71	0.71	0.74
$Re_2 \times 10^{-5}$		0.79	0.55	0.39	0.26	0.09	0.25	0.18	0.21
$Re_3 \times 10^{-5}$		0.69	0.39	0.57	0.41	0.71	0.54	0.62	0.63
K_{12} Eq.(4.6)		-0.1	-0.11	-0.06	-0.04	0.25	0.02	0.09	0.08
K_{13} Eq.(4.8)		1	0.99	1.11	1.16	1.46	1.18	1.31	1.25
K_{13} Eq.(4.12)		0.97	0.95	1.06	1.08	1.39	1.14	1.26	1.22

Table 4.3 Experimental data of dividing closed conduit flow $L/B = 0.22$

tap No.	distance (cm)	pressure head H (cm)							
		test1	test2	test3	test4	test5	test6	test7	test8
1	-159.49	25.4	21.5	13.9	13	20.4	39	9.8	9
2	-124.51	24.8	20.9	13.5	12.6	20.1	38.6	9.4	8.8
3	-101.65	24.2	20.3	12.9	12	19.4	37.9	8.8	8
4	-71.17	23.5	19.5	12.1	11.2	18.5	37.1	8	7.2
5	-48.31	23.2	19.1	11.7	10.7	18	36.5	7.5	6.7
6	-28.37	22.6	18.6	11.1	10.1	17.4	35.9	7	6.2
7	-20.75	22.4	18.4	10.9	9.9	17.2	35.7	6.8	6
8	-13.13	22.2	18.2	10.7	9.7	16.9	35.5	6.6	5.8
9	-10.59	22	18	10.6	9.6	16.8	35.2	6.5	5.7
10	-5.51	21.6	17.6	10.1	9.1	16.1	34.5	6.3	5.3
11	-4.51	21.4	17.5	9.9	8.8	15.9	34.1	6.2	5.2
12	-3.51	21.2	17.3	9.6	8.4	15.4	33.6	6.1	5
13	-2.21	20.7	16.6	8.8	7.6	14.3	32.1	5.9	4.6
14	-1.71	20.3	16.1	8.2	6.9	13.4	31	5.6	4.2
15	-1.21	19.6	15.4	7.2	5.8	11.9	29.3	5.4	3.7
16	-0.81	18.8	14.4	5.8	4.4	10	26.8	5	3
17	-0.41	17.4	12.6	3.5	1.8	6.6	22.1	4.5	1.9
18	-0.21	16	11	0.3	-0.6	3.3	17.6	4	0.9
19	2.24	27.2	23.7	16.5	16	23.6	40.4	9.5	10.6
20	2.44	26.9	23.5	16.8	16.5	24.8	43.1	9.1	10
21	2.84	26.2	22.7	16.2	15.7	24.2	43.2	8.6	9.4
22	3.24	25.6	22	15.3	14.9	23.3	42.4	8.3	8.8
23	3.74	25	21.4	14.7	14.2	22.5	41.4	8	8.4
24	4.24	24.7	21.2	14.4	13.9	22.2	41.1	7.9	8.1
25	5.54	24.2	20.8	13.8	13.2	21.3	40.4	7.6	7.7
26	6.54	24	20.5	13.6	12.9	21	40	7.5	7.5
27	7.54	23.9	20.4	13.4	12.7	20.7	39.8	7.4	7.3
28	12.63	23.6	20	13	12.4	20.3	39.3	7.2	7.1
29	15.16	23.5	19.7	12.9	12.4	20.2	39.2	7.1	7
30	22.79	23.3	19.6	12.8	12.3	20.1	39.1	6.9	6.9
31	30.4	23.2	19.5	12.7	12.2	20	39	6.7	6.8
32	38.02	23.1	19.4	12.6	12.1	19.8	39	6.6	6.6
33	45.64	23	19.3	12.5	12	19.7	38.9	6.4	6.5
34	60.88	22.8	19.2	12.3	11.8	19.5	38.8	6.1	6.2
35	76.13	22.6	18.9	12	11.5	19.2	38.5	5.9	5.9
36	97.16	22.2	18.5	11.7	11.2	18.9	38.3	5.5	5.5

Table 4.3 (continued)

tap No.	distance (cm)	pressure head H (cm)							
		test1	test2	test3	test4	test5	test6	test7	test8
37	112.4	21.9	18.2	11.5	10.9	18.7	38	5.1	5.2
38	135.27	21.5	17.8	11.1	10.5	18.3	37.8	4.5	4.7
39	158.13	21.2	17.6	10.9	10.2	18	37.6	4	4.2
40	180.99	20.8	17.2	10.5	9.8	17.7	37.2	3.6	3.8
41	196.22	20.6	16.9	10.4	9.6	17.4	37.1	3.4	3.6
42	-20.75	22.1	18	10.8	10	17	35.6	6.8	5.8
43	-13.13	21.9	17.9	10.6	9.8	16.8	35.4	6.6	5.6
44	-5.51	22	18.1	10.8	10	17.1	35.8	6.5	5.7
45	2.11	22.7	18.8	11.9	11.3	18.8	37.4	7	6.3
46	17.35	23.4	19.6	12.8	12.3	20	39	7.2	6.8
47	32.6	23	19.4	12.6	12.1	19.8	38.4	6.6	6.5
48	47.83	22.7	19.2	12.4	11.8	19.6	38.3	6.3	6.2
49	63.07	22.5	19	12.2	11.6	19.3	38.1	6	5.9
50	9.45	9.2	2.3	-11.6	-15.2	-18.2	-14.7	2.3	-3.8
51	9.75	8.6	1.5	-12.6	-16.3	-19.8	-17	2.1	-4.2
52	10.05	8.5	1.3	-12.9	-16.7	-20.1	-17.7	2.1	-4.3
53	10.85	8.4	1.2	-13	-16.8	-20.4	-18	2.1	-4.4
54	11.35	8.5	1.3	-12.8	-16.5	-19.9	-16.8	2.2	-4.3
55	12.65	10.6	4.3	-8.4	-11.4	-11.9	-3.9	2.5	-3.1
56	13.65	12.7	6.8	-3.8	-7.3	-6.3	3.1	3.1	-1.6
57	14.65	14	8.4	-2.9	-5	-3.8	5.9	3.6	-0.5
58	19.73	16	10.4	-0.6	-2.9	-1.5	7.5	4.9	1.5
59	24.81	16.3	10.8	-0.4	-2.6	-1.3	7.3	5.1	1.8
60	29.89	16.2	10.7	-0.6	-2.9	-1.6	6.7	5.1	1.8
61	34.97	16.1	10.5	-0.9	-3.2	-2	6	5.1	1.7
62	40.05	15.9	10.3	-1.2	-3.6	-2.4	5.2	5.1	1.6
63	45.13	15.8	10.1	-1.5	-4	-3	4.5	5	1.5
64	50.21	15.6	9.8	-1.9	-4.3	-3.6	3.5	5	1.4
65	55.29	15.4	9.6	-2.2	-4.7	-4.1	2.8	4.9	1.3
66	60.37	15.3	9.3	-2.6	-5.1	-4.8	1.9	4.8	1.1
67	9.45	24.1	19.3	8.9	7.4	11	19.1	10.5	9.3
68	9.75	19.9	14.6	3.1	0.9	2.6	11	8	5.7
69	10.05	17.3	11.7	0.1	-2.3	-1.5	6.2	5.5	3
70	10.85	11.5	5.1	-7.5	-10.4	-11.2	-4.7	2.4	-2.2
71	11.35	10.3	3.7	-9.4	-12.5	-14	-7.9	2.3	-3.2
72	12.65	10.8	4.4	-8.1	-11.1	-11.9	-4.3	2.5	-2.9

Table 4.3 (continued)

tap No.	distance (cm)	pressure head H (cm)							
		test1	test2	test3	test4	test5	test6	test7	test8
73	13.65	12.4	6.4	-5.4	-8.1	-7.7	1.5	3	-1.6
74	14.65	13.8	8.2	-3	-5.6	-4.5	4.8	3.7	-0.4
75	19.73	16	10.7	-0.6	-2.8	-1.3	7.6	5	1.6
76	24.81	16.3	11	-0.3	-2.7	-1.2	7.3	5.3	1.9
77	29.89	16.2	10.9	-0.5	-2.9	-1.6	6.7	5.2	1.9
78	34.97	16.1	10.7	-0.7	-3.2	-2	6.2	5.1	1.8
79	40.05	15.7	10.3	-1.2	-3.6	-2.6	5.3	5	1.6
80	45.13	15.8	10.4	-1.4	-3.8	-2.9	4.7	5.1	1.6
81	50.21	15.6	10.2	-1.7	-4.2	-3.5	3.9	5.1	1.5
82	55.29	15.4	9.9	-2	-4.6	-4.1	2.9	5	1.4
83	60.37	15.2	9.6	-2.3	-4.9	-4.7	2	4.9	1.3
84	82.67	14.7	8.8	-3.4	-6.1	-6.3	-0.2	4.9	0.9
85	97.91	14.1	8.1	-4.4	-7.2	-7.9	-2.8	4.7	0.6
86	113.15	13.6	7.3	-5.3	-8.3	-9.4	-5.1	4.6	0.3
discharges, discharge ratio, Reynolds number, and energy loss coefficients									
Q_1 (*l/s*)		4.02	4.06	4.09	4.2	4.41	4.27	4.15	4.15
Q_2 (*l/s*)		3.41	3.34	3.21	3.24	3.23	2.8	3.88	3.66
Q_3 (*l/s*)		0.62	0.72	0.88	0.96	1.18	1.47	0.26	0.49
Q_3/Q_1		0.15	0.18	0.22	0.23	0.27	0.34	0.06	0.12
$Re_1 \times 10^{-5}$		0.6	0.6	0.61	0.63	0.66	0.64	0.62	0.62
$Re_2 \times 10^{-5}$		0.51	0.5	0.48	0.48	0.48	0.42	0.58	0.55
$Re_3 \times 10^{-5}$		0.2	0.23	0.28	0.31	0.38	0.47	0.08	0.16
K_{12} Eq.(4.6)		-0.11	-0.12	-0.11	-0.11	-0.11	-0.11	-0.09	-0.1
K_{13} Eq.(4.8)		1.44	1.45	1.71	1.65	1.87	2.53	1.05	1.19
K_{13} Eq.(4.12)		1.35	1.4	1.62	1.6	1.79	2.29	1.04	1.19

Notes:

1. Pressure taps 1 to 41 located on the center of the branch side wall of main conduit, taps 42 to 49 on the opposite wall of the main. The distances equate to X.
2. Pressure taps 50 to 66 located on the center of upstream side wall of branch conduit, taps 67 to 86 on the downstream side wall of the branch. The distances equate to Y.

Table 4.3 (continued)

tap No.	distance (cm)	pressure head H (cm)						
		test9	test10	test11	test12	test13	test14	test15
1	-159.49	58.4	77.4	141	116.2	108.2	47.1	136.6
2	-124.51	58.1	77.1	140.6	115.7	108	46.2	135.5
3	-101.65	57.5	76.6	140.2	115.2	107.6	44.7	134.6
4	-71.17	56.9	76	139.5	114.5	107.2	43.9	133.4
5	-48.31	56.5	75.6	139.1	114.1	107	43.2	132.8
6	-28.37	56	75.1	138.6	113.6	106.7	42.5	131.9
7	-20.75	55.8	75	138.5	113.4	106.6	42	131.6
8	-13.13	55.6	74.9	138.2	113.1	106.4	41.7	131.2
9	-10.59	55.4	74.7	138	113	106.3	41.4	130.9
10	-5.51	54.7	73.8	136.7	111.7	105.4	40.5	129.3
11	-4.51	54.2	73.2	136	111	104.8	39.8	128.4
12	-3.51	53.7	72.5	135	110	104	39.2	127.2
13	-2.21	52.1	70.6	132.1	107.3	101.8	37.4	124.9
14	-1.71	50.9	69	129.8	105.3	100	36.1	122.2
15	-1.21	48.8	66.3	126.8	101.4	96.8	33.6	117.6
16	-0.81	45.8	62.4	119.9	95.7	92.1	30.7	111.2
17	-0.41	40.4	55.1	108.4	85.1	82.9	24.8	98.6
18	-0.21	35	47.6	96.7	74.2	73.4	19.2	86.2
19	2.24	56.5	70.2	124.7	102.3	93.4	50.5	127.6
20	2.44	61.6	79	139.3	116.1	104.8	53.2	140.9
21	2.84	62.9	82.2	145.6	121.6	110.3	52.9	145.2
22	3.24	62.3	81.6	145.5	121.4	110.5	51.4	144.1
23	3.74	61.4	80.5	144.4	120	109.9	50.2	142.3
24	4.24	61.2	80.5	144.2	119.7	109.8	49.9	141.9
25	5.54	60.4	79.5	143.6	119	109.1	48.7	140.4
26	6.54	60.1	79.1	142.9	118.5	108.7	48.2	139.7
27	7.54	59.9	78.9	142.2	118.1	108.5	47.7	139.2
28	12.63	59.3	78	141	116.8	108.2	47	137.8
29	15.16	59.2	77.8	140.9	116.6	108.1	46.9	137.6
30	22.79	59.1	77.9	141	116.7	108.3	46.8	137.7
31	30.4	59.2	78	141.2	117	108.4	46.7	137.8
32	38.02	59.2	78.1	141.4	117.1	108.4	46.6	137.9
33	45.64	59.1	78.2	141.5	117.2	108.5	46.5	137.9
34	60.88	59.1	78.2	141.7	117.3	108.6	46.2	137.9
35	76.13	59	78.2	141.6	117.2	108.6	45.9	137.7
36	97.16	58.9	78.1	141.6	117.2	108.6	45.5	137.5

Table 4.3 (continued)

tap No.	distance (cm)	pressure head H (cm)						
		test9	test10	test11	test12	test13	test14	test15
37	112.4	58.8	78	141.6	117.2	108.5	45.1	137.4
38	135.27	58.6	78	141.6	117.1	108.4	44.7	137.2
39	158.13	58.4	77.9	141.5	117.1	108.5	44.3	137
40	180.99	58.3	77.8	141.5	117	108.4	43.9	136.8
41	196.22	58.3	77.7	141.5	116.9	108.4	43.7	136.7
42	-20.75	55.6	75.1	138.2	113.3	106.5	42	131.6
43	-13.13	55.5	75	138.1	113.2	106.5	41.7	131.5
44	-5.51	56	75.6	139.2	114.2	107.2	42.2	132.5
45	2.11	57.7	77.1	140.6	116	107.8	44.8	135
46	17.35	58.6	77.5	140.9	116.3	107.9	46.5	136.2
47	32.6	58.5	77.8				46.3	
48	47.83	58.5	77.9				46.1	
49	63.07	58.5	77.9				45.8	
50	9.45	-9.1	-18	-11.5	-26.3	-17.7	-19.1	-20.5
51	9.75	-12.7	-22.7	-19.7	-34.2	-24.2	-21.9	-29.1
52	10.05	-13.2	-23.9	-21.7	-36.2	-25.6	-22.8	-30.2
53	10.85	-13.3	-23.3	-19.7	-34.3	-24.4	-23.4	-30.1
54	11.35	-10.2	-17.7	-10.2	-25.6	-17.5	-22.3	-21.9
55	12.65	7.9	8.9	32.9	15.1	18.3	-7.3	22.1
56	13.65	20.5	17.8	45.8	27.6	29.5	2.1	38.2
57	14.65	17.4	19.5	48.3	29.8	31.5	6.2	41.5
58	19.73	17.9	19.4	47.5	29.2	30.5	9.1	41.7
59	24.81	17.3	18.3	45.5	27.5	28.9	9.2	40.3
60	29.89	16.3	16.8	43.2	25.2	27.1	8.5	38.3
61	34.97	15.4	15.6	41.1	23.4	25.5	7.9	36.1
62	40.05	14.4	14	38.9	21.2	23.4	7	34.2
63	45.13	13.5	12.5	36.4	18.8	21.4	6.1	31.8
64	50.21	12.4	11	33.8	16.4	19.2	5.1	29.4
65	55.29	11.2	9.4	31.3	14	16.9	4.2	26.8
66	60.37	9.9	7.6	29	11.4	14.5	3.1	24.1
67	9.45	16.3	-9.3	-29.7	-33.7	-33.2	28.8	12.8
68	9.75	20.3	6.3	-9.2	-12	-23.7	14.5	33.7
69	10.05	16.1	17.9	42.1	26.4	14	8.3	38.5
70	10.85	4.5	2	22	4.5	11.1	-7.2	12.1
71	11.35	1.7	-1	17.7	0.7	7.3	-11.5	7.2
72	12.65	6.9	6.6	28.5	11.6	15.4	-7.2	19.3

Table 4.3 (continued)

tap No.	distance (cm)	pressure head H (cm)						
		test9	test10	test11	test12	test13	test14	test15
73	13.65	12.8	13.9	39.7	21.7	23.9	0.2	31.8
74	14.65	15.9	17.6	46.1	26.8	28.5	4.7	38.4
75	19.73	17.9	19.5	47.5	29.2	30.7	9.2	42.5
76	24.81	17.2	18.3	45.4	27.3	29	9.1	40.6
77	29.89	16.2	16.9	43.2	25.3	27.1	8.5	38.5
78	34.97	15.4	15.7	41.3	23.5	25.4	7.8	36.6
79	40.05	14.2	14.1	39.1	21.2	23.3	7.3	35.7
80	45.13	13.6	12.9	37	19.2	21.6	6.2	32.3
81	50.21	12.5	12.2	35.4	16.8	19.4	5.3	29.8
82	55.29	11.3	9.5	26.7	14.3	17.2	4.3	27.2
83	60.37	10.1	7.8	28.8	11.7	14.8	3.2	24.5
84	82.67	7	3.5	22	5.6	9.1	0.5	17.9
85	97.91	3.6	-1.4	14	-1.7	2.3	-2.4	10.3
86	113.15	0.5	-5.7	7	-8.1	-3.6	-5.3	3.5
discharges, discharge ratio, Reynolds number, and energy loss coefficients								
Q_1 (*l/s*)		3.81	3.67	3.75	3.96	2.88	5.24	5.1
Q_2 (*l/s*)		2.08	1.55	0.97	1.32	0.33	3.65	2.39
Q_3 (*l/s*)		1.73	2.12	2.78	2.64	2.55	1.59	2.71
Q_3/Q_1		0.46	0.58	0.74	0.67	0.88	0.30	0.53
$Re_1 \times 10^{-5}$		0.57	0.55	0.56	0.59	0.43	0.78	0.76
$Re_2 \times 10^{-5}$		0.31	0.23	0.15	0.2	0.05	0.54	0.36
$Re_3 \times 10^{-5}$		0.56	0.68	0.89	0.85	0.82	0.51	0.87
K_{12} Eq.(4.6)		-0.08	-0.01	0.13	0.06	0.26	-0.1	-0.03
K_{13} Eq.(4.8)		3.53	4.96	6.5	5.89	8.79	2.12	4.16
K_{13} Eq.(4.12)		3.16	4.39	6.04	5.38	8.15	2.01	3.82

Table 4.4 The Contraction Coefficient C_c

L/B	Q_3/Q_1	C_c (Eq.4.4)	C_c (graphical)
1.0	0.46	0.33	0.31
1.0	0.64	0.38	0.39
1.0	0.97	0.48	0.49
0.77	0.42	0.37	0.38
0.77	0.57	0.43	0.43
0.22	0.30	0.49	0.50
0.22	0.53	0.55	0.56

Table 5.1 Experimental data of combining closed conduit flow $L/B = 1.0$

tap No.	distance (cm)	pressure head H (cm)					
		test1	test2	test3	test4	test5	test6
1	-152.24	88	101	70.4	83.2	87.5	91.4
2	-117.26	87.2	100.1	70	82.7	87.1	91.4
3	-94.4	85.8	98.9	69.6	82.3	86.6	91.3
4	-63.92	84.6	97.6	69.2	81.8	86.2	91.2
5	-41.06	83.7	96.7	68.7	81.4	85.8	91.2
6	-20.74	82.9	95.8	68.4	81.1	85.5	91.1
7	-13.12	82.5	95.5	68.3	80.9	85.4	91.1
8	-10.58	82.5	95.4	68.3	81	85.5	91.2
9	-5.5	82.3	95.5	68.4	81.1	85.5	91.2
10	-4.5	82.5	95.6	68.5	81.2	85.7	91.2
11	-3.5	82.4	95.6	68.4	81.2	85.6	91.2
12	-2.2	82.6	95.8	68.7	81.4	85.9	91.2
13	-1.7	82.6	95.9	68.6	81.4	86	91.2
14	-1.2	82.9	96.2	68.8	81.5	86.2	91.3
15	-0.8	82.8	96.2	68.7	81.6	86.3	91.2
16	-0.4	83	96.4	68.9	81.7	86.4	91.3
17	-0.2	83.1	96.6	69	81.7	86.5	91.3
18	9.35	67.4	71.9	53.6	60.6	57.4	31.3
19	9.55	67.4	71.8	53.5	60.6	57.4	31.2
20	9.95	67.2	71.8	53.5	60.6	57.3	30.9
21	10.35	66.8	71.6	53.4	60.5	57.2	30.7
22	10.85	66.7	71.4	53.4	60.5	57.2	30.6
23	11.35	66.6	71.3	53.4	60.4	57.2	30.6
24	12.65	67.6	71.1	53.3	60.4	57.1	30
25	13.65	69.5	71.3	53.3	60.3	57	29.5
26	14.65	71.3	72.3	53.4	60.4	57.1	29.2
27	19.73	74.6	80.9	56.4	63.6	60.4	31.6
28	22.27	74.8	82.1	58.5	66.4	64	37.1
29	29.89	74.9	82.6	60	68.9	69	53.1
30	37.51	74.8	82.3	59.9	69	69.3	56
31	45.13	74.5	82.4	59.8	69.1	69.4	56.9
32	52.75	74.3	82.1	59.7	69	69.3	57.2
33	60.37	74	81.8	59.5	68.8	69.1	57.3
34	67.99	73.6	81.5	59.4	68.6	68.9	57.2
35	75.61	73.2	81.1	59.2	68.3	68.6	57
36	104.47	71.9	79.6	58.5	67.4	67.5	56

Table 5.1 (continued)

tap No.	distance (cm)	pressure head H (cm)					
		test1	test2	test3	test4	test5	test6
37	119.71	71	78.6	57.9	66.9	66.9	55.1
38	142.57	69.9	77.4	57.4	66.2	66.1	53.8
39	165.43	68.7	76	56.7	65.4	65.1	52.6
40	188.29	67.6	74.8	55.9	64.6	64.1	51
41	203.53	66.9	73.9	55.6	64.2	63.8	47.8
42	-13.82	82.3	95	68.6	80.9	85.5	90.6
43	-6.2	81.7	94.6	68.3	80.6	85.3	90.5
44	1.42	80.7	92.8	67.4	79.5	83.7	89.9
45	9.04	76.4	85.5	62.6	73.2	74.9	77.9
46	14.12	75.2	81.2	58.8	67.6	67.3	54.2
47	19.2	74.8	80.4	58.1	65.8	64.4	41.3
48	24.28	73.3	80.1	58	66.7	64.7	41.5
49	29.36	75	81.5	59.4	68	67.9	49.3
50	34.44	74.8	81.9	59.8	68.6	68.8	53.3
51	39.52	74.9	82.1	60	69	69.4	55.5
52	54.76	74.3	81.6	59.8	68.7	69.3	56.8
53	70	73.7	81.1	59.4	68.3	68.8	56.6
54	9.45	82.9	95.9	69.4	82.1	86.7	91.3
55	9.75	82.9	95.9	69.4	82.1	86.6	91.1
56	10.05	82.9	95.9	69.4	82.1	86.5	90.9
57	10.85	82.9	95.9	69.4	82	86.4	90.4
58	11.35	82.9	95.9	69.4	82	86.3	89.8
59	12.65	82.9	95.9	69.4	81.9	86.2	88.8
60	13.65	82.9	95.9	69.4	81.8	86.2	88.1
61	14.65	82.9	95.9	69.4	81.7	86	87.5
62	19.73	82.7	95.9	69.3	81.4	85.7	86.3
63	24.81	82.7	95.9	69.2	81.5	85.8	86.4
64	29.89	82.8	95.9	69.3	81.5	85.8	86.5
65	34.97	82.8	95.9	69.3	81.6	85.9	86.6
66	40.05	82.9	95.9	69.3	81.6	85.9	86.8
67	45.13	82.9	95.9	69.3	81.6	86	87
68	50.21	82.9	95.9	69.3	81.6	86	87.2
69	55.29	82.9	95.9	69.3	81.7	86	87.4
70	60.37	82.9	95.9	69.3	81.7	86.1	87.6
71	65.45	82.9	95.9	69.3	81.7	86.1	87.9
72	9.45	78.7	87.3	62.9	72.9	73.1	57.7

Table 5.1 (continued)

tap No.	distance (cm)	pressure head H (cm)					
		test1	test2	test3	test4	test5	test6
73	9.75	80.4	90.3	64.9	75.6	76.6	64.9
74	10.05	81.2	91.8	65.8	76.9	78.7	68.3
75	10.85	82	93.3	67.2	78.6	81.2	74.7
76	11.35	82.2	94.1	67.7	79.3	82.2	76.8
77	12.65	82.4	94.9	68.2	80.2	83.5	80.3
78	13.65	82.5	95.2	68.4	80.5	84.1	81.9
79	14.65	82.6	95.3	68.6	80.9	84.7	83.1
80	19.73	82.7	95.4	68.8	81.3	85.4	85.3
81	24.81	82.8	95.6	68.9	81.4	85.5	85.9
82	29.89	82.8	95.6	69	81.5	85.7	86.1
83	34.97	82.9	95.7	68.8	81.5	85.8	86.2
84	45.13	82.9	95.7	69.1	81.5	85.9	86.9
85	55.29	82.9	95.7	69.1	81.6	86	87.4
86	65.45	82.9	95.8	69.2	81.6	86.1	87.8
87	80.45	82.9	95.8	69.2	81.7	86.2	88.9
88	95.69	82.9	95.8	69.2	81.7	86.3	89.6
89	110.93	82.9	95.9	69.3	81.8	86.4	90.2
90	126.17	82.9	95.9	69.4	81.9	86.5	90.3
discharges, discharge ratio, Reynolds number, and energy loss coefficients							
Q_1 (m^3/s) x 10^3		5.8	5.8	3.38	3.38	3.37	0.87
Q_2 (m^3/s) x 10^3		6.37	6.85	4.72	5.12	5.77	6.93
Q_3 (m^3/s) x 10^3		0.61	1.11	1.27	1.8	2.39	6.19
Q_3/Q_2		0.1	0.16	0.27	0.35	0.42	0.88
Re_1 x 10^{-5}		0.87	0.87	0.5	0.5	0.5	0.13
Re_2 x 10^{-5}		0.96	1.03	0.69	0.77	0.86	1.05
Re_3 x 10^{-5}		0.09	0.17	0.19	0.27	0.36	0.92
K_{12}		0.15	0.25	0.35	0.42	0.45	0.6
K_{32}		-0.61	-0.39	0.03	0.19	0.32	1.01

Notes:

1. Pressure taps 1 to 41 located on the center of the branch side wall of main conduit, taps 42 to 53 on the opposite wall of the main. The distances equate to X.
2. Pressure taps 54 to 71 located on the center of upstream side wall of branch conduit, taps 72 to 90 on the downstream side wall of the branch. The distances equate to Y.

Table 5.1 (continued)

tap No.	distance (cm)	pressure head H (cm)					
		test7	test8	test9	test10	test11	test12
1	-152.24	95	88	79.5	71.9	72.8	71.6
2	-117.26	94.9	87.9	79.4	71.8	72.7	71.5
3	-94.4	94.8	87.7	79.3	71.7	72.5	71.2
4	-63.92	94.7	87.6	79.3	71.6	72.4	71
5	-41.06	94.6	87.4	79.2	71.5	72.2	70.8
6	-20.74	94.5	87.3	79.2	71.4	72.1	70.6
7	-13.12	94.4	87.2	79.1	71.3	72	70.5
8	-10.58	94.4	87.3	79.1	71.3	72.1	70.5
9	-5.5	94.5	87.3	79.1	71.3	72.1	70.5
10	-4.5	94.5	87.4	79.2	71.4	72.2	70.6
11	-3.5	94.5	87.4	79.2	71.3	72.2	70.6
12	-2.2	94.6	87.5	79.2	71.5	72.4	70.6
13	-1.7	94.6	87.5	79.3	71.5	72.4	70.7
14	-1.2	94.6	87.6	79.2	71.5	72.5	70.7
15	-0.8	94.6	87.6	79.3	71.5	72.5	70.7
16	-0.4	94.6	87.7	79.4	71.5	72.5	70.8
17	-0.2	94.6	87.7	79.4	71.5	72.6	70.8
18	9.35	44.9	39.5	70.4	60.2	60	65.1
19	9.55	44.9	39.5	70.5	60.2	59.9	65
20	9.95	44.7	39.4	70.3	60.3	59.9	65.1
21	10.35	44.5	39.3	70.3	60.2	59.9	65.1
22	10.85	44.4	39.3	70.3	60.2	59.9	65
23	11.35	44.4	39.3	70.3	60.2	59.8	65
24	12.65	44	39.1	70.2	60.1	59.8	65
25	13.65	43.7	38.7	70.2	60.1	59.8	65
26	14.65	43.5	38.6	70.2	60.1	59.8	65.1
27	19.73	46.1	41.3	71	61.1	61	66.4
28	22.27	50.7	46.5	71.9	62.4	62.3	67
29	29.89	63.5	58.3	73.9	64.9	65	67.4
30	37.51	66.2	60.4	74.3	65.3	65.3	67.3
31	45.13	66.9	61	74.4	65.2	65.3	67.3
32	52.75	67.2	61.2	74.4	65.2	65.3	67.2
33	60.37	67.3	61.2	74.3	65.1	65.2	67.1
34	67.99	67.2	61.1	74.2	65	65.1	67
35	75.61	67.1	60.9	74.1	64.9	65	66.9
36	104.47	66.1	59.9	73.8	64.5	64.5	66.6

Table 5.1 (continued)

tap No.	distance (cm)	pressure head H (cm)					
		test7	test8	test9	test10	test11	test12
37	119.71	65.5	59.2	73.6	64.3	64.2	66.4
38	142.57	64.3	58	73.4	63.9	63.8	66.1
39	165.43	63.1	56.8	73.1	63.5	63.4	65.8
40	188.29	57.2	52.1	72.7	63.2	63	65.5
41	203.53	53.1	49.8	72.5	62.9	62.7	65.3
42	-13.82	94.1	87.1	79	70.9	72.1	70.3
43	-6.2	94	86.8	78.9	70.8	71.9	70.2
44	1.42	93.1	85.3	78.6	70.3	71.3	69.8
45	9.04	81	72.3	76	68.8	67.3	68.3
46	14.12	64.6	58.3	73.4	64	64.2	67
47	19.2	54.5	49.2	72.9	63.6	62.7	66.7
48	24.28	52.3	47	71.8	61.7	62.3	66.8
49	29.36	60.9	55.7	73.2	64	64.3	67.1
50	34.44	64.2	58.6	73.6	64.5	64.7	67.2
51	39.52	65.9	60.1	73.8	64.7	65	67.2
52	54.76	67.1	61.1	74	64.8	65.1	67.1
53	70	67	60.9	73.7	64.6	64.8	66.9
54	9.45	94.9	87	79.3	71.7	72.7	70.5
55	9.75	94.7	86.8	79.4	71.7	72.6	70.5
56	10.05	94.6	86.7	79.4	71.6	72.6	70.4
57	10.85	94.2	86.5	79.3	71.6	72.6	70.4
58	11.35	94	86.3	79.3	71.5	72.5	70.3
59	12.65	93.1	85.8	79.3	71.5	72.5	70.3
60	13.65	92.4	85.3	79.2	71.4	72.4	70.3
61	14.65	91.9	84.8	79.1	71.3	72.3	70.3
62	19.73	90.7	83.5	78.8	71.1	72	70.2
63	24.81	90.8	83.5	78.8	71.2	72.1	70.2
64	29.89	91	83.5	78.9	71.2	72.1	70.2
65	34.97	91.1	83.6	78.9	71.3	72.2	70.2
66	40.05	91.3	83.7	79	71.3	72.2	70.3
67	45.13	91.5	83.9	79	71.3	72.2	70.3
68	50.21	91.7	84.1	79	71.3	72.2	70.3
69	55.29	91.9	84.3	79.1	71.4	72.3	70.3
70	60.37	92.1	84.4	79.1	71.4	72.3	70.3
71	65.45	92.3	84.6	79.1	71.5	72.3	70.3
72	9.45	65.5	59.5	74.4	65.6	66.3	68.2

Table 5.1 (continued)

tap No.	distance (cm)	pressure head H (cm)					
		test7	test8	test9	test10	test11	test12
73	9.75	72.3	65.7	75.7	67.1	67.9	69
74	10.05	74.9	68.9	76.3	67.9	68.7	69.2
75	10.85	80.5	74.2	77.2	69	69.9	69.6
76	11.35	82.6	76.5	77.6	69.5	70.3	69.9
77	12.65	85.7	79.5	78.1	70	71.1	70
78	13.65	87	80.9	78.3	70.5	71.4	70.2
79	14.65	87.9	81.9	78.5	70.6	71.6	70.2
80	19.73	89.8	83.5	78.8	71	71.9	70.2
81	24.81	90.2	84	78.8	71.1	72	70.2
82	29.89	90.4	83.2	78.9	71.1	72.1	70.2
83	34.97	89.7	83.3	78.8	71	72.1	70.2
84	45.13	91.3	83.9	79	71.2	72.2	70.3
85	55.29	91.7	84.2	79	71.3	72.3	70.3
86	65.45	92.2	84.5	79.1	71.4	72.3	70.3
87	80.45	93	85.1	79.2	71.5	72.4	70.3
88	95.69	93.5	85.7	79.3	71.5	72.4	70.3
89	110.93	94	86.1	79.4	71.7	72.5	70.3
90	126.17	94.1	86.1	79.4	71.7	72.5	70.3
discharges, discharge ratio, Reynolds number, and energy loss coefficients							
Q_1 (m^3/s) x 10^3		1.3	1.82	1	1.47	1.86	2.24
Q_2 (m^3/s) x 10^3		6.72	6.65	2.94	3.46	3.72	3
Q_3 (m^3/s) x 10^3		5.36	4.86	1.8	1.85	1.76	0.66
Q_3/Q_2		0.81	0.73	0.64	0.56	0.49	0.23
Re_1 x 10^{-5}		0.19	0.27	0.15	0.22	0.28	0.33
Re_2 x 10^{-5}		0.99	1	0.42	0.5	0.54	0.43
Re_3 x 10^{-5}		0.8	0.72	0.27	0.28	0.26	0.1
K_{12}		0.59	0.55	0.51	0.5	0.48	0.32
K_{32}		0.92	0.73	0.68	0.54	0.43	-0.13

Table 5.2 Experimental data of combining closed conduit flow $L/B = 0.77$

tap No.	distance (cm)	pressure head H (cm)					
		test1	test2	test3	test4	test5	test6
1	-154.36	89.2	100.3	93.3	117.3	95.6	121.4
2	-119.38	89	99.4	92.4	116.4	94.9	121.4
3	-96.52	88.6	98.5	91.5	115.5	94.2	121.3
4	-66.04	88.3	97.4	90.5	114.5	93.4	121.4
5	-43.18	88.1	96.8	89.8	114	93	121.3
6	-20.74	87.8	96.1	89	113.1	92.4	121.3
7	-13.12	87.7	95.9	88.8	112.9	92.2	121.2
8	-5.5	88	96	89	113.2	92.5	121.2
9	-4.5	88.1	96.1	89.1	113.4	92.7	121.2
10	-3.5	88.3	96.2	89.3	113.7	93	121.3
11	-2.2	88.4	96.4	89.7	114.2	93.4	121.2
12	-1.7	88.7	96.7	90	114.6	93.7	121.3
13	-1.2	88.7	96.9	90.1	114.7	93.9	121.3
14	-0.8	88.9	97.1	90.5	115	94.2	121.3
15	-0.4	88.8	97.3	90.7	115.3	94.3	121.3
16	-0.2	88.7	97.4	90.8	115.5	94.4	121.3
17	7.24	54.1	76	60.1	72.6	52.8	81.3
18	7.44	54.1	76	60.1	72.7	52.8	81.4
19	7.84	54	76	60	72.6	52.8	80.9
20	8.24	54	75.8	59.9	72.5	52.7	81
21	8.74	54	75.6	59.7	72.3	52.6	80.6
22	9.24	54	75.7	59.7	72.5	52.6	80.8
23	10.54	53.8	75.4	59.5	72.2	52.4	80.4
24	11.54	53.6	75.6	59.4	72	52.2	80
25	12.54	53.7	76.2	59.8	72.3	52.4	79.7
26	17.62	56.9	82.9	67.4	80	58.2	79.6
27	20.16	67.4	84.4	70.7	85.4	63.4	79.1
28	27.78	68.5	85.2	72.9	90	69.5	84.7
29	35.4	68.6	85.1	73	90.3	70.1	96.4
30	43.02	68.7	84.9	72.7	90.1	70	99
31	50.64	68.9	84.8	72.5	90.1	70	99.5
32	58.26	68.8	84.6	72.4	89.8	69.8	99.7
33	65.88	68.7	84.3	72.1	89.5	69.6	99.9
34	73.5	68.4	84	71.7	89.1	69.2	99.8
35	81.12	68.2	83.7	71.3	88.7	68.8	99.7
36	102.36	67.5	82.8	70.3	87.5	67.8	99.2

Table 5.2 (continued)

tap No.	distance (cm)	pressure head H (cm)					
		test1	test2	test3	test4	test5	test6
37	117.6	66.9	82	69.5	86.5	66.9	98.5
38	140.46	66	81	68.3	85.1	65.6	97.7
39	163.31	65	79.9	67	83.5	64.3	96.7
40	186.18	64.1	78.8	65.9	82.3	63.1	95.8
41	201.42	64	78.3	65.1	81.5	62.4	94.4
42	-15.74	87.6	96	88.7	112.9	92.2	121.3
43	-8.12	87.4	95.7	88.3	112.4	92.1	121.2
44	-0.5	84.2	94.3	86.5	110.1	90.1	121.1
45	7.12	76.7	88.3	77.7	98.3	78.2	119
46	12.2	66.6	84	70.8	87.2	67.3	99.7
47	17.28	61.9	83	68.8	83.8	63.1	87.1
48	22.36	62.7	83.3	69.7	85.5	64.7	87.2
49	27.44	65.6	82.7	69.8	86	66.5	91.4
50	32.52	65.3	84.5	71.8	88.4	68.1	93.9
51	37.6	68.4	84.7	72.4	89.6	69.8	98.5
52	52.84	68.7	84.5	72.2	89.5	70	99.7
53	68.08	68.3	83.9	71.6	88.9	69.4	99.6
54	9.45	89.2	99.6	91.3	115.3	94.1	122.5
55	9.75	89	99.4	91.2	115.2	93.8	122.3
56	10.05	88.9	99.1	91.2	115.1	93.7	122.1
57	10.85	88.8	99.1	91.2	115.1	93.6	121.1
58	11.35	88.7	99.5	91.1	115.1	93.5	120.5
59	12.65	88.1	99.4	91	114.8	93.1	119.4
60	13.65	87.7	99.4	90.9	114.5	92.8	118.4
61	14.65	87.4	99.3	90.8	114.4	92.5	117.8
62	19.73	86.8	99.1	90.5	113.8	91.9	117.3
63	24.81	86.9	99.1	90.5	113.7	91.9	117.4
64	29.89	87	99.1	90.5	113.8	92	117.7
65	34.97	87.1	99	90.6	114	92.1	117.9
66	40.05	87.2	99.1	90.6	114	92.2	118.2
67	45.13	87.3	99.2	90.7	114.1	92.3	118.5
68	50.21	87.4	99.1	90.7	114.2	92.4	118.7
69	55.29	87.5	99.1	90.8	114.3	92.5	119
70	60.37	87.6	99.2	90.9	114.4	92.6	119.2
71	65.45	87.7	99	90.9	114.5	92.7	119.5
72	9.45	71.5	92.1	79.3	97.1	75.2	98

Table 5.2 (continued)

tap No.	distance (cm)	pressure head H (cm)					
		test1	test2	test3	test4	test5	test6
73	9.75	76.1	94.7	83.3	102.7	79.5	102.8
74	10.05	78.4	95.7	85	105.2	83.3	105.5
75	10.85	81.5	97	87.4	108.7	86.7	109.3
76	11.35	82.8	97.7	88.2	110	88	110.9
77	12.65	84.5	98.3	89.3	111.7	89.7	113.3
78	13.65	85.3	98.5	89.8	112.5	90.5	114.3
79	14.65	85.8	98.7	90	112.9	90.9	115.1
80	19.73	86.5	98.8	90.4	113.7	91.8	116.5
81	24.81	86.7	98.9	90.4	113.8	91.9	117
82	29.89	86.9	99	90.5	113.9	92.1	117.3
83	34.97	86.8	99	90.6	114	92.2	117.6
84	45.13	87.4	99	90.6	114.1	92.3	118.2
85	55.29	87.7	99.1	90.7	114.4	92.5	118.6
86	65.45	88	99.1	90.8	114.5	92.6	119
87	80.55	88.4	99.2	91	114.9	93	120.1
88	95.79	88.7	99.2	91.1	115.1	93.3	121.2
89	111.03	89.1	99.3	91.3	115.3	93.6	122.2
90	126.27	89.4	99.4	91.4	115.5	93.9	123
discharges, discharge ratio, Reynolds number, and energy loss coefficients							
Q_1 (m^3/s) x 10^3		2.78	5.11	5.11	5.11	4.29	0.55
Q_2 (m^3/s) x 10^3		5.8	6.15	6.88	7.33	6.8	5.54
Q_3 (m^3/s) x 10^3		2.96	1.05	1.6	2.24	2.56	5
Q_3/Q_2		0.52	0.17	0.24	0.31	0.37	0.9
Re_1 x 10^{-5}		0.41	0.76	0.76	0.76	0.64	0.08
Re_2 x 10^{-5}		0.86	0.92	1	1.1	1.02	0.83
Re_3 x 10^{-5}		0.53	0.19	0.28	0.4	0.45	0.89
K_{12}		0.59	0.26	0.35	0.42	0.48	0.67
K_{32}		0.72	-0.11	-0.01	0.17	0.3	1.5

Notes:

1. Pressure taps 1 to 41 located on the center of the branch side wall of main conduit, taps 42 to 53 on the opposite wall of the main. The distances equate to X.
2. Pressure taps 54 to 71 located on the center of upstream side wall of branch conduit, taps 72 to 90 on the downstream side wall of the branch. The distances equate to Y.

Table 5.2 (continued)

tap No.	distance (cm)	pressure head H (cm)					
		test7	test8	test9	test10	test11	test12
1	-154.36	91.6	70.9	104.1	57	69.6	96.1
2	-119.38	91.6	70.8	103.9	56.8	69.3	95.9
3	-96.52	91.5	70.7	103.6	56.5	68.8	95.6
4	-66.04	91.6	70.8	103.3	56.3	68.4	95.4
5	-43.18	91.5	70.5	103.1	56.1	68	95.3
6	-20.74	91.5	70.5	102.9	55.9	67.8	95.1
7	-13.12	91.4	70.4	102.8	55.8	67.6	95
8	-5.5	91.6	70.6	103.1	56	67.9	95.2
9	-4.5	91.5	70.6	103.2	56.1	68	95.3
10	-3.5	91.6	70.7	103.4	56.5	68.1	95.4
11	-2.2	91.5	70.6	103.5	56.3	68.3	95.5
12	-1.7	91.6	70.8	103.7	56.2	68.5	95.7
13	-1.2	91.5	70.8	103.8	56.6	68.7	95.7
14	-0.8	91.7	70.9	103.9	56.7	68.8	95.8
15	-0.4	91.5	70.8	103.9	56.6	68.9	95.7
16	-0.2	91.6	70.8	103.8	56.6	68.9	95.7
17	7.24	57.9	24.9	46.7	15.9	35.9	38.4
18	7.44	57.8	24.8	46.6	15.9	35.9	38.3
19	7.84	57.6	24.7	46.4	15.8	35.9	38.1
20	8.24	57.5	24.5	46.3	15.7	35.8	38
21	8.74	57.4	24.3	46.2	15.7	35.8	37.9
22	9.24	57.4	24.3	46.2	15.7	35.8	37.9
23	10.54	57	23.8	45.7	15.4	35.6	37.4
24	11.54	56.6	23.4	45.2	15.1	35.4	37
25	12.54	56.5	23.3	45.1	15.1	35.5	36.9
26	17.62	56.8	25.3	49	18.2	39.3	40.4
27	20.16	60.7	29.9	54.7	22.6	43.5	45.9
28	27.78	69.9	40.5	67.6	30.6	49.2	59.2
29	35.4	71.9	43.1	70.2	32.2	49.8	61.9
30	43.02	72.5	44	71	32.7	49.9	62.8
31	50.64	72.9	44.4	71.4	32.9	49.8	63.2
32	58.26	73	44.6	71.5	32.9	49.7	63.4
33	65.88	73.1	44.7	71.6	32.8	49.5	63.3
34	73.5	73	44.5	71.4	32.6	49.3	63.2
35	81.12	72.9	44.4	71.2	32.4	49.1	63
36	102.36	72.5	43.8	70.3	31.8	48.3	62.2

Table 5.2 (continued)

tap No.	distance (cm)	pressure head H (cm)					
		test7	test8	test9	test10	test11	test12
37	117.6	72.1	43.2	69.4	31.2	47.7	61.3
38	140.46	71.2	42.1	68.1	30.2	46.7	60
39	163.31	70.4	41.2	66.6	29.3	45.8	58.7
40	186.18	69.6	40.2	65.3	28.3	44.8	57.3
41	201.42	69.5	39.6	64.4	27.5	44.2	56.4
42	-15.74	91.2	70.9	102.5	55.5	67.4	94
43	-8.12	91.1	70.8	102.2	55.4	67.1	94.6
44	-0.5	90.9	70.1	100.8	54.1	65.6	93.5
45	7.12	85.8	61	87.1	44.3	56.4	80
46	12.2	72.4	43.3	68.1	30.6	47.6	62.3
47	17.28	62.7	32.7	57.5	24.1	43.8	50.3
48	22.36	62.3	34.2	57.9	25.7	44.1	49.9
49	27.44	65.8	36.8	62.6	28.1	47.1	55.5
50	32.52	67.1	38.9	64.8	29.1	47.8	57.8
51	37.6	71.4	42.9	69.4	31.9	49.5	61.2
52	52.84	72.6	44.5	71	32.7	49.7	63.1
53	68.08	72.5	44.6	70.9	32.5	49.4	62.9
54	9.45	91.7	72.1	101.9	56.7	69.6	97.2
55	9.75	91.3	71.6	101.5	56.4	69.4	96.7
56	10.05	91.1	71.5	101	56.3	69.3	96.5
57	10.85	90.6	70.7	100.6	56	69.4	95.8
58	11.35	90	70.4	100	55.6	69.1	95.1
59	12.65	88.9	69	99.5	54.9	68.7	93.9
60	13.65	88.6	68.4	99.2	54.4	68.4	93.1
61	14.65	88.1	67.7	98.6	54	68.1	92.6
62	19.73	87.7	66.9	97.5	53.3	67.5	91.5
63	24.81	87.8	67	98	53.4	67.6	91.7
64	29.89	87.8	67.3	98.2	53.6	67.7	91.9
65	34.97	88	67.5	98.7	53.7	67.8	92.2
66	40.05	88.3	67.7	99	53.7	67.9	92.4
67	45.13	88.4	68	99.4	53.8	67.9	92.6
68	50.21	88.6	68.1	99.7	54	68	92.8
69	55.29	88.8	68.3	100	54.2	68.2	93.1
70	60.37	89	68.5	100.7	54.3	68.3	93.2
71	65.45	89.2	68.6	100.8	54.5	68.4	93.5
72	9.45	71.1	45.7	72.7	35.5	53.3	65

Table 5.2 (continued)

tap No.	distance (cm)	pressure head H (cm)					
		test7	test8	test9	test10	test11	test12
73	9.75	75.5	51.7	80.3	40.7	57.9	73.1
74	10.05	77.7	54.6	84.1	43.3	60	77.1
75	10.85	81.2	58.9	89.6	47	62.9	82.6
76	11.35	82.6	60.5	91.8	48.5	64	84.7
77	12.65	84.5	63	95.1	50.6	65.5	86.5
78	13.65	85.4	64.1	96.4	51.5	66.3	88.7
79	14.65	86.1	64.8	97.2	52.1	66.8	89.6
80	19.73	87.2	66.2	98.7	52.9	67.6	91.2
81	24.81	87.5	66.6	99.2	53.3	67.7	91.7
82	29.89	87.8	66.9	99.6	53.4	67.8	92
83	34.97	87.9	67	99.7	53.6	67.7	92
84	45.13	88.5	67.6	100.2	53.9	68	91.5
85	55.29	88.9	68	100.7	54.2	68.2	93.2
86	65.45	89.2	68.4	101	54.5	68.4	93.5
87	80.55	90.1	69.4	102.1	55	68.7	94.7
88	95.79	90.9	70.2	103	55.6	69	95.7
89	111.03	91.6	71.1	103.8	56.1	69.4	96.5
90	126.27	92.3	71.7	104.6	56.5	69.6	97.2
discharges, discharge ratio, Reynolds number, and energy loss coefficients							
Q_1 (m^3/s) x 10^3		0.83	1.57	2.36	2.37	3.2	2.21
Q_2 (m^3/s) x 10^3		5.14	6.06	7.03	5.94	5.89	7.01
Q_3 (m^3/s) x 10^3		4.33	4.62	4.62	3.67	2.62	4.73
Q_3/Q_2		0.84	0.75	0.66	0.61	0.45	0.68
Re_1 x 10^{-5}		0.12	0.23	0.35	0.35	0.48	0.33
Re_2 x 10^{-5}		0.77	0.92	1.04	0.9	0.87	1.04
Re_3 x 10^{-5}		0.77	0.82	0.82	0.65	0.46	0.84
K_{12}		0.66	0.63	0.65	0.62	0.53	0.65
K_{32}		1.3	1.14	0.99	0.84	0.55	1.06

Table 5.3 Experimental data of combining closed conduit flow $L/B = 0.22$

tap No.	distance (cm)	pressure head H (cm)					
		test1	test2	test3	test4	test5	test6
1	-159.49	69.8	68.7	91.9	68	87.7	86
2	-124.51	69	68.5	91.8	68.1	87.2	85.4
3	-101.65	68.2	68.1	91.7	68	87	85.2
4	-71.17	67.3	67.9	91.7	68.1	86.5	84.7
5	-48.31	66.6	67.5	91.6	68.1	86.2	84.4
6	-28.37	65.9	67.3	91.5	68	85.8	84
7	-20.75	65.8	67.1	91.5	68	85.7	83.9
8	-13.13	65.6	67.2	91.5	67.8	85.6	84
9	-10.59	65.5	67.4	91.5	67.5	85.7	83.9
10	-5.51	66	67.8	91.6	66.9	86	84.6
11	-4.51	65.4	67.9	91.6	66.8	86.1	84.7
12	-3.51	66.6	68.3	91.7	66.9	86.5	84.9
13	-2.21	67.4	68.4	91.7	67.1	86.6	85.3
14	-1.71	67.6	68.5	91.8	67.2	86.9	85.4
15	-1.21	68.2	68.7	91.8	67.3	87.2	85.5
16	-0.81	68.6	68.8	91.7	67.3	87.3	85.6
17	-0.41	68.8	68.8	91.7	67.3	87.4	85.7
18	-0.21	68.9	68.9	91.8	67.4	87.5	85.8
19	2.25	50.2	20.5	47.6	33	71.5	60.8
20	2.45	50.2	20.4	47.5	32.9	71.4	60.8
21	2.85	50.3	20.1	47.2	32.7	71.5	60.6
22	3.25	50	20	47.1	32.6	71.5	60.6
23	3.75	49.6	19.9	47.1	32.2	71.5	60.5
24	4.25	49.7	20	47.2	32.6	71.4	60.6
25	5.55	49.8	19.5	46.7	32.1	71.4	60.4
26	6.55	50.4	19.1	46.4	31.9	71.4	60.3
27	7.55	51.1	19	46.3	31.7	71.5	60.4
28	12.63	56.8	19.5	43.2	24.1	73.6	62.2
29	15.17	58.4	21.1	42.6	26	75.1	63.4
30	22.79	58.6	28	50	42.5	78.3	68.5
31	30.41	58.5	35.9	57.7	45.6	79.2	72.1
32	38.03	58.5	41.9	63.2	47.4	79.3	73.2
33	45.65	58.2	45	67.3	49.4	79.3	73.6
34	60.89	57.5	47.4	73.9	54	79.1	73.6
35	76.13	57	47.8	77	57.2	78.8	73.3
36	97.17	56.2	47.3	77.6	58.2	78.2	72.7

Table 5.3 (continued)

tap No.	distance (cm)	pressure head H (cm)					
		test1	test2	test3	test4	test5	test6
37	112.41	55.5	46.6	77.1	57.9	77.7	72.2
38	135.27	53.9	45.7	76.5	57.5	77.2	71.5
39	158.13	53.6	44.7	75.9	57.3	76.6	70.7
40	180.99	52.5	43.6	75.2	56.8	76	70
41	196.23	52	43.2	75.1	56.7	75.8	69.8
42	-20.75	65.5	67.8	91.5	68	86.3	84.1
43	-13.13	65.3	67.6	91.4	67.8	86.1	83.9
44	-5.51	64.6	66.9	91.4	66.6	85.6	83.4
45	2.12	60.9	59.7	91.1	64.8	82.1	78.1
46	7.2	57.2	41	87.7	65	77.5	70.6
47	12.28	56.7	29.2	46.6	31	75.7	65.9
48	17.36	57.7	25.1	43.6	30.2	76.4	66.3
49	22.44	58.6	31.2	52.1	43	78.4	69.5
50	27.52	58.4	33.3	54.6	44.2	78.5	70.9
51	32.6	58.3	37.7	59	46	78.9	72
52	47.84	57.8	45	68.3	50.2	79.2	73.3
53	63.08	57.4	47.2	73.9	54.4	79	73.6
54	9.45	68.9	66.5	88.5	64	87.7	84.7
55	9.75	68.6	63.8	85.7	61.9	87.1	83.5
56	10.05	68.3	62.2	84	60.5	86.8	82.8
57	10.85	67.8	58.4	79.5	56.7	85.9	81.1
58	11.35	67.6	57.4	78.5	56	85.8	80.7
59	12.65	67.5	57.1	78.4	56.1	85.6	80.5
60	13.65	67.4	57.2	78.4	56	85.7	80.5
61	14.65	67.5	57	78.2	55.9	85.7	80.5
62	19.73	67.6	59.1	81.3	59	86	81.2
63	24.81	67.8	60.9	84	61.7	86.4	81.9
64	29.89	67.9	62.7	86.7	64.3	86.6	82.5
65	34.97	68.1	65	89.9	67.7	87.1	83.6
66	40.05	68.3	67	92.9	70.8	87.4	84
67	45.13	68.4	69.1	96	74	87.6	85
68	50.21	68.5	70.6	98.5	76.5	87.8	85.7
69	55.29	68.7	71.9	100	77.9	88	86
70	60.37	68.8	73	101.8	79.7	88.4	86.5
71	9.45	63.2	41.7	63.6	44.6	80.3	72.5
72	9.75	65.1	48.4	70.1	49.7	82.5	76.2

Table 5.3 (continued)

tap No.	distance (cm)	pressure head H (cm)					
		test1	test2	test3	test4	test5	test6
73	10.05	66.1	51.5	73	51.9	83.6	77.3
74	10.85	66.8	54.5	75.6	53.7	84.7	79.2
75	11.35	67	55.4	76.4	54.3	85	79.7
76	12.65	67.3	56.5	77.4	55.1	85.3	80.1
77	13.65	67.4	55.7	76.2	53.8	85.3	80
78	14.65	67.4	57	78	55.6	85.5	80.5
79	19.73	67.5	58.3	79.9	57.4	85.9	81.2
80	24.81	67.6	60.5	83.3	61.1	86.1	81.6
81	29.89	67.7	61.6	85.2	62.6	86.4	82.5
82	34.97	68	65.2	90.2	68	86.9	83.5
83	40.05	67.9	67	92.9	70.8	87.4	84
84	45.13	68.2	68	95.9	73.5	87.4	84.8
85	50.21	68.4	69.9	98.1	75.7	87.6	85.1
86	55.29	68.5	71.4	100.6	78.4	88	85.9
87	60.37	68.7	72.8	102.1	79.9	88.4	86.4
88	82.67	69.5	80.5	114.1	91.8	89.7	89.5
89	97.91	69.9	86.9	123.8	101.5	90.9	91.9
90	113.15	70.5	94.6	135	112.9	92.3	94.8
discharges, discharge ratio, Reynolds number, and energy loss coefficients							
Q_1 (m^3/s) x 10^3		5.07	3.01	0.9	0	3.27	3.28
Q_2 (m^3/s) x 10^3		5.68	5.61	4.3	3.32	4.24	4.78
Q_3 (m^3/s) x 10^3		0.61	2.64	3.32	3.32	0.95	1.48
Q_3/Q_2		0.11	0.47	0.79	1	0.23	0.31
Re_1 x 10^{-5}		0.76	0.45	0.13	0	0.49	0.49
Re_2 x 10^{-5}		0.85	0.84	0.63	0.5	0.63	0.71
Re_3 x 10^{-5}		0.2	0.85	1.07	1.07	0.31	0.48
K_{12}		0.16	0.62	0.88	1.08	0.33	0.43
K_{32}		-0.18	3.08	8.9	14.39	0.71	1.3

Notes:

1. Pressure taps 1 to 41 located on the center of the branch side wall of main conduit, taps 42 to 53 on the opposite wall of the main. The distances equate to X.
2. Pressure taps 54 to 70 located on the center of upstream side wall of branch conduit, taps 71 to 90 on the downstream side wall of the branch. The distances equate to Y.

Table 5.3 (continued)

tap No.	distance (cm)	pressure head H (cm)					
		test7	test8	test9	test10	test11	test12
1	-159.49	77.3	80.1	60.1	81.8	53.8	92.5
2	-124.51	76.8	80	60	81.7	53.1	92
3	-101.65	76.8	79.8	59.3	81.4	52.2	91.7
4	-71.17	76.8	79.7	58.9	81.3	51.2	91.3
5	-48.31	76.7	79.5	58.5	81.2	50.8	90.9
6	-28.37	76.7	79.2	58.3	81.1	50.1	90.6
7	-20.75	76.6	79.1	58.2	81	49.6	90.5
8	-13.13	76.6	79.2	58.3	81.1	49.5	90.5
9	-10.59	76.6	79.1	58.3	81.1	49.3	90.5
10	-5.51	76.7	79.5	58.7	81.3	50	91.2
11	-4.51	76.6	79.5	58.9	81.3	50.4	91.3
12	-3.51	76.7	79.7	59.2	81.4	50.7	91.7
13	-2.21	76.6	79.8	59.4	81.5	51.4	91.9
14	-1.71	76.7	79.9	59.6	81.6	51.6	92
15	-1.21	76.6	79.9	59.6	81.6	52	92.2
16	-0.81	76.7	79.9	59.8	81.6	52.4	92.2
17	-0.41	76.7	80	59.8	81.6	52.6	92.2
18	-0.21	76.7	80	59.9	81.7	52.6	92.3
19	2.25	26.7	29.3	21	20.1	31.5	19.2
20	2.45	26.6	29.1	20.9	19.9	31.5	19
21	2.85	26.3	28.8	20.7	19.4	31.5	18.6
22	3.25	26.2	28.7	20.5	19.3	31.4	18.4
23	3.75	26.3	28.9	20.5	19.2	31	18.3
24	4.25	26.1	28.7	20.5	19.3	31	18.5
25	5.55	25.7	28.3	20.1	18.8	31	17.6
26	6.55	25.4	27.7	19.8	18.2	31.3	17
27	7.55	25.2	27.5	19.7	17.9	31.8	16.7
28	12.63	21.6	25.8	21.2	14.8	37.1	16.5
29	15.17	20.5	26.8	23	15.3	39.7	18.8
30	22.79	28.9	33.7	29.4	23.9	41.2	28.5
31	30.41	38.4	42	36.2	34.2	41	40.9
32	38.03	43.9	48.6	40	42.5	40.9	50.6
33	45.65	48.6	53.1	41.8	48.3	40.6	56.3
34	60.89	56.1	57.8	42.7	55.6	40.1	60.9
35	76.13	60.1	59.6	42.6	58.7	39.7	62
36	97.17	61	59.8	41.7	59.3	38.9	61.4

Table 5.3 (continued)

tap No.	distance (cm)	pressure head H (cm)					
		test7	test8	test9	test10	test11	test12
37	112.41	60.6	59.3	41	58.8	38.2	60.5
38	135.27	59.9	58.5	40.2	57.9	37.4	59.4
39	158.13	59.3	57.7	39.3	57	36.6	58
40	180.99	58.6	56.8	38.3	56	35.6	56.6
41	196.23	58.2	56.5	37.9	55.6	35	56.1
42	-20.75	76.6	79	58.1	80.9	49.3	90.4
43	-13.13	76.6	79	57.9	81	49.4	90.2
44	-5.51	76.5	78.6	57.1	80.8	48.4	89.3
45	2.12	76.4	73.8	50.1	77.3	43.3	79.4
46	7.2	74.1	57.1	37.2	61.2	39.3	53.5
47	12.28	24.7	34.2	27.1	23.1	38.4	28.1
48	17.36	22.7	30.6	26.7	19.4	39.3	24.7
49	22.44	26.9	33.2	29.7	22.2	40.3	27.9
50	27.52	35.1	39.3	33.9	31.1	40.6	36.6
51	32.6	39.3	43.3	36.2	36.2	40.4	43.3
52	47.84	49.3	53.5	41.2	49.2	40.3	56
53	63.08	56.1	57.9	42.4	55.8	39.9	60.3
54	9.45	72.8	76.1	58.9	76.7	51.5	85.2
55	9.75	69.7	73.1	57	73.1	51.2	81.1
56	10.05	67.3	70.9	55.6	70.6	50.7	78.3
57	10.85	62.9	67.8	52.8	65.6	50.5	72.7
58	11.35	61.8	66.7	52	64.2	50.3	70.9
59	12.65	61.4	65.4	51.6	63.7	50.5	70.2
60	13.65	60	64.3	51.3	63.8	50.6	70.3
61	14.65	62.1	65.9	52	64.4	50.6	71
62	19.73	65.2	68.2	53.1	67.2	50.7	73.4
63	24.81	68.5	70.7	54.5	70.6	50.9	76.6
64	29.89	71.7	73.1	55.9	74.2	51.1	80
65	34.97	75.8	76.3	57.7	77.9	51.5	83.3
66	40.05	79	78.7	59.1	80.3	51.9	85.7
67	45.13	81.4	80.8	60.2	84.3	52.2	89.4
68	50.21	84.2	82.9	61.1	86.7	52.5	91.5
69	55.29	86	84.7	62.4	88.7	52.7	93.2
70	60.37	88.7	86.7	63.5	91.8	52.9	96.1
71	9.45	45.3	49.7	39.2	44.6	45	48.4
72	9.75	51.7	56.3	44	53	47.6	57.7

Table 5.3 (continued)

tap No.	distance (cm)	pressure head H (cm)					
		test7	test8	test9	test10	test11	test12
73	10.05	55	59.6	47.2	57.7	48.7	63.1
74	10.85	58	62.6	49.1	60.6	50.1	66.1
75	11.35	59.4	63.8	50.2	61.5	50.3	68.5
76	12.65	61.1	65.3	51	63.8	50.6	69.8
77	13.65	61	65.2	50.9	63.7	50.6	69.8
78	14.65	60.9	65.2	51.3	64.2	50.7	71.5
79	19.73	64.9	68.2	52.7	66.7	50.9	73.7
80	24.81	67.2	69.9	54	70.5	51.2	77.4
81	29.89	71.2	73	55.5	73.6	51.6	80.1
82	34.97	75.2	76.2	57.2	77.5	51.8	83.3
83	40.05	78.3	78.4	58.6	80.2	52	86
84	45.13	81.9	81.2	59.8	83.6	52.4	89.3
85	50.21	84.6	83.3	61.2	86.2	52.5	91.6
86	55.29	87	85	62.1	89.5	52.8	94.3
87	60.37	88.6	86.4	63.1	91.1	53	95.9
88	82.67	102.3	96.8	68.9	105.1	53.8	108.4
89	97.91	113.2	105.1	73.7	116.3	54.5	118.1
90	113.15	126.2	114.8	79.1	129.2	55.4	129.9
discharges, discharge ratio, Reynolds number, and energy loss coefficients							
Q_1 (m^3/s) x 10^3		0.82	2.14	3.23	1.78	4.87	3.32
Q_2 (m^3/s) x 10^3		4.42	5.16	5.41	5.41	5.59	6.62
Q_3 (m^3/s) x 10^3		3.58	3.08	2.17	3.61	0.79	3.37
Q_3/Q_2		0.81	0.59	0.4	0.67	0.14	0.5
Re_1 x 10^{-5}		0.12	0.32	0.48	0.27	0.73	0.5
Re_2 x 10^{-5}		0.66	0.78	0.81	0.8	0.84	1
Re_3 x 10^{-5}		1.15	0.99	0.7	1.16	0.25	1.08
K_{12}		0.92	0.75	0.55	0.81	0.22	0.65
K_{32}		9.89	5.13	2.39	6.39	-0.01	3.45

Table 5.4 Contraction coefficient for combining flows

L/B	Q_3/Q_2	C_c (Eq.5.8)	C_c (Figs.5.4, 5.5, 5.6)
1	0.49	0.6	0.6
1	0.23	0.69	0.71
0.77	0.68	0.53	0.51
0.77	0.45	0.61	0.58
0.22	0.5	0.41	0.41
0.22	0.14	0.74	0.73

Table 5.5 Average entry angle "δ" for momentum transfer

L/B	Q_3/Q_2	Method 1 δ	Method 2 δ	Method 3 δ
1	0.49	61.6	63.0	65.6
1	0.23	49.8	46.7	52.2
0.77	0.68	78.4	71.7	75.1
0.77	0.45	72.0	63.4	70.7
0.22	0.5	87.4	82.6	83.6
0.22	0.14	75.6	71.2	75.0

Appendix 4 Experimental Uncertainties

A. 4.1 Uncertainty in the measurements

1. Conduit dimensions	Length = X ± 0.02 mm
	Height = B ± 0.02 mm
	Width = W ± 0.02 mm
2. Open channel dimensions	Length = X ± 0.02 mm
	Diameter = D ± 1 mm
	Sill height = s ± 0.02 mm
	Length of weir = L ± 0.02 mm
3. V-notch readings	Notch height = h ± 0.05 mm
4. Pressure measurements	Pressure head = P/γ ± 0.5 mm
	(water column)
5. LDV measurements	Mean velocity = U ± 0.05 m/s
	Turbulent intensity = u' ± 0.5 %
6. Temperature	T ± 0.25°C

A. 4.2 Uncertainty in computed results

1. Discharge	$Q \pm 3\ \%$
2. Mean velocity	$V \pm 3\ \%$
3. Reynolds number	$Re \pm 3.5\ \%$

Appendix 5 Specimen Computations

A. 5.1 Two-dimensional slot flow:

Given data: $V_1 = 195.5$ cm/s, $H_1 = p_1 / \gamma = 34.1$ cm, $L/B = 1.0$

$H_o = p_o / \gamma = 0$ cm (the pressure outside conduits)

Find: discharge coefficient C_d

$$h = H_1 - H_3 = 34.1 \text{ cm}$$

$$\eta_1 = \frac{V_1}{\sqrt{V_1^2 + 2gh}} = \frac{195.5}{\sqrt{195.5^2 + 2 \times 981 \times 34.1}} = 0.603$$

From Eq.(2.2)

$$C_d = 0.52$$

A. 5.2 Dividing rectangular closed conduit flow:

Given data: $V_1 = 241.7$ cm/s, $H_1 = p_1 / \gamma = -8.25$ cm,

$H_c = p_c / \gamma = -27.8$ cm (the pressure at point c, Fig. 4.1)

$Q_r = 0.354$, $L/B = 1.0$

Find: energy loss coefficient K_{12} and K_{13}

$$\Delta\ p/\gamma = H_1 - H_c = 19.55 \text{ cm}$$

$$V_3 = V_1 \times [Q_r / (L/B)] = 85.6 \text{ cm/s}$$

$$V_j = \sqrt{V_1^2 + 2g(\frac{\Delta p}{\gamma})} = 311.1 \text{ cm/s}$$

$$C_c = V_3 / V_j = 0.275$$

From Eq.(4.12),

$$K_{13} = (\frac{1}{C_c} - 1)^2 (\frac{Q_r}{L/B})^2 = 0.871$$

From fit curve in Fig.4.3,

$$K_{12} = -0.11$$

A. 5.3 Combining rectangular closed conduit flow:

Given data: $V_1 = 89.3$ cm/s, $V_3 = 63.3$ cm/s, $L/B = 1.0$

Find: energy loss coefficient K_{12} and K_{13}

From Table 5.1, one may get following relations (by curve fitting):

$$K_{12} = 0.077 + 1.14\, Q_r - 0.64\, Q_r^2$$

$$K_{32} = -0.88 + 3.53\, Q_r - 1.63\, Q_r^2$$

and here,

$$Q_r = \frac{V_3}{\frac{V_1}{L/B} + V_3} = 0.415$$

then,

$$K_{12} = 0.440$$

$$K_{32} = 0.304$$